2011

A Flexible Syntactic Foam For Shock Mitigation

Jogi C. Gowda
North Carolina Agricultural and Technical State University

A FLEXIBLE SYNTACTIC FOAM FOR SHOCK MITIGATION

by

JOGI C. GOWDA

A dissertation submitted to the graduate faculty
in partial fulfillment of the requirements for the degree of
DOCTOR OF PHILOSOPHY

Department: Mechanical Engineering
Major: Mechanical Engineering
Advisor: Dr. Kunigal Shivakumar

North Carolina A&T State University
Greensboro, North Carolina
2011

ABSTRACT

Gowda, Jogi. A FLEXIBLE SYNTACTIC FOAM FOR SHOCK MITIGATION. (**Major Advisor Dr. Kunigal Shivakumar**), North Carolina Agricultural and Technical State University.

This dissertation focused on the development and assessment of flexible microballoons filled elastomeric foam for shock mitigation applications. The overall goal of the research was to develop a flexible syntactic foam that has controllable bulk modulus, compressibility and shock mitigation characteristics and to validate these characteristics by experiments. Elastomer LP-2 with solid manganese dioxide and uncured BJO-093 hollow Pµb were chosen for making the syntactic foam. Hand mixing and room temperature curing was used to make foams of 0 to 30% weight of filler, which amounts to 0 to 60% of volume of the filler. Analysis using gas laws and simple elasticity equations showed that the compressibility of the foam and the resulting bulk modulus vary as a function of microballoon content. Confined compression tests confirmed these results and demonstrated that the bulk modulus can be changed from 19 MPa to 9 MPa as the filler content was increased from 0 to 30% by weight. The compressive high strain rate behavior of the foam was determined using the Split Hopkinson Pressure Bar test apparatus at strain rates ranging from 3,000/s to 4,600/s. The peak strain and strain rate values remain unaffected irrespective of the amount of filler. Both peak stress and stress rise rate decreased with increased filler content. Decrease in peak stress and stress rates were as high as 50% of the base material for filler content of 20% by weight. These characteristics show the potential of this material for shock mitigation applications.

School of Graduate Studies
North Carolina Agricultural and Technical State University

This is to certify that the Doctoral Dissertation of

Jogi C. Gowda

has met the dissertation requirements of
North Carolina Agricultural and Technical State University

Greensboro, North Carolina
2011

Approved by:

Dr. Kunigal Shivakumar Major Advisor	Dr. Huanchun Chen Co-advisor
Dr. Vinayak N. Kabadi Committee Member	Dr. Leonard C. Uitenham Committee Member
Dr. Dhananjay Kumar Committee Member	Dr. Samuel P. Owusu-Ofori Department Chairperson

Dr. Sanjiv Sarin
Interim Associate Vice Chancellor for
Research and Graduate Studies

BIOGRAPHICAL SKETCH

Jogi C. Gowda was born in Chandagalu, Mandya located in the state of Karnataka in India. He received his bachelor's degree in mechanical engineering from the BMS College in Bangalore, India in 1964 and worked until 1970 with NGEF (AEG, West German Collaboration), also in India. He later moved to the U.S.A. and earned his master's degree in Systems & Industrial Engineering from Pennsylvania State University in 1978 while working full-time. His professional engineering career spans over 40 years and includes Fortune 500 companies such as NCR, Shick Electric, Data General, Kaiser Fluid Technology, BE Aerospace and IBM. He was recognized in 1989 by IBM for the patent and publication of "Reduction of Noise & Vibrations in High Speed Scanner Motor for Laser Printers". At Luminescent Systems in 1983, he contributed to product and tool design, stock room layout, and eliminated deflash operations to achieve cost savings. At Schick Electric in 1977, he optimized moving assembly line balancing, reduced scrap and layout, and eliminated repair stations to achieve major cost reductions.

He enrolled in the Ph.D. program in 2005 at North Carolina Agricultural and Technical State University in the Department of Mechanical Engineering. His research dissertation for his PhD in Mechanical Engineering is in the area of syntactic foam for shock mitigation.

DEDICATIONS

"With salutations to that God whose compassion makes the mute eloquent and cripple cross mountains; whom the singers of sama sing by the Vedas with their full complement of parts, consecutive sections, and Upanishads; whom the Yogis see with their minds absorbed in him through perfection in meditation; and whose limit the hosts of devas and Asuras know not," according to Bhagavad Gita translation from Swami Swarupananda.

I would like to dedicate this accomplishment to my late grandmother (who nourished me from 10 months of age), uncles, and Gurus (who taught me until 15 years of age) whose love, teachings and blessings encouraged me to start grammar school and continue at colleges to earn a Bachelor's degree, Master's degree and finally, a doctorate. Finally, to my wife, daughters and son-in-law for their loving care and service throughout this effort.

ACKNOWLEDGMENTS

I am greatly indebted to my major adviser, Dr. Kunigal N. Shivakumar, for his constructive inputs, helpful support, and advice throughout my research activity to complete this research and the development of dissertation. I am honored to receive his knowledge to make this a successful doctoral research dissertation. My heartfelt thanks to my distinguished dissertation committee: Dr. Leonard C. Uitenham, Dr. Dhananjay Kumar, Dr.Vinayak N. Kabadi, and Dr. Huanchun Chen for their time, input and support. Special thanks to the Funding agencies, Office of Naval Research (Grant # N00014-01-1-1033 and Dr. Yapa Rajapakse), U.S. Army Research Office (Grant # W911NF-04-D-0002 and Dr. Bruce LaMattina), and NAAS URC-Center for Aviation Safety (Grant # NNX09AV08A). Many thanks to Dr. Raghu Panduranga, Professor Bob Sadler, Mathew Sharpe, John Skujins, and Dr. Shivalingappa Lingaiah for their continual help to prepare specimens, make tools, and instrumentation.

I also acknowledge the former and current students of CCMR: Dr. Feras Hilmi Darwish, Dr. Gowtham Swaminathan, Paul Akangah, Anthony Cunninghen, and Ebonni J. Adams, who helped me when needed. Thanks to Dr. Bill Sachina of High Land Industries, who permitted the use of its DMA equipment and facility for nearly two months and Ms. Sharon at N.C. State University for their Instron tensile tester. Additionally, Transpo Industries supplied TP48 epoxy-based polysulfide, PRC-DesSoto International supplied cartridges of PRC1422 class A, and Expancel Industries supplied samples of DE40d42 Expancel for evaluations.

TABLE OF CONTENTS

LIST OF FIGURES x

LIST OF TABLES xvi

NOMENCLATURE xvii

CHAPTER 1. INTRODUCTION 1

1.1 Background and Challenges 1

1.2 Syntactic Foams 5

1.3 Confined Compression Test 6

1.4 High Strain Rate Testing of Material 8

1.5 Objective of the Research 11

1.6 Scope of the Dissertation 12

CHAPTER 2. ANALYSIS 13

2.1 Introduction 13

2.2 Analysis 13

2.3 Assumptions 16

2.3.1 Case 1: Elastomer and microballoon walls perfectly plastic 17

2.3.2 Case 2: Analysis including compressibility of elastomer and Pμb wall 19

2.4 Summary 23

CHAPTER 3. MATERIALS SELECTION, PROCESSING AND PHYSICAL CHARACTERIZATION 25

3.1 Introduction 25

3.2 Material Selection 25

3.2.1 Polysulfides (Matrix Material)....................25
3.2.2 Curing Agent....................29
3.2.3 Phenolic Microballoon....................31
3.3 Material Processing and Specimen Preparation.................... 34
3.3.1 Compounding Process 34
3.3.2 Molding Process....................36
3.3.2.1 Molding Cylindrical Specimen....................36
3.3.2.2 Molding Rectangular Flat Specimen....................38
3.4 Physical Properties of the Material 39
3.4.1 Volume Fraction of Pμbs....................39
3.4.2 Computation of Void Fraction 41
3.5 Morphology of Material.................... 42
3.6 Summary 45
CHAPTER 4. STATIC CHARACTERIZATION 46
4.1 Introduction.................... 46
4.2 Tensile Test.................... 46
4.2.1 Test Specimen and Testing 47
4.2.2 Test Results and Discussion....................49
4.3 Confined Compression Test.................... 52
4.3.1 Test Specimen and Fixture....................52
4.3.2 Test Procedure 54
4.3.3 Test Results and Discussion....................55

4.3.3.1 Mechanism of Compression 55

4.3.3.2 Axial Stress-Strain Response...56

4.3.4 Comparison of Analysis with Experiment...64

4.4 Morphology of Microballoons at Different Stress Levels 66

4.5 Summary 70

CHAPTER 5. HIGH STRAIN RATE CHARACTERIZATION OF POLYSULFIDE SYNTACTIC FOAMS 71

5.1 Introduction.. 71

5.2 Sample Preparation 71

5.3 High Strain Rate Testing.. 74

5.3.1 Test Apparatus and Procedure 74

5.3.2 Data Collection and Analysis..78

5.3.3 Test Matrix..85

5.4 Results and Discussions 87

5.4.1 Effect of % wt. of Pμbs on Materials Dynamic Response..........................87

5.4.2 Effect of % wt. of Pμbs on Stress-Strain Response....................................90

5.4.3 High Strain Test Results for 0.11MPa Breech Pressure 95

5.4.4 High Strain Test Results for 0.19 MPa Breech Pressure 103

5.4.5 Effect of Strain Rate on Base and Pμb Filled Polysulfide.........................111

5.5 Summary 115

CHAPTER 6. CONCLUDING REMARKS AND FUTURE WORK 117

6.1 Concluding Remarks.. 117

6.2 Future Work 120

REFERENCES 121

APPENDIX. STRESS VS. TIME AND STRAIN VS. TIME PLOTS 125

LIST OF FIGURES

FIGURE **PAGE**

1.1 Typical layup of a composite integral armor and stress state in the elastomer layer 1

1.2 Stress wave modification for (a) $\upsilon = 0.5$ and (b) $\upsilon < 0.5$ 3

1.3 Stress-Strain response of different material system 4

1.4 An approach for making syntactic foam 4

1.5 Typical syntactic foam 6

1.6 Test fixture for ASTM D7012 7

1.7 Confined compression test apparatus 7

1.8 Schematic of Split Hopkinson Bar Apparatus 9

1.9 Typical Strain Signal for Aluminum Specimen (Al 6061-T651-1) in a Split Hopkinson Pressure Bar Test 9

1.10 Typical compressive stress-strain response of foam material 10

2.1 Morphology and deformation of Pμb under hydrostatic pressure 14

2.2 Schematic and SEM of LP2 polysulfide elastomer filled with Pμb 15

2.3 Confined Compression Test 15

2.4 Axial stress versus volumetric contraction of Pμb alone (Equation 2.5) 18

2.5 Axial Stress versus Strain for $\nu_e = 0.5$ (Eq. 2.10) 21

2.6. Axial stress vs. strain for (a) $\nu_e = 0.4995$ and (b) $\nu_e = 0.4990$ 22

2.7 Comparison of axial stress vs. strain based on Eqs. 2.5 & 2.10 for ($\nu_e = 0.5$) 23

3.1 Shear modulus against time for cure of polysulfide with MnO_2 30

3.2. Chemical structure of Pμb 32

3.3 Morphology of as-received Pμb 32

3.4 Deformation of microballoon under hydrostatic stress 32

3.5 (a) Compression test on a single microballoon and (b) typical compressive load vs. displacement response 33

3.6 Compounds (a) measured, (b) mixed, and (c) homogeneous elastomer............... 35

3.7 (a) Tension and (b) Compression test specimen configuration 36

3.8 (a) Round mold, (b) Closed mold assembly, and (c) Specimen configuration 37

3.9 (a) Flat mold, (b) Molding assembly, and (c) Specimen configuration................ 39

3.10 (a) Specimen, (b) Specimen slice, and (c) Mounted on test button 43

3.11 Scanning electron microscopy for morphology characterization 44

3.12 Morphology of specimen (a) Base, (b) 10% Pμbs, (c) 20% Pμbs, and (d) 30% Pμbs 44

4.1 Instron 5542 electro-mechanical testing system 47

4.2 Instron tension test specimen configuration 48

4.3 Tensile test plots for polysulfide LP2 neat resin (base) specimens 49

4.4 Tensile test plots for 10% wt. Pμb filled LP2 tensile specimens.......................... 50

4.5 Variation of tensile modulus with Pμb content for LP2 specimens 51

4.6 Comparison of Halpin-Tsai semi-empirical equation with experimental data 52

4.7 Specimen and test apparatus for confined compression test 53

4.8 Typical stress-strain response of Pμb and unfilled LP2 composite 56

4.9 (a) Complete stress-strain, and (b) Bulk modulus response of base LP2 specimen 57

4.10 (a) Complete stress-strain, and (b) Bulk modulus response of 10% wt. Pμb specimen 58

4.11 (a) Complete stress-strain, and (b) Bulk modulus response of 20% wt. Pμb specimen 59

4.12 (a) Complete stress-strain, and (b) Bulk modulus response of 30% wt. Pμb specimen 60

4.13 Average confined compression stress vs. strain for various Pμb contents 61

4.14 Polysulfide bulk modulus vs. percent wt. Pμb specimens 63

4.15 Polysulfide specimens compressibility vs. percent wt. Pμb 64

4.16 Comparison of analysis and experiment data 65

4.17 Comparison of experiment and exponential equation 66

4.18 Confined compression-decompression at various stress level 67

4.19 SEM morphology at 2.8 MPa stress level 68

4.20 SEM morphology at 4.2 MPa stress level 68

4.21 SEM morphology at 5.6 MPa stress level 69

4.22 SEM morphology at 6.9 MPa stress level 69

5.1 (a) Specimen schematic, (b) base polysulfide, and (c) Pμb filled polysulfide 72

5.2 Photograph of main SHPB test apparatus 75

5.3 (a) Transmitter-Specimen-Incident bars, (b) Specimen bars assembly, (c) Striker hitting incident bar, and (d) Display of wave forms 76

5.4 Specimen deformation state and strain waves in incident and transmitter bars 76

5.5 Typical strain pulses measured from the strain gages mounted on the incident and transmission bars (LP2-0-9) 77

5.6 Block diagram of typical data processing procedure 78

5.7 Strain Rate vs. Time plot for base polysulfide specimen LP2-0-9 82

5.8 Strain vs. Time plot for base polysulfide specimen LP2-0-9................................ 83

5.9 Stress vs. Time plot for base polysulfide specimen LP2-0-9................................ 83

5.10 Stress vs. Strain plot for base polysulfide specimen LP2-0-9 84

5.11 Illustration of computing Strain Rate at 10%, 25%, and at 70% (Half Power Point) of peak strain.. 84

5.12 Illustration of computing Stress Rise Rate at 10%, 25%, and at 70% (Half Power Point) of peak stress... 85

5.13 Plot of normalized Peak Stress vs. Amount of Pµbs at breech pressure of 0.16 MPa 89

5.14 Plot of normalized Stress Rise Rate vs. Amount of Pµbs at breech pressure of 0.16 MPa 90

5.15 Stress-Strain response of base LP2 at breech pressure of 0.16 MPa 93

5.16 Stress-Strain response of 10 wt.% Pµb-filled LP2 at breech pressure of 0.16 MPa... 93

5.17 Stress-Strain response of 20 wt.% Pµb-filled LP2 at breech pressure of 0.16 MPa... 94

5.18 Stress-Strain response of 30 wt.% Pµb-filled LP2 at breech pressure of 0.16 MPa... 94

5.19 Average Stress-Strain Response of Pµb-filled LP2 at breech pressure of 0.16 MPa... 95

5.20 Plot of normalized Peak Stress vs. Amount of Pµbs at breech pressure of 0.11 MPa 98

5.21 Plot of normalized Stress Rise Rate vs. Amount of Pµbs at breech pressure of 0.11 MPa 98

5.22 Stress-Strain response of base LP2 at breech pressure of 0.11 MPa 101

5.23 Stress-Strain response of 10 wt.% Pµb-filled at breech pressure of 0.11 MPa 101

5.24 Stress-Strain response of 20 wt.% Pµb-filled at breech pressure of 0.11 MPa 102

5.25 Stress-Strain response of 30 wt.% Pµb-filled at breech pressure of 0.11 MPa 102

5.26 Average Stress-Strain response of Pµb-filled LP2 at breech pressure of 0.11 MPa 103

5.27 Plot of normalized Peak Stress vs. Amount of Pµbs at breech pressure of 0.19 MPa 105

5.28 Plot of normalized Stress Rise Rate vs. Amount of Pµbs at breech pressure of 0.19 MPa 106

5.29 Stress-Strain response of base LP2 at Breech Pressure 0.19 MPa...................... 109

5.30 Stress-Strain response of 10 wt.% Pµb-filled LP2 at Breech Pressure 0.19 MPa 109

5.31 Stress-Strain response of 20 wt.% Pµb-filled LP2 at Breech Pressure 0.19 MPa 110

5.32 Stress-Strain response of 30 wt.% Pµb-filled LP2 at Breech Pressure 0.19 MPa 110

5.33 Average Stress-Strain response of Pµb-filled LP2 at Breech Pressure 0.19 MPa 111

5.34 Average Stress-Strain response of base polysulfide at strain rates ranging from 3,017/s to 4,569/s 112

5.35 Average Stress-Strain response of 10 wt.% Pµb-filled polysulfide at strain rates ranging from 3,376/s to 4,787/s.................... 113

5.36 Average Stress-Strain response of 20 wt.% Pµb-filled polysulfide at strain rates ranging from 3,131/s to 4,530/s.................... 114

5.37 Average Stress-Strain response of 30 wt.% Pµb-filled polysulfide at strain rates ranging from 2,861o 4,497/s 115

LIST OF TABLES

TABLE **PAGE**

3.1 Polysulfide elastomers characteristics 27

3.2 Physical properties of different microballoons 34

3.3 Summary of specimen volume, weight, density and volume fraction of Pμb and voids.. 41

4.1 Tension and Confined Compression Test Matrix. 46

4.2 Pμb filled LP2 tensile test specimen geometry and tensile modulus.................... 48

4.3 Confined compression test specimen geometries 54

4.4 Summary of bulk modulus and compressibility of the specimens 62

5.1 Specimen Number, Avg. Diameter, and Avg. Length.. 73

5.2 Dynamic Test Matrix for Base & Pμb-filled Polysulfide 86

5.3 Summary of High Strain Rate Test Results for Base & Microballoon Filled Polysulfide Tested at Breech Pressure of 0.16 MPa.................................. 88

5.4 Summary of Peak Strain, Strain Rate, Peak Stress, and Stress Raise Rate at Breech Pressure of 0.16 MPa.. 89

5.5 Summary of High Strain Rate Test Results for Base & Pμb-filled Polysulfide Tested at Breech Pressure of 0.11 MPa 96

5.6 Summary of Peak Strain, Strain Rate, Peak Stress, and Stress Raise Rate at Breech Pressure of 0.11 MPa.. 97

5.7 High Strain Rate Test Results for Base & Microballoon Filled Polysulfide Tested at Breech Pressure of 0.19 MPa 104

5.8. Summary of Peak Strain, Strain Rate, Peak Stress, and Stress Raise Rate at Breech Pressure of 0.19 MPa.. 105

NOMENCLATURE

A	cross-sectional area
A_b	cross-sectional area of the pressure the bar
A_s	cross-sectional area of the pressure the specimen
A	ampere
ASME	American Standard Code for Information Interchange
ASTM	American Society of Testing and Materials
avg.	average
C_b	wave speed in the bar
CC	confined compression
cps	cycles per second
CV	co-efficient of variation
DC	direct current
D_s	specimen diameter
DSO	Digital Storage Oscilloscope
E	elastic modulus
E_b	elastic modulus of the bar
ε_I	Incident strain signal
ε_R	reflected strain signal
ε_T	transmitted strain signal
g	gram

g/cc	gram/cubic centimeter
GPa	giga pascal
H_s	height of specimen
I_b	Incident bar
in	inch
mN	milli Newton
L/D	Length-Diameter Ratio
m/s	meter/second
mg	milligram
MHz	mega hertz
min	minute
mm	millimeter
MPa	mega pascal
µs	microsecond
N	Newton
Psi	pounds per square inch
ρ	density
σ	stress
SEM	Scanning electron microscopy
DMA	Dynamic Mechanical Analyzer
SHPB	Split Hopkinson Pressure Bar
LP2	Liquid Polysulfide 2

MnO2	Manganese Dioxide
Pµb	Pµb
V_e	Volume fraction of elastomer
V_0	Volume fraction of microballoon
V_w	*V*olume fraction of microballoon wall
V_f	*V*olume fraction of fluid in the microballoon
V_{f1}	Volume fraction of fluid at pressures P_1
V_{f2}	Volume fraction of fluid at pressures P_2
V_c	Volume of composite
E_e	Elastic modulus of elastomer
E_w	Elastic modulus of microballoon wall
ν_e	Poisson's ratio of elastomer
ν_w	Poisson's ratio of microballoon wall

CHAPTER 1

INTRODUCTION

1.1 Background and Challenges

Protection of soldiers and vehicles that carry personnel and material in combat or noncombat against an ever-increasing firepower of ammunitions and improvised ammunitions by the enemy is a challenging task of the military. The lightweight and more agile armors are essential so that soldiers can handle it with no loss of war fighting capability. A continuous development and improvement of materials (metals, ceramic and polymer composites) have been going on for a number of years. Advancement of nanotechnology, computer power, and simulation models has provided an opportunity to develop materials by simulations. Sometimes a simple idea could also result in a good solution to practical problems. Figure 1.1 is typical composite armor layup.

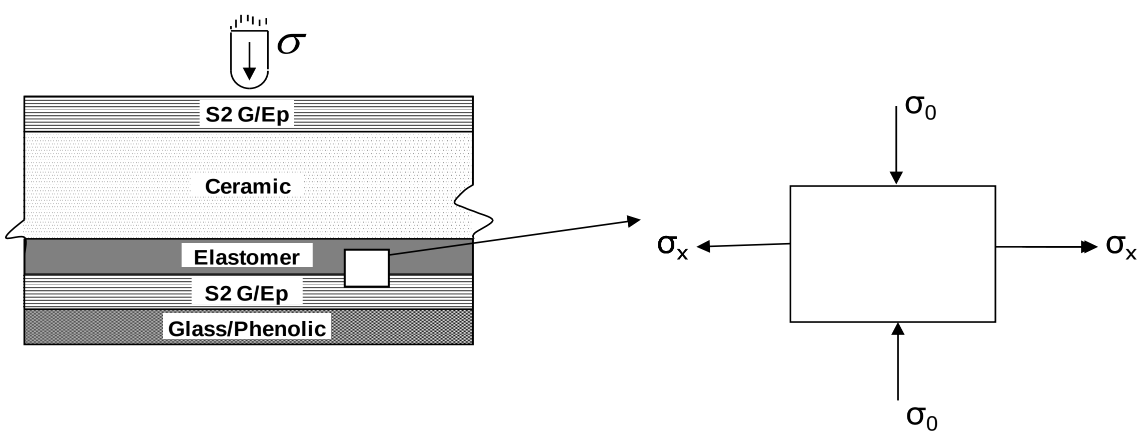

Figure 1.1 Typical layup of a composite integral armor and stress state in the elastomer layer

This research is about one such idea and its assessment. Elastomers are proposed to be used under ceramic tiles to provide softer media and to distribute the stress shock waves over a larger area. Elastomers being plastic (Poisson's ratio of 0.5) would develop lateral stress waves of equal magnitude of the impact stress wave (see Fig. 1.1). This can be derived from the theory of three dimensional elasticity; $\sigma_x = \sigma_z = 2\nu\sigma_0$ for a constrained lateral boundary condition. Also, the bulk modulus (K) of the elastomer $K = \frac{E}{3(1-2\nu)}$ could be infinite for ν = 0.5. In such a scenario, the incoming shock pulse from the tile directly transfers to the supporting structure (composite panels). If the elastomer material is modified such that its Poisson's ratio is less than 0.5, the bulk modulus is finite, or a part of the energy is dissipated by compressing the elastomer and the transmitted stress wave will be less severe. Based on a number of research reported in the literatures, one can hypothesize that the modification of the stress wave means reducing the peak stress, reducing stress rise rate and increasing the pulse width.

Figure 1.2 shows transmitted stress waves for bulk modulus of infinite and finite values. Note that the area under the two stress waves are identical but the peak and rise rate of stress and the bandwidth of the curve are different. For convenience of assessment of half-power bandwidth, pulse width at stress value of $\sigma_{peak}/\sqrt{2}$ is chosen for comparison.

The challenge of this problem is how to mitigate the shock pulse without altering the general characteristics of the elastomer.

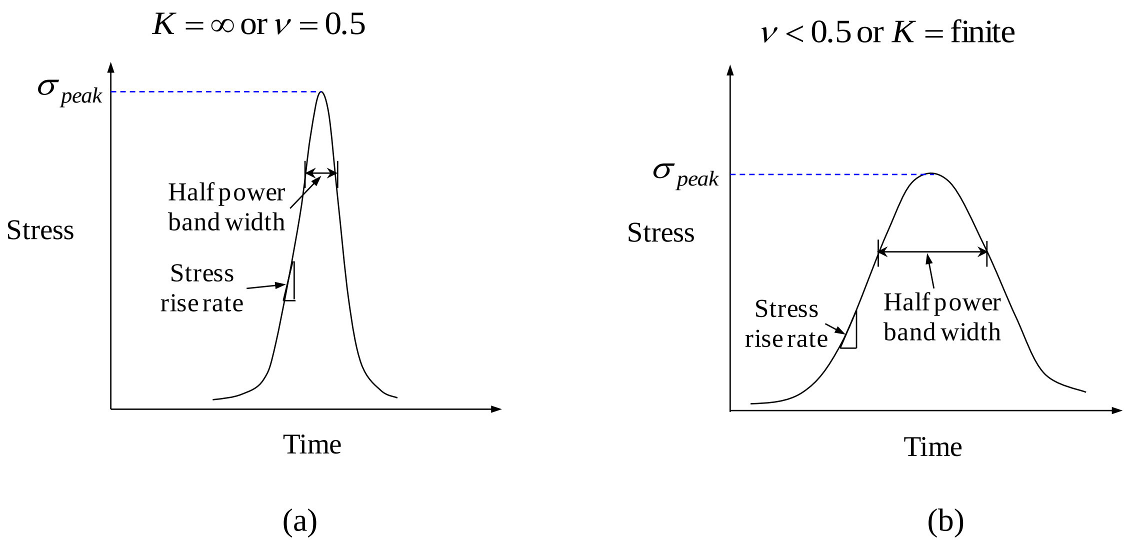

Figure 1.2 Stress wave modification for (a) υ = 0.5 and (b) υ < 0.5

Figure 1.3 shows the stress-strain diagrams of rigid-plastic, elastic, and elastic-plastic-solidification (foam) type of materials. Among the three materials, the foam type has large compressibility followed by solidification. The compressibility of the material with reasonable compression strength could be chosen as a shock mitigation material. Furthermore, the material should also take multiple loading (shocks) and unloading so that it can survive multiple hits. Therefore, the challenge is how to design and develop elastomer material that can be hydrostatically compressible and recovers upon unloading. The proposed approach is to use elastomer with collapsible microballoons in a syntactic process to make a flexible foam. The filler content controls the bulk modulus and the compressibility of the material. A schematic of manufacturing the flexible syntactic foam is shown in Figure 1.4. These materials could also be used in packing sensitive instruments against shock and or protect structural components against shock and impact.

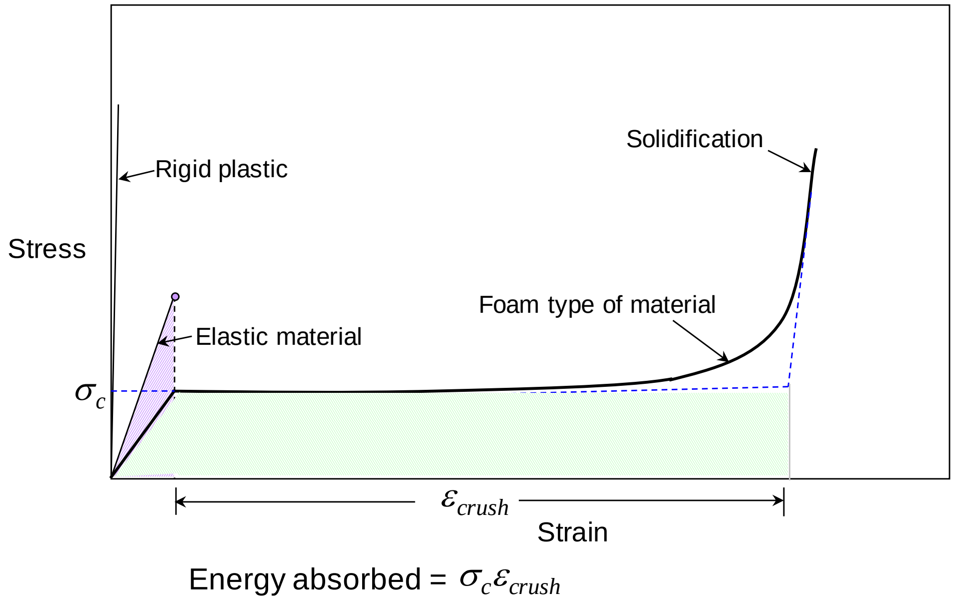

Figure 1.3 Stress-Strain response of different material system

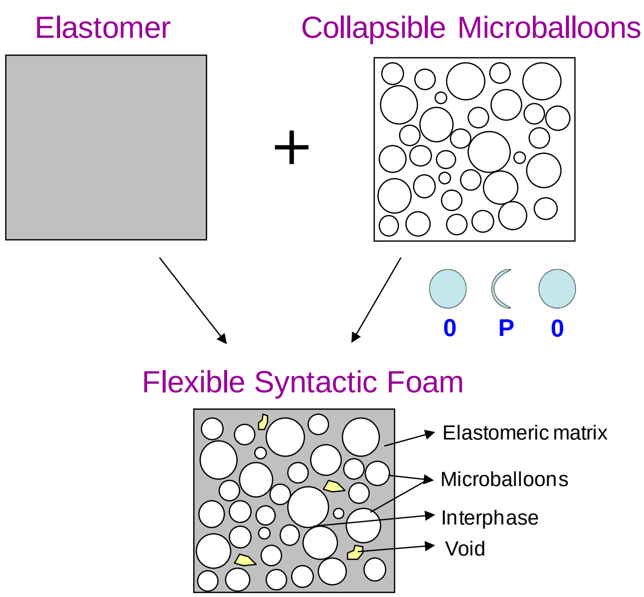

Figure 1.4 An approach for making syntactic foam

1.2 Syntactic Foams

Syntactic foams are composite materials synthesized by filling a metal, polymer or ceramic matrix with hollow particles called microballoons. The word "syntactic" means "put together"[1]. Presence of hollow particles results in lower density, higher strength, a lower coefficient of thermal expansion, and, in some cases, radar or sonar transparency.

Tailorability is one of the biggest advantages of syntactic foams. The matrix material can be selected from almost any metal, polymer or ceramic. A wide variety of microballoons are available, including cenospheres, glass microspheres, and carbon and polymer microballoons. The most widely used and studied foams are glass microballoon-epoxy, glass microballoon-aluminum and cenosphere-aluminum [2]

The compressive properties of syntactic foams primarily depend on the properties of microballoons, whereas the tensile properties depend on the matrix material that holds the microballoons together. Changing the volume fraction and/or changing the wall thickness of the microballoons can adjust properties of syntactic foams. In general, the compressive strength of the material is proportional to its density [2]

Syntactic foams were developed in early 1960s as buoyancy aid materials for marine applications [3] the other characteristics led these materials to aerospace and ground transportation vehicle applications [4]. Current applications for syntactic foam include buoyancy modules for marine riser tensioners, boat hulls, deep-sea exploration, underwater vehicles, parts of helicopters and airplanes, and sporting goods such as soccer balls [5].

Another class of syntactic foams that is finding wide applications in potting, sealing, and packaging is the elastomer-soft microballoons foams. These materials provide flexibility to fill all gaps and voids and can offer shock mitigation properties. Again, there is a wide variety of elastomers (example, polysulfides) and microballoons (such as phenolic and expancel) that are available to choose from. This study focuses on polysulfide elastomer and Pμbs. Figure 1.5 shows the morphology of a syntactic foam.

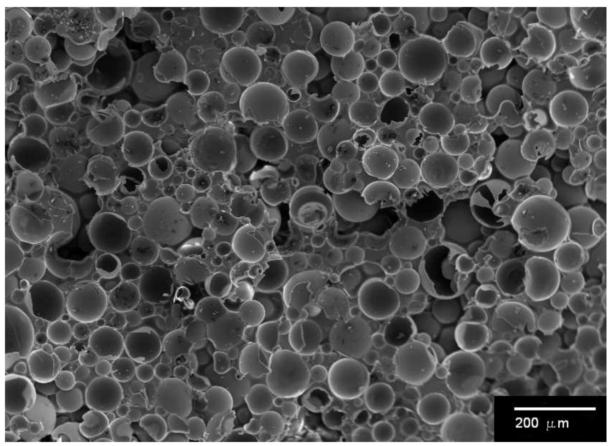

Figure 1.5 Typical syntactic foam

1.3 Confined Compression Test

Genesis of confined compression test starts from soil mechanics where shear strength of soils are measured under triaxial stress state and it dates back to 19th Century. The method has been standardized for soils and concrete and the details are found in ASTM D7012 [6]. The ASTM D7012 test fixture is shown in Figure 1.6.

Matsuoka and Maxwell [7] developed a test fixture (see Figure 1.7) to study the compressibility of Nylon 66 and polystyrene matrices. Warfield [8] used the same test fixture to study polyethylene. Burchett, et al. [9] studied the effect of specimen length to diameter on volumetric stress and strain and highlighted its importance. The current study uses a slightly modified version of Matsuka and Maxwell's test fixture for ease of conducting the tests. The purpose of this test is to measure the bulk modulus and compressibility of the syntactic foam.

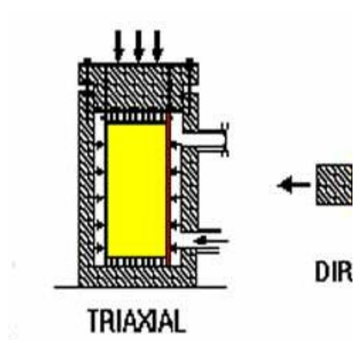

Figure 1.6 Test fixture for ASTM D7012

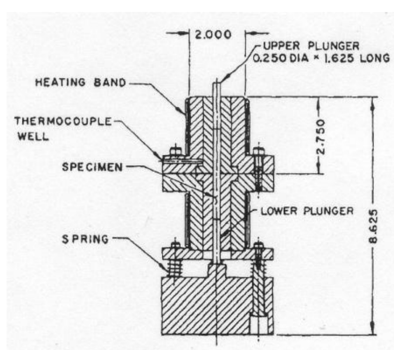

Figure 1.7 Confined compression test apparatus

1.4 High Strain Rate Testing of Material

The most widely used test for determining strain rate properties of materials over the range of 100 and 10,000 s^{-1} is the Split Hopkinson Pressure Bar (SHPB). The test method was first proposed by Hopkinson [10-12] and the present form of the test apparatus was developed by Kolsky [13] with all the mathematical details required for one-dimensional wave propagation theory. The analysis was refined by Bancroft [14] and Davies [15]. Later on, the method was extended from compression to tension and torsional loadings [16,17], ceramic materials [18], and soft and viscoelastic materials [19,20]. The reference quoted here is only a few, but one can find a wealth of publications in the literature.

The compressive SHPB consists of two elastic pressure bars that sandwich the specimen between them Figure 1.8. Upon impact of the striker bar on an incident bar, an elastic compressive wave is generated in the incident bar and that travels through the specimen (some reflected back) and into the transmitting bar. The strain-time response is measured by strain gages on bars. The velocity of the striker controls the strain rate while the length of the striker determines the duration of the test. By adjusting the striker bar velocity, a desired strain rate can be achieved. At the incident bar/specimen interface, the wave is partially reflected and partially transmitted into the specimen. The reflected and transmitted wave response is measured by the strain gages on the two bars. Typical incident, reflected and transmitted waves for an aluminum alloy specimen is shown in Fig. 1.9.

From these strain-time response, a complete stress-strain response of the material can be determined. A detailed analysis and testing of the SHPB test facility at A&T is presented by Panduranga [21].

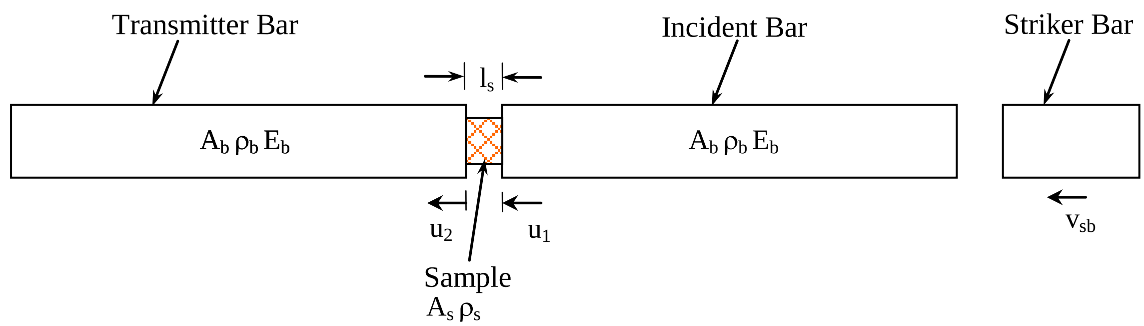

Figure 1.8 Schematic of Split Hopkinson Bar Apparatus

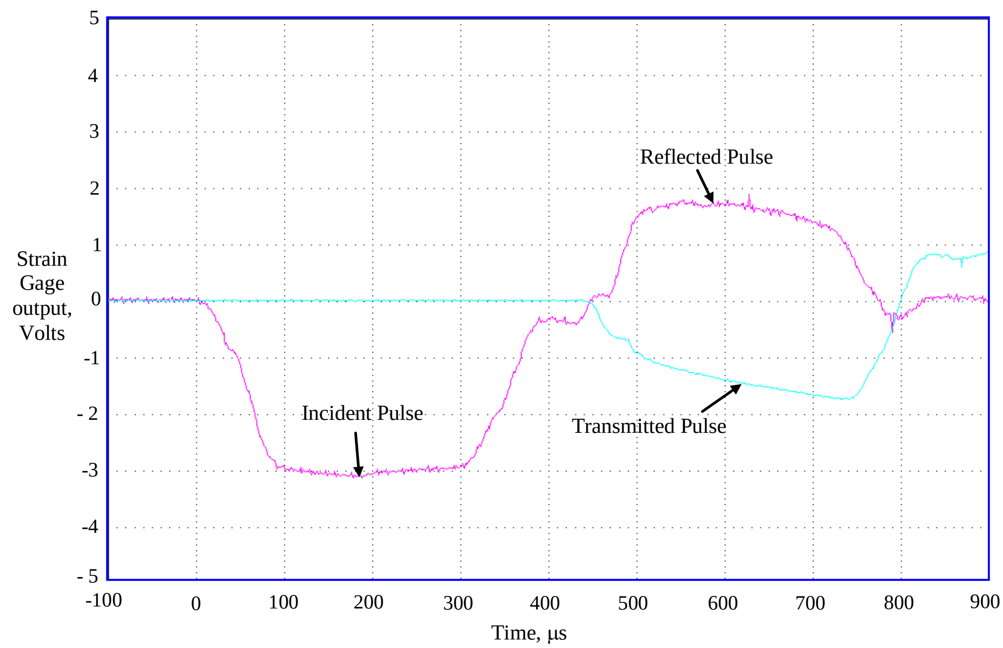

Figure 1.9 Typical Strain Signal for Aluminum Specimen (Al 6061-T651-1) in a Split Hopkinson Pressure Bar Test

An ideal static or dynamic stress-strain response for a microballoon filled syntactic foam is shown in Figure 1.10. Notice the failure onset (compressive strength), microballoon collapse (crushing) and solidification/densification parts of the curve in Figure 1.10. Crushing strain (ε_{crush}) is an important component in energy dispersion of the material. In these cases, the energy absorption can be approximated by the ($\sigma_o \varepsilon_{crush}$).

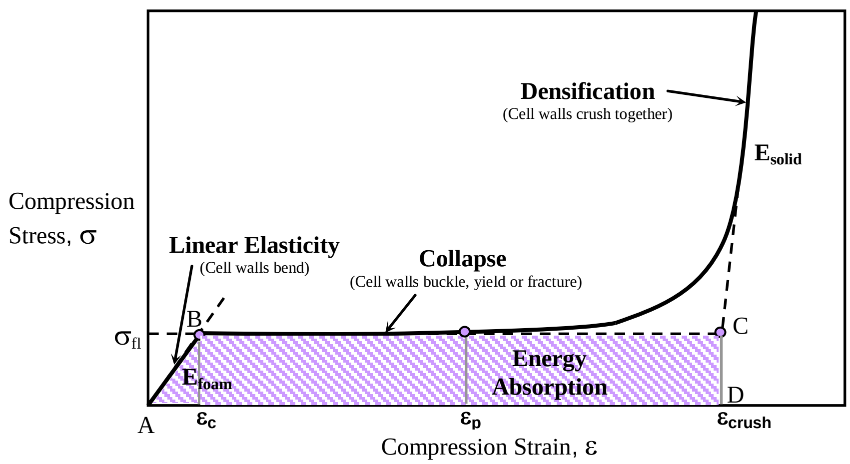

Figure 1.10 Typical compressive stress-strain response of foam material

The idea of proposed research is filling the matrix with microballoon to increase the ε_{crush} strain of the material. In the present research, flexible microballoon will be selected because of multiple compressibility and is used to make a syntactic foam.

An extensive study on high strain rate characteristics of metallic materials and foams can be found in the literature. However, the studies of elastomer materials are very limited [22, 23] and no reference was found on soft microballoon filled elastomers. The work of Sandia Lab [22, 23] was all on commercial materials, no details of material composition was provided and the results were inconclusive.

The study of Wasley et al. [24] on various organic foams such as polyurethane foams, phenolic microballoons, and polystyrene bead foam provided a guidance for good shock mitigation material: pulse duration was greatly lengthened, Peak stress and stress rise rate reduction and increased stress pulse width. This guidance was used in the present study to assess the flexible microballoon filled elastomer foam. Selected phenolic microballoons dispersed in a liquid polysulfide resin binder at 0.23 g/cc.

1.5 Objective of the Research

The overall objective of the research is to develop a flexible syntactic foam that has controllable bulk modulus, compressibility and shock mitigation characteristics and to validate the material performance by experiments. The specific activities of the research are:

- To demonstrate that a variable bulk modulus can be developed using an elastomer matrix and flexible microballoons. It is also required to assess the material compressibility as function of microballoon content.
- To develop flexible syntactic foams using commercial materials and to characterize its physical properties as a function of filler content.
- To characterize the tensile and bulk moduli of the foam and to express the compressibility as a function of filler content.
- To use A&T's Split Hopkins Pressure Bar test apparatus to characterize high strain rate properties and shock mitigation performance of the foam.

1.6 Scope of the Dissertation

The dissertation consists of six chapters. Chapter 1 presents the importance of problem, background on elastomeric syntactic foams, confined compression test, and compression high strain rate test. Chapter 1 also includes the objectives of the research and scope of the dissertation. Chapter 2 presents the concept of variable bulk modulus using flexible microballoons to fill the composite and analyzed through simple gas laws analysis. It also includes discussions on the elastic deformation of the elastomer and the microballoon wall materials. Chapter 3 focuses on the materials selection, processing of the foam, fabrication of the specimen, physical and the morphology characterization. Chapter 4 presents the tension and confined compression testing procedure, and the results. Chapter 5 presents details of compression high strain rate testing, test results, analysis and discussions. The strain rate is limited to 3,000/s to 4,600/s to get the first order effect and viability of the concept. Finally, concluding remarks and future work are presented in Chapter 6.

CHAPTER 2

ANALYSIS

2.1 Introduction

This chapter derives a relation between volumetric stress and volumetric strain in a confined compression testing of Pμbs filled LP2 elastomer composite using gas laws and elastic deformation of the LP2 elastomer. A number of realistic assumptions are made to reduce the equation to a simple form. The lateral constraint due to a nearly rigid mold, the slope of axial stress and strain would yield the bulk modulus of the composite.

2.2 Analysis

The Pμbs are filled with inert gas such as Nitrogen during the manufacturing process. The wall material of the microballoon is highly flexible and non-breakable under repeated loading and unloading. Figure 2.1 shows the morphology of Pμb (Fig. 2.1a) and the deformation states under hydrostatic stress (Fig. 2.1b). At the normal atmospheric pressure (1 bar), the microballoon is spherical and at 6 bar or 0.62 MPa hydrostatic pressure, the balloon completely collapses. Upon releasing the pressure, the microballoon bounces back to the original spherical shape.

This expansion and contraction upon de-pressurizing and pressurizing follows the ideal gas laws. At constant temperature, it follows the Boyle's law. The composite is a mixture of elastomer and Pμb, therefore, the amount of compressibility depends on the volume fraction of Pμb. The rate of change of compressibility will directly influence the bulk modulus of the material. For an elastic material of modulus (E) and Poisson's ratio of (ν), the bulk modulus is given by $K = \frac{E}{3(1-2\nu)}$.

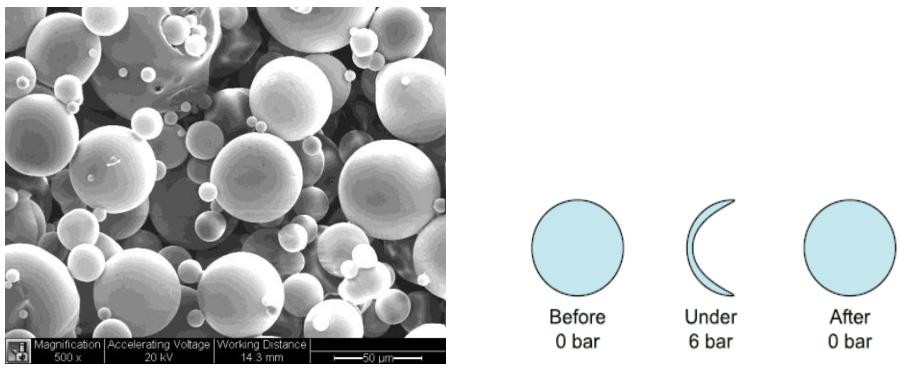

(a) As-received microballoon **(b) Under hydrostatic stress**

Figure 2.1 Morphology and deformation of Pμb under hydrostatic pressure

As noted in the above equation, the bulk modulus is infinite for ν = 0.5 for elastomer type material. For ν not equal to 0.5, the bulk modulus is finite. It is possible to vary K by adding Pμb, which are enclosed air pockets. Figure 2.2 shows the schematic and the SEM of Pμb filled LP2 polysulfide elastomer. This is assuming that Pμb is spherical and well dispersed. This composite is tested in a steel test cylinder under axial stress as shown in Figure 2.3. Because the cylinder is rigid compared to the composite, the lateral strains are zero and the axial strain is hydrostatic strain. The analysis is conducted for two cases as shown in Figures 2.2 and 2.3 with a schematic, morphology and test cylinder:

1.Elastomer and microballoon walls are perfectly plastic and do not deform under hydrostatic stress and;

2. Elastomer and Pμb wall are elastic and deform under hydrostatic stress state.

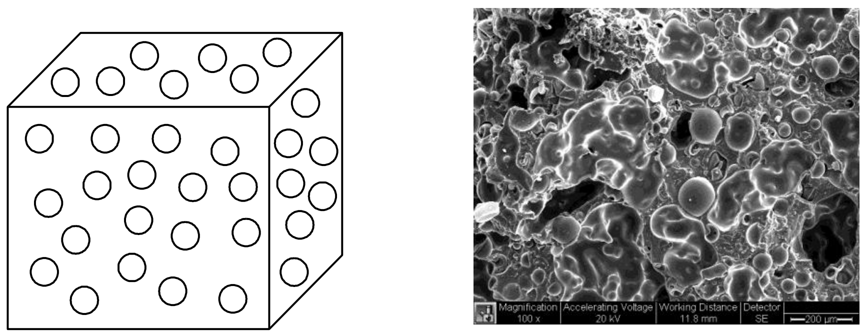

(a) Schematic (b) SEM

Figure 2.2 Schematic and SEM of LP2 polysulfide elastomer filled with Pμb

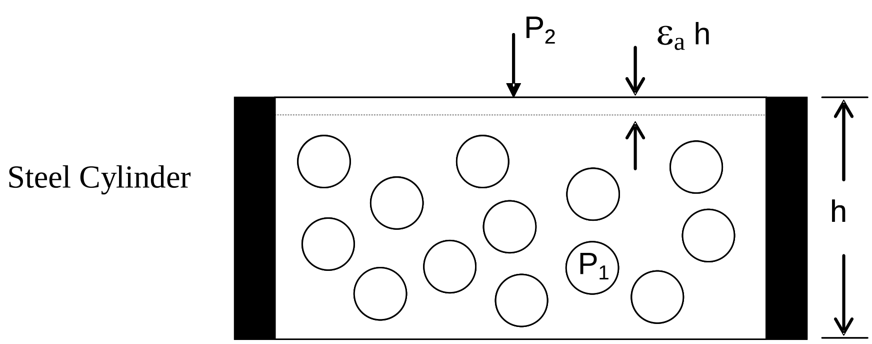

Figure 2.3 Confined Compression Test

2.3 Assumptions

The analysis is based on the following assumptions:

1. Composite consists of elastomer, Pμb, and no voids
2. Volume fraction of elastomer is V_e
3. Volume fraction of microballoon is V_0
4. V_0 consists of volume fraction of microballoon walls (V_w) + volume fraction of fluid (V_f) in the microballoons. Therefore $V_0=V_w+V_f$
5. V_{f1} and V_{f2} are the volume fraction of fluid (filler) at pressures P_1 and P_2, respectively.
6. Volume fraction of the composite is V_c=1. and $V_c=V_e+V_0$
7. Initial pressure in the Pμb is P_1, which is the atmospheric pressure
8. Applied pressure or the axial stress is P_2, which is over and above the atmospheric pressure.
9. Elastic modulus and Poisson's ratio of elastomer are E_e and ν_e, respectively
10. Elastic modulus and Poisson's ratio of microballoon wall is E_w and ν_w, respectively
11. The test cylinder is made of steel jacket and is considered rigid. Material leakage in the test system is zero

2.3.1 Case 1: Elastomer and microballoon walls perfectly plastic

Here all the expansion and contraction of composite are due to the fluid inside the microballoon and the pressure-volume relation is governed by Boyle's law.

$$P_1 V_{f1} = P_2 V_{f2} \tag{2.1}$$

In a confined compression test shown in Figure 2.3, the axial strain ε_a can be calculated as follow:

Volume fraction of the fluid (V_{f2}) at pressure P_2 is:

$$V_{f2} = \frac{P_1 V_{f1}}{P_2} \tag{2.2}$$

Change in volume fraction is:

$$\frac{\Delta V_f}{V_c} = V_{f1} - \frac{P_1 V_{f1}}{P_2} = \left(1 - \frac{P_1}{P_2}\right) V_{f1}$$

Because volume fraction of the composite, V_c, is 1, we get the volumetric strain ε_f , which is same as the axial strain, ε_a, is:

$$\varepsilon_a = \left(1 - \frac{P_1}{P_2}\right) V_{f1} \tag{2.3}$$

The applied axial stress in a uniaxial compression test is given by:

$$\sigma_a = (P_2 - P_1) \tag{2.4}$$

Substituting equation 2.4 in 2.3 and simplifying will lead to:

$$\varepsilon_a = \left(1 - \frac{1}{(1 + \sigma_a / P_1)}\right) V_{f1} \tag{2.5}$$

Here P_1 = 1 bar (0.1 MPa).

Figure 2.4 shows axial stress versus strain response from Equation 2.5 for different values of filler volume fraction (V_{f1}). The amount of shift to the right depends on volume fraction of the filler, V_{f1}. Notice the almost zero slope in the initial stress-strain response because of low modulus of Pμb. Once the Pμbs are compressed, the stress-strain curve is very steep or vertical because of infinite bulk modulus (ν_e = 0.5).

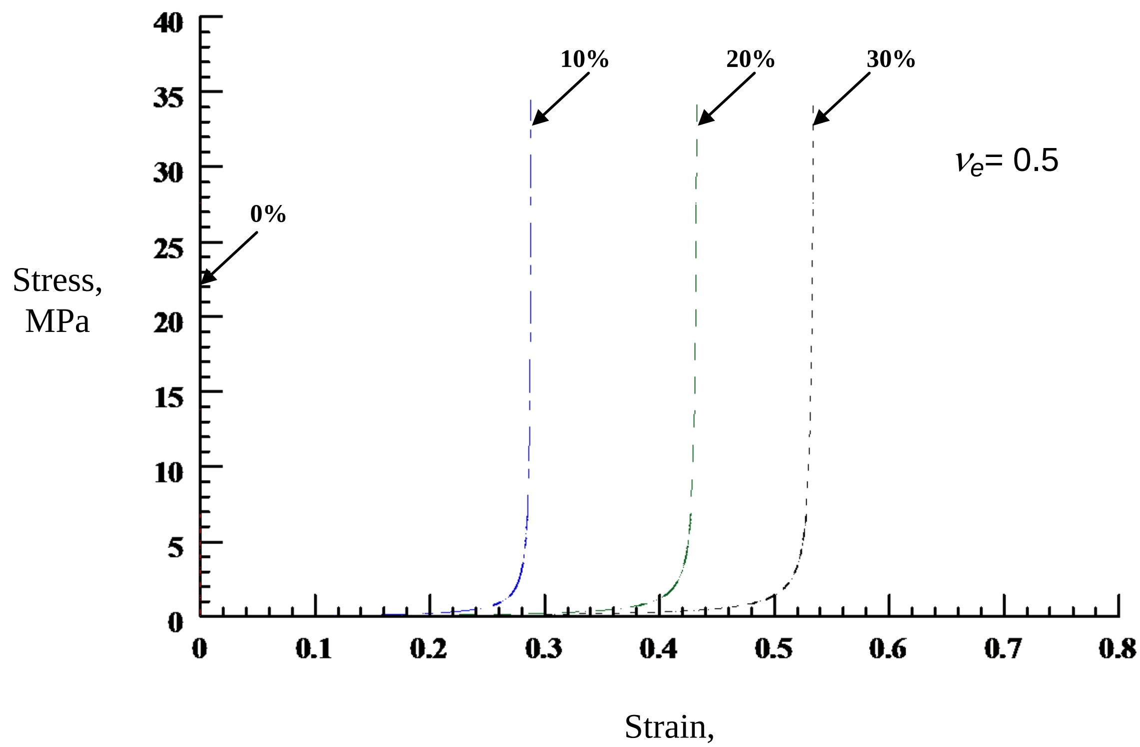

Figure 2.4 Axial stress versus volumetric contraction of Pμb alone (Equation 2.5)

2.3.2 Case 2: Analysis including compressibility of elastomer and Pμb wall

Here, in addition to the compressibility of the fluid in the microballoon, the compressibility of elastomer and the Pμb wall materials will be included in establishing axial stress-strain equation. Although the elastomer's Poisson's ratio is nearly 0.5, it is assumed to be ν_e for the purpose of analysis and the microballoon wall's Poisson's ratio is ν_w. Both these materials deform as per the three-dimensional elasticity theory.

Deformation due to compressibility of the composite using the rule of mixtures elastic modulus (E_c) and Poisson's ratio (ν_c) of the composite is calculated as follows [27]. The volume fraction of the composite excluding the filler content is ($1-V_{f1}$), the resulting elastic modulus when applying the rule-of-mixture and the volume fraction correction, is:

$$E_c = \frac{E_e V_e + E_w V_w}{1 - V_{f1}} \tag{2.6}$$

and

$$\nu_c = \frac{\nu_e V_e + \nu_w V_w}{1 - V_{f1}} \tag{2.7}$$

For a confined compression test, the lateral strains are zero and the corresponding lateral stresses can be derived from the elasticity equations [28]. Combining these two stresses and the axial stress σ_a, the reduced axial strain due to elastic deformation of the composite becomes:

$$\varepsilon_{El} = \frac{\sigma_a}{E_c}\left(1 - \frac{2\nu_c^{\ 2}}{1-\nu_c}\right) \tag{2.8}$$

The total axial strain, ε_t, is the sum of the compressibility of the fluid in the Pμb (Eq. 2.3) and the elastic deformation of the composite (Eq. 2.8), that is:

$$\varepsilon_t = \left(1 - \frac{P_1}{P_2}\right)V_{f1} + \frac{\sigma_a}{E_c}\left(1 - \frac{2\nu_c{}^2}{1-\nu_c}\right) \tag{2.9}$$

Invoking Eq. 2.4 in Eq. 2.9, it simplifies to:

$$\varepsilon_t = \left(1 - \frac{1}{1+\frac{\sigma_a}{P_1}}\right)V_{f1} + \frac{\sigma_a}{E_c}\left(1 - \frac{2\nu_c{}^2}{1-\nu_c}\right) \tag{2.10}$$

As noted in the above equation, the limiting strain is V_{f1} (volume fraction of the filler). The reference pressure P_1 is assumed as 1 atm or 0.1 MPa. The material properties used in the calculation are:

Elastomer:

E_m = 1.42 MPa (206 psi)

ν_e = 0.48 to 0.5; V_{f1} = 0, 0.34, 0.51 and 0.63 corresponding to 0,10, 20, and 30 % weight fraction of Pμb.

Phenolic microballoons (Pμb):

Wall: E_f = 3 GPa (400 ksi)

ν_w = 0.3

The stress (σ_a) and strain (ε_a) curves are shown in Figure 2.5 for the filler volume fraction of 0, 0.34, 0.51 and 0.63 corresponding to filler weight fraction of 0%, 10%, 20% and 30%. If the ν_e is different from 0.5, then for a small variation of ν_e that is for ν_e=0.4995 and 0.499 the results are shown in Figure 2.5, 2.6a and 2.6b, respectively.

Figure 2.7 comparison of results from Eq. 2.10 (including wall material deformation and Eq. 2.5 not including) is shown in Figure 2.7 (ν_e of 0.5). The effect of Pμb wall deformation is small compared to the total deformation and it can be neglected.

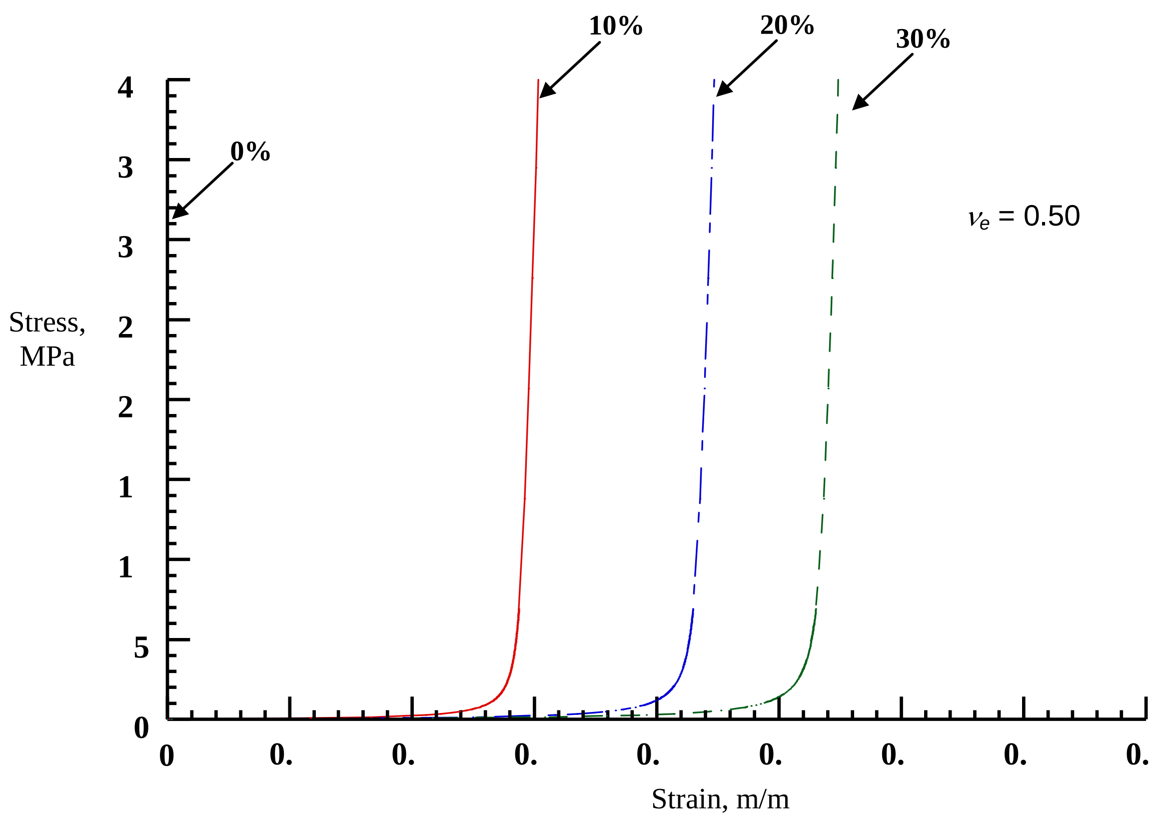

Figure 2.5 Axial Stress versus Strain for ν_e = 0.5 (Eq. 2.10)

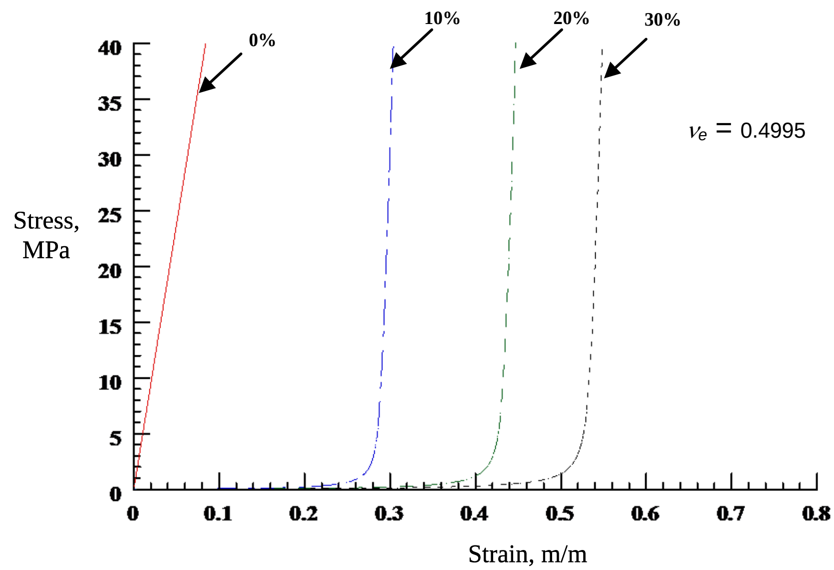

(a)

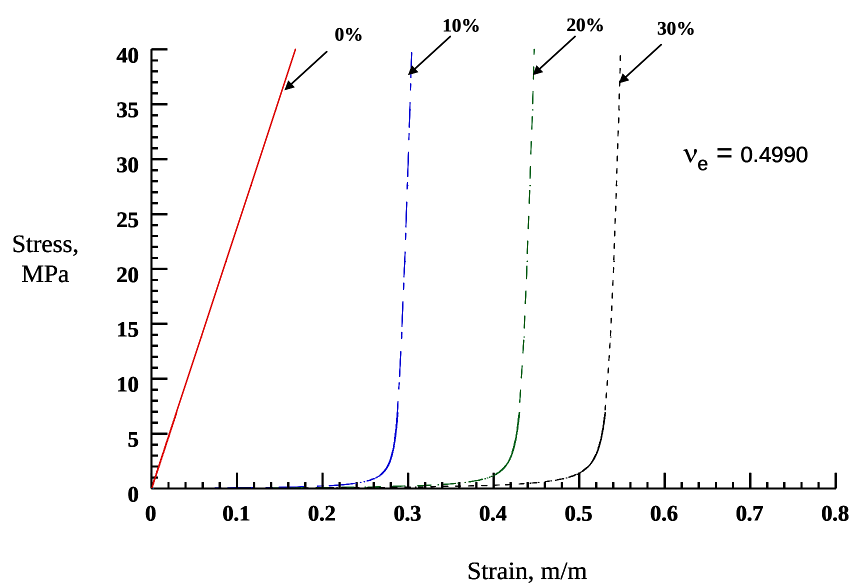

(b)

Figure 2.6. Axial stress vs. strain for (a) ν_e = 0.4995 and (b) ν_e = 0.4990

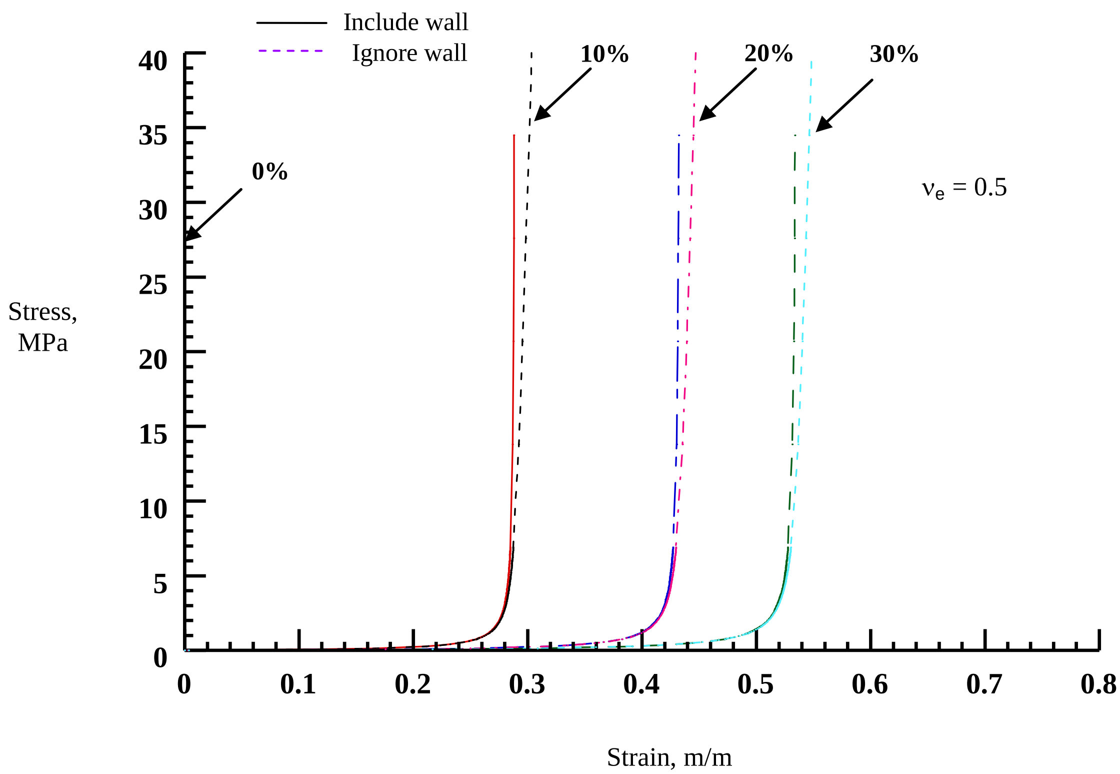

Figure 2.7 Comparison of axial stress vs. strain based on Eqs. 2.5 & 2.10 for (ν_e = 0.5)

2.4 Summary

A simple relation between axial stress and axial strain was derived for a confined compression test based on the gas laws and realistic assumptions. The equation is given by $\varepsilon_a = \left(\frac{1}{1+\sigma_a/P_1}\right)V_f$, where ε_a and σ_a are the applied axial strain and calculated axial strains, respectively. The equation's limiting strain is V_{fl} (volume fraction of the fluid in the filler). The equation extended to include the elastic deformation of the elastomer and the microballoon wall materials and found this has only a marginal improvement. The slope of the axial stress and strain curve gives the bulk modulus. The bulk modulus and the limiting strain are dependent on the percent weight or volume of the Pμb.

CHAPTER 3

MATERIALS SELECTION, PROCESSING AND PHYSICAL CHARACTERIZATION

3.1 Introduction

This chapter describes the materials, their selection, processing, and physical and morphological characterization of the variable bulk modulus composite. The specific objectives of this chapter are:

1. To select elastomeric elastomer matrix, curing agent and microballoon filler.
2. To compound the elastomer matrix with curing agent, and various percent weight Pμb filler.
3. To determine physical properties including density and volume fraction of test specimens.
4. To determine the morphology of the syntactic foam.

3.2 Material Selection

3.2.1 Polysulfides (Matrix Material)

Polysulfides are a class of elastomers comprising alternating chains of sulfur atoms and hydrocarbons. The general formula is $–[(CH_2)_m\text{-}S_x]_n–$, where “x” indicates the number of sulfur atoms, “m” and “n” the number of repeating units [29].

Thiokol Corporation introduced liquid polysulfide polymers in 1943 [30]. They are available in molecular weights ranging from 1,000 to 8,000 and with different weight percent of cross linking agent (0 and 2%). The higher cross linking amount increases the modulus and hardness of the cured elastomeric foam.

Polysulfides are widely used in various applications because of their rapid curing at room temperature, good adhesion to most surfaces, toughness, and chemical resistance to most dilute acids, alkalis, and solvents. They can be easily compounded into sealants, adhesives, coatings, potting compounds, and flexible molding compositions. Polysulfide compounds are used in residential and commercial building construction, insulating glass, aerospace, electronic, aviation, and marine applications. Because of these wide applications, polysulfide has been selected as the right matrix material to develop a variable bulk modulus flexible elastomeric foam.

Five polysulfide materials were evaluated to select the best matrix material: Polysulfide elastomer LP2, Polysulfide elastomer LP980, Polysulfide epoxy TP48, Polysulfide elastomer CS3100 and Polysulfide elastomer PRC1422A. The following Table 3.1 summarizes the important properties, such as physical form, viscosity, molecular weight, moisture content, mercapatan content and cross linking agent percentages, density, compatible base fillers and curing agent of these five different polysulfides. The material properties and technical data are taken from references [31] through [33]. They have been carefully evaluated for process ability to develop the variable bulk modulus elastomeric foam specimens.

Table 3.1 Polysulfide elastomers characteristics

Properties	Polysulfide Rubber LP2	Polysulfide Rubber LP980	Polysulfide Epoxy TP48	Polysulfide Rubber CS3100	Polysulfide Rubber PRC1422A
Physical form	liquid	liquid	liquid	liquid	liquid
Viscosity, pa.s	41-48	10- 12.5	12-16'	55	25
Average molecular wt.	4000	2500	NA	NA	NA
Mositure content, %	0.15 – 0.25	0.15 – 0.25	NA	NA	NA
Mercaptan content,%	1.5 – 2.0	2.5 – 3.5	NA	NA	NA
Crosslinking agent, %	2	0.5	NA	NA	NA
Density, g/cc	1.29	1.25	1.25	1.25	1.45
Base fillers	None	None	Unknown	Unknown	$CaCO_3$
Curing agent	Grain MnO_2	Grain MnO_2	Liquid	Liquid	Liquid

The polysulfide polymers considered were assessed to choose a suitable elastomeric system that would vary the elongation and modulus of the compound. Toray Fine Chemicals Co., Ltd. supplied the liquid polysulfide LP2 & LP980. They were made of bis(ethelenoxy)methane containing disulfide linkages. The ether linkages in the polymer provided mobility and flexibility whereas disulfide and high sulfur content along with its chemical saturation provided the polymer an excellent fuel resistance. The user could vary the elongation and modulus of the specimen by varying the amount of tri-functional organic halide, which was co-reacting to obtain varying amounts of crosslink sites. Although they became the high-performance sealants used in building construction, these elastomeric sealants have found applications in large-scale projects, such as fuel tanks, aircraft, insulating glass, canal and marine sealants around the world. A major advantage is that the base chemical has no fillers and the disadvantage is that there is the need for complex equipments for processing, such as sigma blade mixers, kneader-extruders, high-speed disperators, transferring and packing of compound requires heavy-duty processing pumps.

The polysulfide epoxy TP48 supplied by Transpo Industries [31] was made of a two-component (2 resin:1 hardener) epoxy based blended sealer and an aggregate system. This specially made system could penetrate deep into cracks and provide bonding to the inner walls of the crack. This seal prevents the ingress of moisture and salts into the substrate while providing skid resistant surface. This seal adds one third to one half pound of dead load per square foot of deck area. A major disadvantage is that the base chemical has unknown fillers, the chemical formulae and physical properties are not available, and the material adds additional dead weight.

The Polysulfide elastomer CS3100 was supplied by Chem Seal Products [32] and consisted a two-component (100 base:10 curing agent) elastomer which was applied within 1-3 hours time to seal or pott the electrical connectors and components for protection from moisture, fuels, dirt and other contaminants. Major advantages are that the material is widely used for potting and sealing electrical components and adheres to most commonly used surfaces. Major disadvantages are that the base chemical has unknown fillers and the chemical formulae and physical properties are not available.

The Polysulfide elastomer PRC-1422 class A was supplied by PRC-DeSoto International [33] and consist of two-part (part A 10:part B100), dichromate cured polysulfide compound for fuel tank sealant. It has an excellent adhesion capability to common aircraft substrates having tensile strength of 350 psi, elongation of 250 percent and flexible - no cracks after bending 180 degrees over 0.125 inch. Major disadvantages are that the base chemical has known fillers (calcium carbonate) which are brittle compared to hollow microballoons and the physical properties are not available.

After evaluating these five polysulfide material system, study concluded that polysulfide epoxy TP48, polysulfide elastomer CS3100 have unknown fillers in the base chemical which is a disadvantage for the development of the variable bulk modulus composite foam. Therefore, the polysulfide elastomer LP2 was selected as the matrix material for the expanded study.

3.2.2 Curing Agent

Manganese Dioxide (MnO_2) is a very widely used curing agent for liquid polysulfide elastomer in industrial applications because of no toxicity, better pot life stability and being able to be pre-mixed with fillers. Therefore, MnO_2 was chosen as the curing agent for the LP2 polysulfide elastomers. Figure 3.1 shows a shear modulus versus cure time for a typical polysulfide for catalyzed and uncatalyzed with MnO_2 in adhesives and sealants.

The reaction of liquid polysulfide elastomer with manganese dioxide converts mercapatan (-SH) groups to disulfide (-S-S) bonds [34] as shown below. This results in a high molecular weight polymer with elastomeric properties.

$$2RSH + MnO_2 \longrightarrow RSSR + MnO + H_2O$$
$$2RSH + MnO \longrightarrow RSMnRS + H_2O$$
$$RSMnSR + MnO_2 \longrightarrow RSSR + 2MnO$$

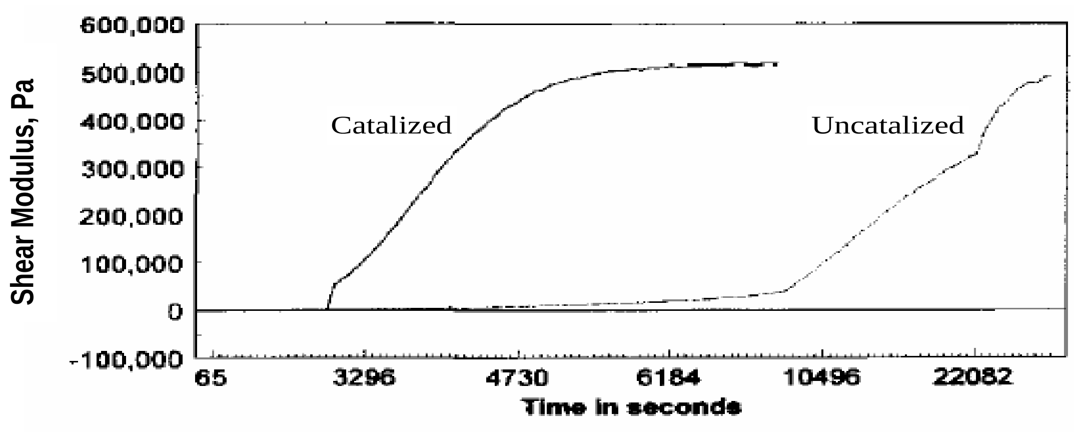

Figure 3.1 Shear modulus against time for cure of polysulfide with MnO_2

Properties of MnO_2 are:

- Chemical formula MnO_2
- Physical Form Blackish brown solid
- Molar mass 87 g/mol
- Density 5.02 g/cc
- Melting point 535 ^{o} C
- Solubility in water Insoluble

The reaction of liquid polysulfide elastomer with manganese dioxide converts mercapatan (-SH) groups to disulfide (-S-S) bonds [34] as shown below. This results in a high molecular weight polymer with elastomeric properties. The curing reaction is shown here:

$$2RSH + MnO_2 \longrightarrow RSSR + MnO + H_2O$$
$$2RSH + MnO \longrightarrow RSMnRS + H_2O$$
$$RSMnSR + MnO_2 \longrightarrow RSSR + 2MnO$$

3.2.3 Phenolic Microballoon

Phenolic microballoon BJO-093 supplied by Asia specific company [35] was selected as the filler material and designated as "Pμb" in this dissertation. Figure 3.2 shows the chemical structure and networkings of a microballoon made out of phenol-formaldehyde that has a 3-D network from tri-functional polymers [36]. This microstructure property enables interfacial adhesion between Pμb and the polysulfide base leading to a material that is chemically stable and stiffer.

Figure 3.3 shows the size and morphology of the BJO-093 Pμb as-received from the supplier. These microballoons can withstand several cycles of loading/unloading without breaking (up to 4.2 MPa). The deformation of the microballoon under hydrostatic compression loading is shown in Figure 3.4 [37]. The microballoons completely collapse at 6.9 MPa pressure and expand back upon release of pressure. Figure 3.5a illustrates the compression test on a single microballoon. The microballoon is compressed to a certain displacement and the load is released. Figure 3.5b shows the load vs. displacement response of different types of Pμbs: as received and cured Pμb, glass and carbon (brittle) Pμbs during the test. Careful examination of load vs. displacement indicates that as-received Pμb does not break but deform to 45 μm under load 60 mN (milli Newton) where as cured Pμb breaks at about 20 μm deformation under 8 mN load. Glass microballoon and carbon microballoon are brittle and break under 30 mN and 15 mN, respectively. This data suggests that as-received Pμb is better choice for making the variable bulk modulus composite.

Table 3.2 compares the physical properties of different types of Pμb supplied by various companies as well as two types of glass microballoons. Based on the combination of low density and high hydrostatic strength, BJO-093 Pμb fillers are chosen for the present research.

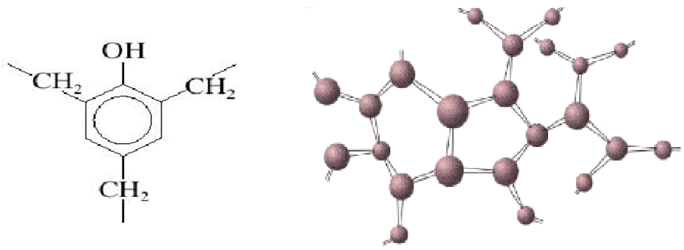

Figure 3.2. Chemical structure of Pμb

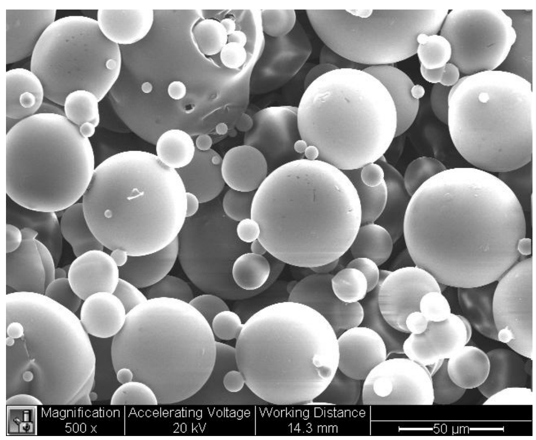

Figure 3.3 Morphology of as-received Pμb

Figure 3.4 Deformation of microballoon under hydrostatic stress

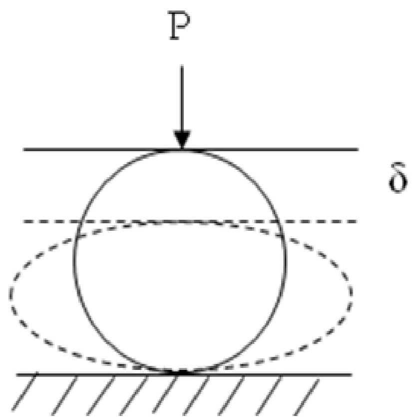

(a)

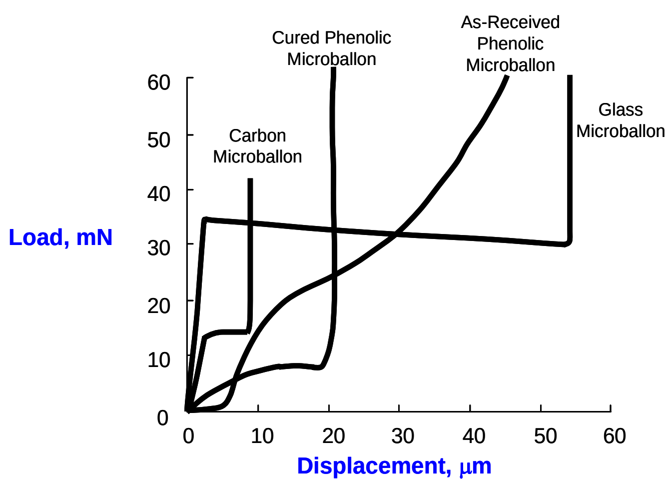

(b)

Figure 3.5 (a) Compression test on a single microballoon and (b) typical compressive load vs. displacement response

Table 3.2 includes the BJO-093 Pμb as-received type, which will not break till 4.2 MPa loading compare to flexible thermoplastic expancel and the other two brittle glass microballoons considered for evaluation in this research.

Table 3.2 Physical properties of different microballoons

Type of Microballoon	True Density (g/cc)	Hydrostatic Compressive Strength (MPa)	Mean Diameter (μm)	Ave. Wall Thickness (μm)	Thickness-to-radius ratio	Supplier
BJO-093 Phenolic	0.25	3.44	71.5	1.84	0.052	Asia specific*
DE40d42 Expancel	0.02-0.05	0.6	36 to 49	0.1 to 0.2	0.02 to 0.04	Expancel, Inc.
K15 3M Glass	0.15	2.07	70	0.7	0.02	3M
K46 3M Glass	0.46	41.37	43.6	1.37	0.063	3M

* www.phenoset.com

In conclusion, liquid polysulfide elastomer LP-2, hollow Pμb (BJO-093) having covalent and secondary bonding and a manganese dioxide curing agent are chosen to prepare the variable bulk modulus elastomeric foam composite for the study. The next section focuses on material processing, and molding of specimen.

3.3 Material Processing and Specimen Preparation

3.3.1 Compounding Process

The compounding process and specimen preparation for this study involved the dispersion of microballoon fillers and curing agent, manganese dioxide in liquid polysulfide elastomer resin. The required amount of liquid polysulfide elastomer base chemical 100 parts by weight, manganese dioxide curing agent 7.5 parts by weight and Pμbs of 0%, 10%, 20% and 30% by weight was measured. Although typical equipment includes sigma blade mixers, kneader-extruders, high-speed disperators, transferring and packing of compound requires heavy-duty processing pumps this study used manual mixing method in a beaker or on flat steel plate with the help of hand tools (flat or round) and squeegees (plastic/steel blades). Figure 3.6a shows the accurately measured amount of microballoons, curing agent and base resin. Figure 3.6b shows mixing of the three compositions in steel pan using plastic tool and flexible steel tools, Figure 3.6c shows homogeneous mixture spreader on a steel plate. The stiffness of the composites increases with 30% weight by Pμb–matrix interactions either due to particle clustering or a network of filler interactions. This is where the continual and constant mixing, spreading, squeezing to disperse the microballoon evenly and achieve near zero voids.

(a)

(b)

(c)

Figure 3.6 Compounds (a) measured, (b) mixed, and (c) homogeneous elastomer

3.3.2 Molding Process

After making the homogeneous mixture, the mixture was transferred to a mold and cured in to form the test specimen of different configurations. Two types of specimen were made; cylindrical specimen for confined compression and high strain rate tests and flat rectangular specimen for tension test. The test specimen configurations are shown in Figure 3.7.

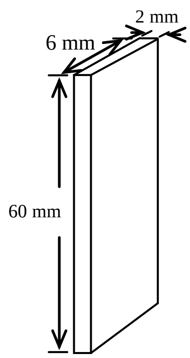

(a)

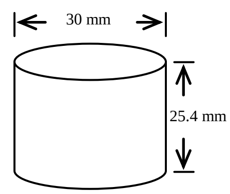

(b)

Figure 3.7 (a) Tension and (b) Compression test specimen configuration

3.3.2.1 Molding Cylindrical Specimen

First, top surface of the bottom flat plate, inside surface of the cylindrical mold, and bottom surface of the top flat plate were coated with mold release wax (TREWAX). Secondly, a pile of freshly prepared homogeneous composite mixture on top surface of the bottom flat plate was made. Thirdly, the cylindrical mold was forced over the mixture on to the flat plate so that the composite completely filled the mold from the bottom-up with nearly no air entrapments.

Additional squeezing and forcing the mixture into the mold was essential to fill the cavity completely. This manual filling and forcing methodology using simple hand tools was crucial to make the homogeneous identical syntactic foam composite specimens. Finally, place a steel flat plate (90-130 N weight) was placed over the overly filled compression-mold assembly as shown in Figure 3.8.

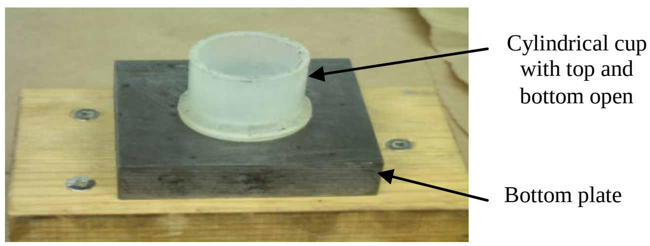

(a)

(b)

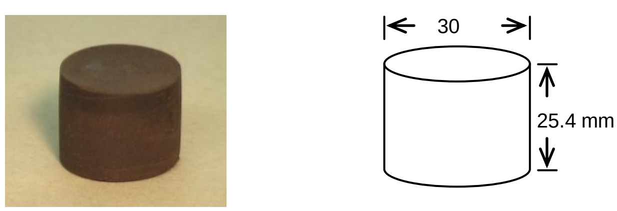

(c)

Figure 3.8 (a) Round mold, (b) Closed mold assembly, and (c) Specimen configuration

Then, the top steel plate was tapped for about 3 minutes using a 12-20 N weight plastic hammer to fill the cavity and to drive-out voids. The whole assembly was left to cure for 24 hours at room temperature. The viscoelastic behavior of the syntactic foam, where the material slowly moved around and filled the cavity completely, reduced the void content. After curing for 24 hours, the cylindrical specimens were demolded, measured, weighed, and identified by a number. The specimen is about 30 mm in diameter and about 25.4 mm in height.

3.3.2.2 Molding Rectangular Flat Specimen

Similar molding process described in the previous section was followed here to make the rectangular specimen by using the mold plate shown in Figure 3.9a. A pile of freshly prepared homogeneous composite mixture was spread on top surface of the bottom flat plate. Then the flat rectangular steel mold was forced over the mixture on to the flat plate so that the composite completely filled the mold from the bottom-up with nearly no air entrapments. Additional squeezing and forcing the mixture into the mold was essential to fill the cavity completely. Then a flat plate (about 90-130 N) was placed on the mold and the top plate was tapped with 12-20N plastic hammer for about 3 minutes. Then the whole assembly was left for 24 hours for curing and readjustment of mold filling. The specimen was removed from the mold. The specimen is 60 mm x 6 mm x 2 mm and is shown in Figure 3.9c.

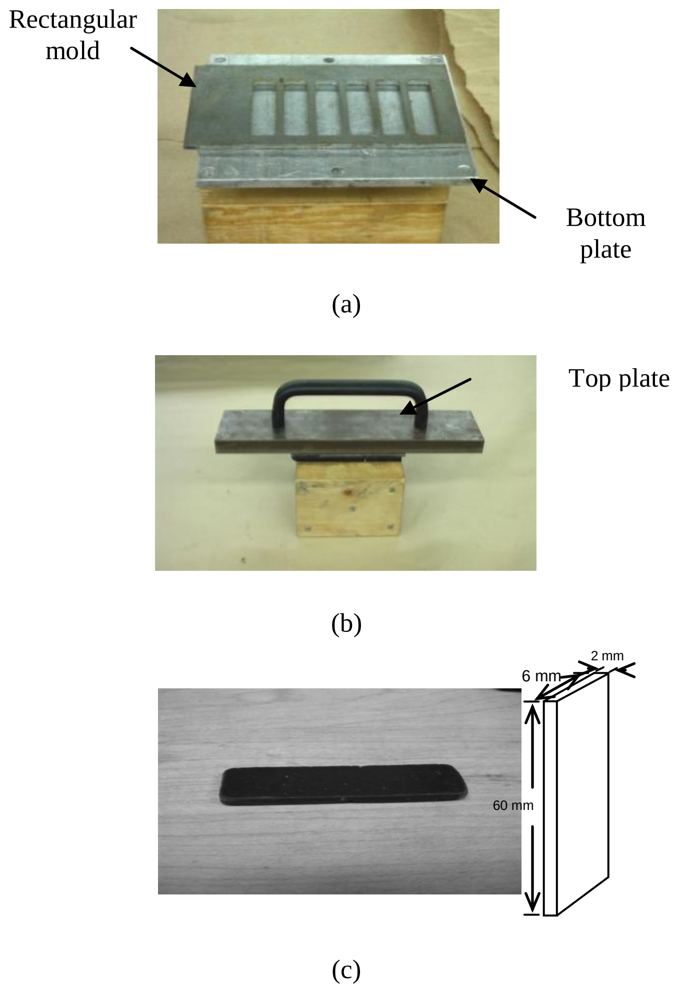

Figure 3.9 (a) Flat mold, (b) Molding assembly, and (c) Specimen configuration

3.4 Physical Properties of the Material

3.4.1 Volume Fraction of Pµbs

The analysis is performed based on the weights of constituents added to the composite and their true densities provided by the supplier to calculate density, volume fraction, and void content. Furthermore, the compound was processed well so that it was almost free from voids. The composite was made of matrix polysulfide, catalyst MnO_2

and Pμbs. Their respective weights were W_m, W_{Mn} and $W_{\mu b}$. The values of densities were ρ_m=1.29 g/cc, ρ_{Mn}=5.02 g/cc and $\rho_{\mu b}$=0.25 g/cc. The volumes of the constituents were determined by the ratio of weight to their respective densities. Note that the specific gravity and density terms were used interchangeably by ignoring the gravitational effect.

Therefore, the volume of Matrix = $\frac{W_m}{\rho_m}$, Catalyst = $\frac{W_{Mn}}{\rho_{Mm}}$, and the $P_{\mu b}$=$\frac{W_{\mu b}}{\rho_{\mu b}}$. The volume fraction of Pμb ($V_{\mu b}$) is the ratio of volume of Pμb and the total volume. Therefore:

$$V_{\mu B} = \frac{\frac{W_{\mu b}}{\rho_{\mu b}}}{\frac{W_m}{\rho_m} + \frac{W_{Mn}}{\rho_{Mn}} + \frac{W_{\mu b}}{\rho_{\mu b}}} \tag{3.1}$$

For example, the 20% weight fraction of Pμb composite contains 100g of matrix, 7.5g of MnO_2 and 20g of Pμb. Substituting these values and the respective densities in Eq. 3.1 results in the volume fraction of Pμb, Vμb=0.503. Similarly, volume fraction of matrix (V_m=0.488) and the catalyst (V_{Mn}=0.009) can be computed. The calculated volume fractions of Pμb for 10, 20, and 30% weight fraction of Pμbs were 33.6, 50.3 and 60.3%, respectively. The values are rounded to a whole number in the Table 3.3.

Table 3.3 Summary of specimen volume, weight, density and volume fraction of Pμb and voids

Material	Specimen No.	Diameter (cm)	Height (cm)	Volume (cc)	Weight (g)	Density (g/cc)	Volume Fraction (%)	
							Pμb	Void
Base	LP2-1	1.280	0.457	0.588	0.75	1.28	0.0	6
	LP2-2	1.302	0.382	0.509	0.67	1.32		3
	LP2-3	1.265	0.287	0.361	0.48	1.32		3
	LP2-4	1.231	0.451	0.537	0.72	1.34		2
10% Pμb	LP2_10MB-1	1.283	0.366	0.473	0.43	0.91	34	10
	LP2_10MB-2	1.285	0.339	0.440	0.39	0.89		12
	LP2_10MB-3	1.289	0.344	0.449	0.41	0.91		10
	LP2_10MB-4	1.282	0.357	0.461	0.42	0.91		10
20% Pμb	LP2_20MB-1	1.290	0.349	0.456	0.34	0.75	50	6
	LP2_20MB-2	1.289	0.347	0.453	0.35	0.77		4
	LP2_20MB-3	1.276	0.335	0.428	0.34	0.79		2
	LP2_20MB-4	1.276	0.337	0.431	0.34	0.79		2
30% Pμb	LP2_30MB-1	1.286	0.377	0.490	0.31	0.63	60	9
	LP2_30MB-2	1.283	0.391	0.505	0.34	0.67		3
	LP2_30MB-3	1.285	0.397	0.515	0.35	0.68		2
	LP2_30MB-4	1.270	0.396	0.502	0.34	0.68		2

3.4.2 Computation of Void Fraction

The approach used here was similar to the computation of volume fraction of Pμb. The measured density of the samples was used to reduce the volume fraction of voids.

The volume fractions of three constituents were derived from the weight fractions in the composite. Since the voids did not contribute to weight, it was the difference between composite volume and the total volume of the constituents. If W_m, W_{Mn} and $W_{\mu b}$ represent the weights of the three constituents in the composite then the total volume of the constituents is:

$$V_1 = \frac{W_m}{\rho_m} + \frac{W_{Mn}}{\rho_{Mn}} + \frac{W_{\mu b}}{\rho_{\mu b}} \tag{3.2}$$

If this volume is normalized to weight of the specimen (W_c), then the volume of the solid constituents (V_2) is:

$$V_2 = \left(\frac{W_m}{\rho_m} + \frac{W_{Mn}}{\rho_{Mn}} + \frac{W_{\mu b}}{\rho_{\mu b}}\right)\frac{W_c}{\left(W_m + W_{Mn} + W_{\mu b}\right)} \tag{3.3}$$

The volume of the voids is the difference between the volume of the composite and the volume of the solid constituents (V_2). Normalizing the volumes by the total volume of the composite specimen (V_c) results in the void fraction (V_0):

$$V_0 = 1 - \left(\frac{W_m}{\rho_m} + \frac{W_{Mn}}{\rho_{Mn}} + \frac{W_{\mu b}}{\rho_{\mu b}}\right)\frac{\rho_c}{\left(W_m + W_{Mn} + W_{\mu b}\right)} \tag{3.4}$$

Table 3.3 lists composite (ρ), (V) of Pμb and voids of each sample. The void content is highest for the 10% Pμb composite, which is 10-20%. Except for sample #1 of base, 20%, and 30% Pμb specimens the void content was reasonably low (2 to 3%).

3.5 Morphology of Material

The morphology of confined compression tested specimen was studied using a Scanning Electron Microscopy (SEM). A specimen of 5x5x5 mm was sliced from the tested cylindrical specimen. The sliced specimen was broken into two-halves. One of the pieces was chosen for the SEM study. The broken surface was coated with gold using a sputter coater to increase conductivity, electrically grounded to prevent electrostatic charge at the surface. This non-conductive specimen tended to charge, especially in secondary electron imaging mode. Coated samples were analyzed in SEM. Figure 3.10 shows the steps of specimen preparation for SEM imaging.

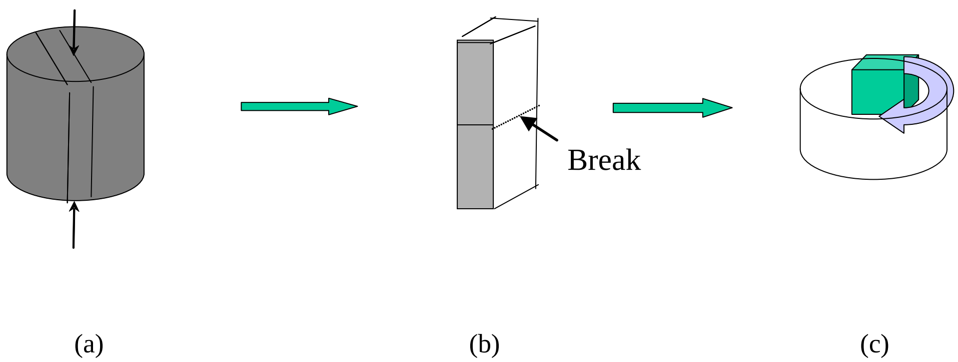

Figure 3.10 (a) Specimen, (b) Specimen slice, and (c) Mounted on test button

This specimen-mounted holder was placed in the SEM apparatus as shown in Figure 3.11 and specimen images were scanned. Figure 3.12 summarizes the SEM images of 0%, 10%, 20% and 30% weight Pμb content specimens. The images show some voids and dispersed Pμbs. Dispersing of Pμbs was good in all cases except 10%, where the void content was higher.

Figure 3.11 Scanning electron microscopy for morphology characterization

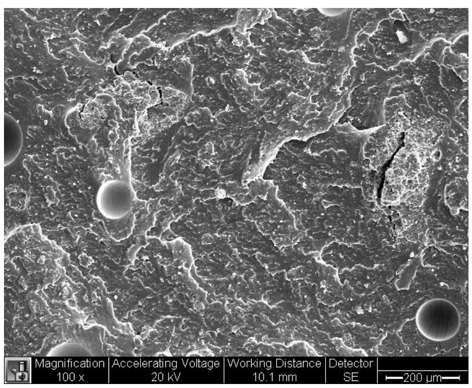

(a)

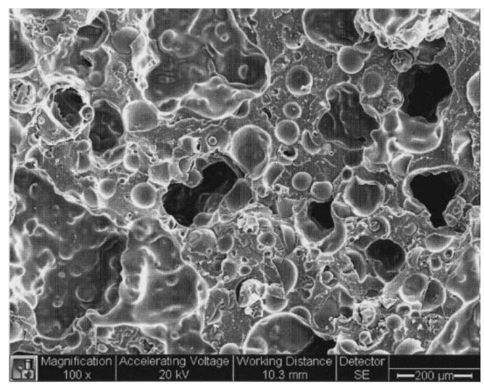

(b)

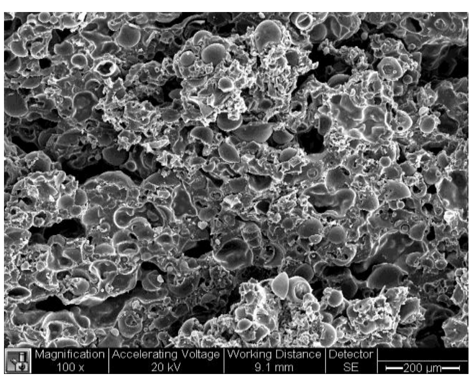

(c)

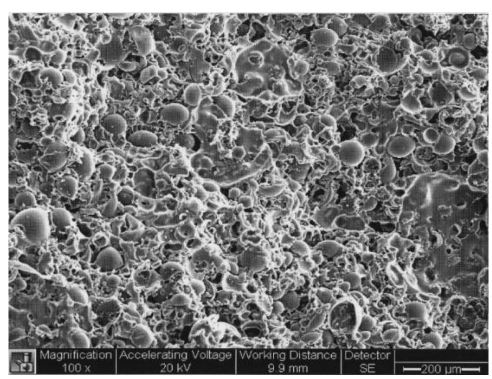

(d)

Figure 3.12 Morphology of specimen (a) Base, (b) 10% Pμbs, (c) 20% Pμbs, and (d) 30% Pμbs

3.6 Summary

Five different elastomers and four different microballoon materials were evaluated for their physical properties and compositions. Selected liquid polysulfide elastomer LP-2, uncured hollow Pμb (BJO-093), and a solid manganese dioxide curing agent were used to prepare the flexible syntactic foam. Weight percentages of Pμb chosen were 0, 10, 20, and 30% that worked out to be 0, 34, 50, and 60% volume percentages. The composite had void that varied from 2 to 12% of the composite volume. Both confined compression and tension test specimens were prepared for testing. The morphology of the specimens was examined using Scanning Electron Microscopy and it was found that microballoons were distributed uniformly.

CHAPTER 4

STATIC CHARACTERIZATION

4.1 Introduction

This chapter describes the tensile and confined compression tests and results of Pμb filled LP2 polysulfide syntactic foam. The tensile modulus, bulk modulus and compressibility of the composite are determined from the test results. Morphology of the specimen before and after loading is assessed by Scanning Electron Microscopy (SEM). The change in moduli with filler content is examined. The test matrix used for the two tests is listed in Table 4.1.

Table 4.1 Tension and Confined Compression Test Matrix.

Test case	Type of Testing	
	Tension	Confined Compression
Baseline	√	√
5 wt.% Pμb	-----	√
10 wt.% Pμb	√	√
15 wt.% Pμb	-----	√
20 wt.% Pμb	√	√
25 wt.% Pμb	-----	√
30 wt.% Pμb	-----	√

4.2 Tensile Test

A tensile test was conducted using Instron 5542 electro-mechanical testing systems shown in Figure 4.1. It is a screw-driven crosshead that can apply tension or compression loading. The test machine had a load capacity of 5kN, cross head speed ranged from 0.05 to 550 mm/minute. Cross head speed for the tensile test was set to 50 mm per minute. Rectangular strip specimens (rubbery) were carefully gripped using mechanically actuated wedge grips.

Figure 4.1 Instron 5542 electro-mechanical testing system

4.2.1 Test Specimen and Testing

A rectangular specimen of 60 mm long, 12 mm wide and 2 mm thick was chosen for the tension test per ASTM D412. The specimen configuration is shown in Figure 4.2. The geometry is more sensitive to loading and positioning of the sample than the tabbed specimens. Any damage to the edges of the sample causes inaccuracies in the measurements.

The specimen was aligned in the load frame such that there was no twisting in the specimen. Tension tests were conducted on LP2 specimens with 0, 10, and 20 % weight of Pμb (see Table 4.1). Five specimens were tested for base LP2 and each for Pμb filled samples. Table 4.2 summarizes the geometry of all specimens tested. During the test, load and displacements were recorded. Corresponding stresses and strains were calculated and plotted to determine the elastic modulus. Table 4.2 summarizes the modulus of each specimen including the average and the standard deviation.

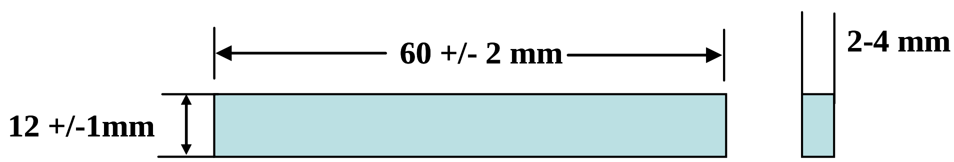

Figure 4.2 Instron tension test specimen configuration

Table 4.2 Pμb filled LP2 tensile test specimen geometry and tensile modulus

Material	Specimen No.	Length (mm)	Thickness (mm)	Width (mm)	Modulus (MPa)
LP2/0% Pμb	1	18.0	3.6	13.2	1.2
	2	18.0	3.1	15.0	1.3
	4	18.0	3.0	15.0	1.6
	5	18.0	3.2	15.0	1.6
	6	18.0	3.2	14.5	1.4
	Average	**18.0**	**3.2**	**14.5**	**1.4**
	STD	**0.0**	**0.2**	**0.8**	**0.2**
LP2/10% Pμb	1	18.0	4.2	12.0	3.7
	2	18.0	4.3	13.0	3.6
	4	18.0	4.5	13.2	3.8
	Average	**18.0**	**4.3**	**12.7**	**3.7**
	STD	**0.0**	**0.2**	**0.6**	**0.1**
LP2/20% Pμb	1	18.0	4.2	13.0	8.4
	2	18.0	3.2	13.0	12.4
	3	18.0	4.5	13.0	8.9
	Average	**18.0**	**4.0**	**13.0**	**9.9**
	STD	**0.0**	**0.6**	**0.0**	**1.8**

4.2.2 Test Results and Discussion

Figures 4.3 and 4.4 show the stress versus strain responses of typical 0% and 10% Pμb weight content of LP2 specimens, respectively. The material behavior was initially linear and then became nonlinear elastic. The initial slope of the stress-strain curve was used for the tensile modulus. Moduli of all specimens are listed in Table 4.2. The measured tensile moduli of 0%, 10% and 20% Pμb content LP2 specimens are 1.4 MPa, 3.7 MPa and 9.9 MPa, respectively. The average modulus increased with the percentage of Pμb. This initial stiffening behavior of the material was attributed to loss of ductility of the material by the addition of microballoons. Note also that the fracture strain decreased (see Figures 4.3 and 4.4) with increased percent of Pμb. This was again due to loss of ductility in the material.

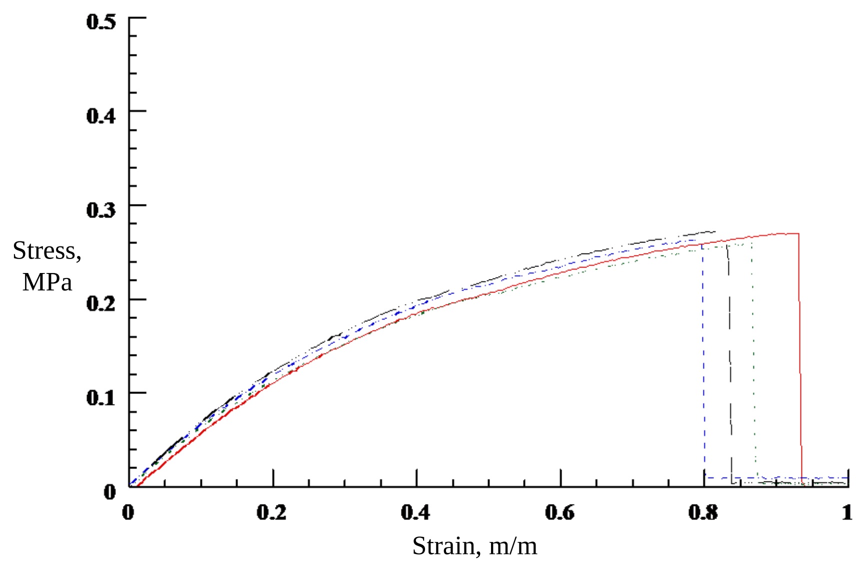

Figure 4.3 Tensile test plots for polysulfide LP2 neat resin (base) specimens

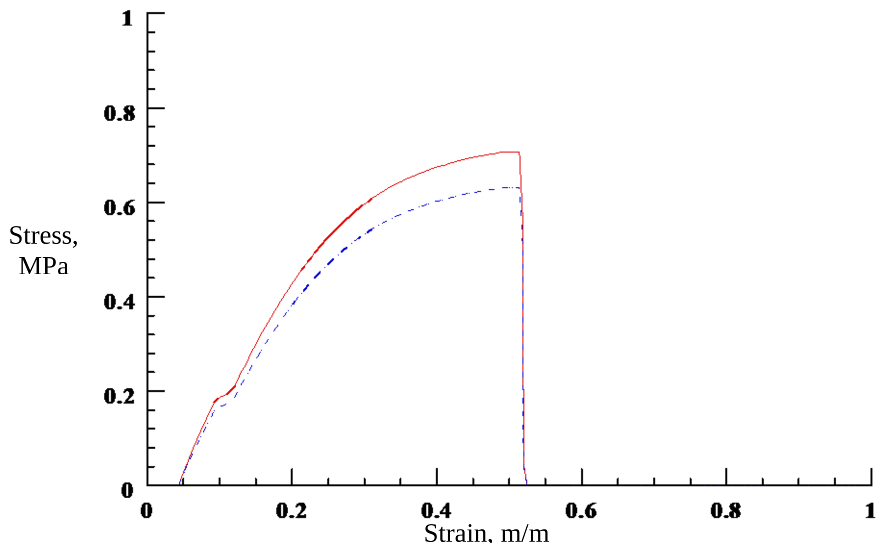

Figure 4.4 Tensile test plots for 10% wt. Pμb filled LP2 tensile specimens

A plot of tensile modulus versus percent weight Pμb content is shown in Figure 4.5. The data can be approximated by a linear relation between tensile modulus and percent weight Pμb. This relationship is given by:

$$E = 0.75 + 0.43w_f \tag{4.1}$$

where E is the tensile modulus and w_f is the weight percent of the Pμb. The significant modulus increase with the weight percentage increase of Pμb is observed. This is due to the stiffening effect by the addition of microballoon filler, which reduces the ductility of the elastomer. Note also that the increase in modulus is almost three times from 10% weight of Pμb and seven times from 20% weight of Pμb as shown in Figure 4.5.

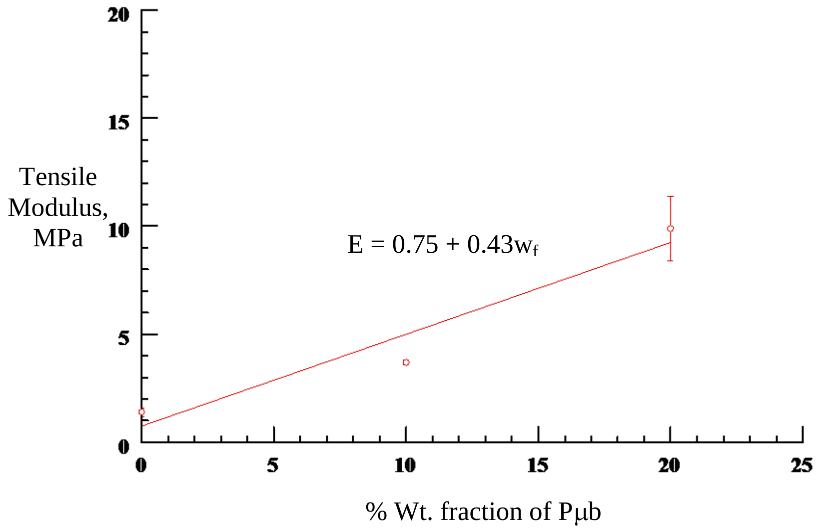

Figure 4.5 Variation of tensile modulus with Pμb content for LP2 specimens

Halpin and Tsai [40] have derived a semi-empirical equation for elastic modulus for elastic modulus for elliptical fillers distributed randomly. That equation is given by:

$$E_c = \left(\frac{1+\xi\eta V_f}{1-\xi\eta V_f}\right)E_m \tag{4.2}$$

where E_c is the modulus of the composite, E_m is the modulus of the matrix (elastomer), ξ is the shape factor (2, for spherical fillers). V_f is the volume fraction of the filler. Results of Halpin –Tsai equation is represented by the solid line in the Figure 4.6.

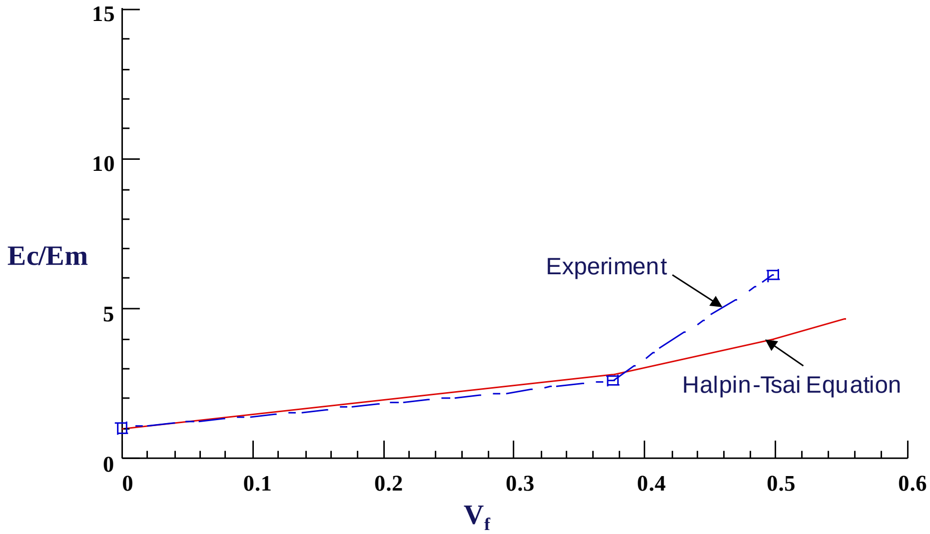

Figure 4.6 Comparison of Halpin-Tsai semi-empirical equation with experimental data

4.3 Confined Compression Test

The confined compression test was conducted in a hardened steel tube using a smooth fit specimen. The load was applied by a steel plunger and the axial deformation is measured. The axial stress and strain represented the hydrostatic stress and volumetric

The axial stress and strain represented the hydrostatic stress and volumetric strain. Slope of stress versus strain curve gave the bulk modulus. Tests were conducted on base and Pμb filled LP2 elastomers.

4.3.1 Test Specimen and Fixture

The test specimen was 25.4 mm (1 inch) thick and about 30.1 mm (1.185 inch) in diameter and is shown in Figure 4.7a. The dimensions and the material of confined compression test fixture are shown in Figure 4.7b. The machined steel sleeve having an inner diameter of 30.2 mm, outer diameter of 50.8 mm and a length of 88.9 mm.

The compression load was applied using a steel plunger of outer diameter of 29.5 and length of 114.3 mm. The dimensional tolerance for all parts was ± 0.127 mm. The specimen was compressed between the top and bottom plungers of outer diameter of 30.2 mm (having smooth fit with sleeve) and their thickness of 12.5 mm. The base plate had a recess of depth 6.4 mm and diameter 51 mm to hold the steel sleeve in place. Three specimens each of 0%, 5%, 10%, 15%, 20%, 25% and 30% weight Pμb composite samples were tested. Table 4.3 lists test specimen geometries and the calculated density of the composite. Test fixture as shown in Figure 4.7 is a simpler version of apparatus as referenced in [6-9].

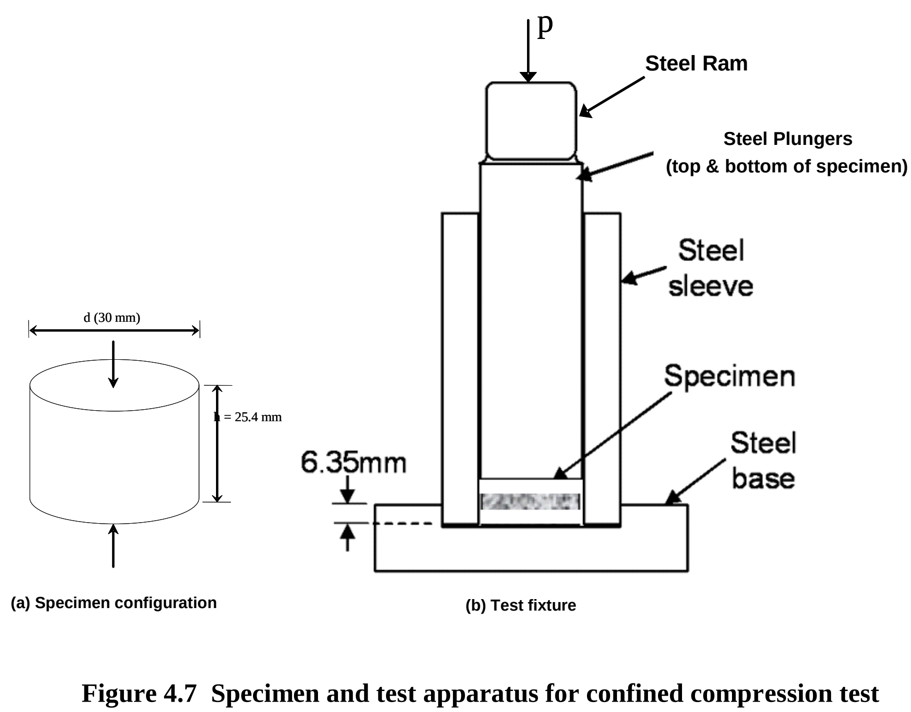

Figure 4.7 Specimen and test apparatus for confined compression test

Table 4.3 Confined compression test specimen geometries

Material	Specimen no.	Diameter (cm)	Height (cm)	Volume (cc)	Weight (g)	Density (g/cc)
Base Polysulfide (Rubber Based)	LP2-1	2.94	2.06	14.0	18.6	1.33
	LP2-2	2.96	2.58	17.8	23.3	1.31
	LP2-3	3.00	2.49	17.6	25.8	1.47
	Average (STD)					**1.37 (0.09)**
5% Pμb/LP2	LP2_5MB-1	2.85	2.42	15.4	16.7	1.08
	LP2_5MB-2	2.96	2.88	19.8	21.9	1.11
	LP2_5MB-3	2.98	2.51	17.5	19.3	1.10
	Average (STD)					**1.10 (0.01)**
10% Pμb/LP2	LP2_10MB-1	2.95	3.02	20.6	19.4	0.94
	LP2_10MB-2	2.95	2.95	20.1	18.9	0.94
	LP2_10MB-3	2.95	2.98	20.4	19.0	0.93
	LP2_10MB-4	2.95	2.91	19.9	18.9	0.95
	Average (STD)					**0.94 (0.01)**
15% Pμb/LP2	LP2_15MB-1	2.96	2.95	20.3	16.6	0.82
	LP2_15MB-2	2.96	2.85	19.6	16.2	0.83
	LP2_15MB-3	2.96	2.67	18.4	15.2	0.83
	Average (STD)					**0.82 (0.00)**
20% Pμb/LP2	LP2_20MB-1	2.97	2.80	19.4	13.7	0.70
	LP2_20MB-2	2.96	2.61	18.0	13.9	0.78
	LP2_20MB-3	2.98	3.02	21.0	14.1	0.67
	LP2_20MB-4	3.04	3.06	22.2	14.1	0.63
	Average (STD)					**0.70 (0.06)**
25% Pμb/LP2	LP2_25MB-1	2.96	2.90	19.9	14.3	0.72
	LP2_25MB-2	2.96	2.94	20.2	14.6	0.72
	LP2_25MB-3	2.96	2.93	20.2	14.2	0.70
	Average (STD)					**0.71 (0.01)**
30% Pμb/LP2	LP2_30MB-1	2.71	3.01	17.3	14.8	0.85
	LP2_30MB-2	2.98	2.59	18.0	13.6	0.75
	LP2_30MB-3	2.98	3.01	21.0	16.0	0.76
	Average (STD)					**0.79 (0.05)**

4.3.2 Test Procedure

The test specimen was inserted into the bore of the test apparatus. Care was taken to ensure that the specimen fit smoothly into the bore of the apparatus. In the present case, a clearance of 0.05 mm (0.002 in) was found to be suitable. Then two case-hardened sliding fit steel plungers 12.7 mm long and 30.2 mm in diameter were inserted into the open end of the bore. The entire assembly was next placed in a test machine and the specimen was loaded in compression by moving the ram over sliding fit plungers down. The plunger load and displacements were recorded continuously to determine stress and strain. From the data, stress and strain were calculated. The normal loading rate was 1.27 mm (0.05 in) per minute. Tests were conducted to a maximum stress level of 50 MPa. All tests were conducted at room temperature (approximately 25 °C).

4.3.3 Test Results and Discussion

4.3.3.1 Mechanism of Compression

Typical confined compression stress and strain responses of base LP2 (a pure plastic material) and Pμb filled LP2 are shown in Figure 4.8. If LP2 is a pure fluid/plastic material of Poisson's ratio 0.5, the stress-strain curve would have been a straight line along the Y axis. In real experiment, short linear shape followed by very steep line is observed because of the initial re-adjustment of specimen and leakage of material around the plunger. However, in the case of filled LP2 composite, one can observe an initial linear line, because of compressibility of Pμb, followed by a transition curve indicative of partial collapse of Pμb (top and bottom faces start touching each other) finally leading to complete collapse or incompressible state of the composite. The last part of the curve is almost parallel to Y axis, representing the plastic response of completely the collapsed state of microballoons. Inserts in Figure 4.8 show the state of Pμb at various stress levels. The slope of the linear (first) portion of the curve gives the bulk modulus of the material.

4.3.3.2 Axial Stress-Strain Response

Compressibility of the syntactic foam is determined by the intersection of tangent lines from the compression and solidification portions of the stress-strain curves. The construction is shown in Figure 4.8. The strain at the intersection point gives the compressibility of the material.

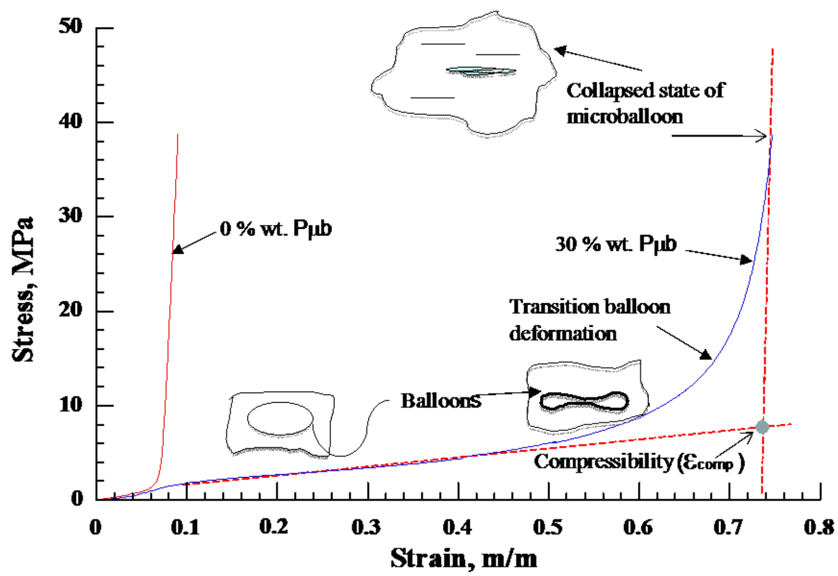

Figure 4.8 Typical stress-strain response of Pμb and unfilled LP2 composite

Figures 4.9 through 4.12 show the confined compressive stress-strain responses of base, 10, 20, and 30% Pμb content in LP2 elastomer, respectively. Each of these figures contains the complete axial stress-strain response till solidification (figure a) and the initial linear portion of the curve (figure b) to determine the slope, which is the bulk modulus of the foam.

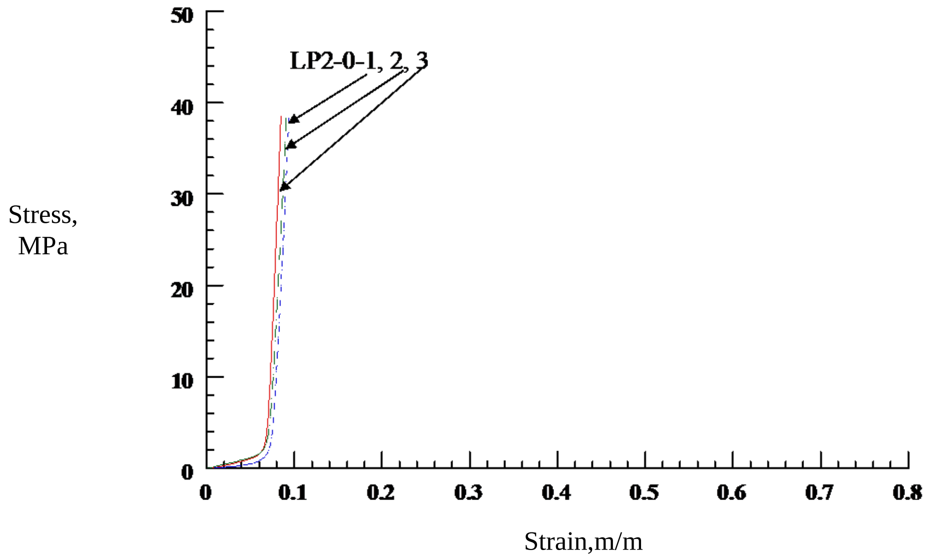

(a)

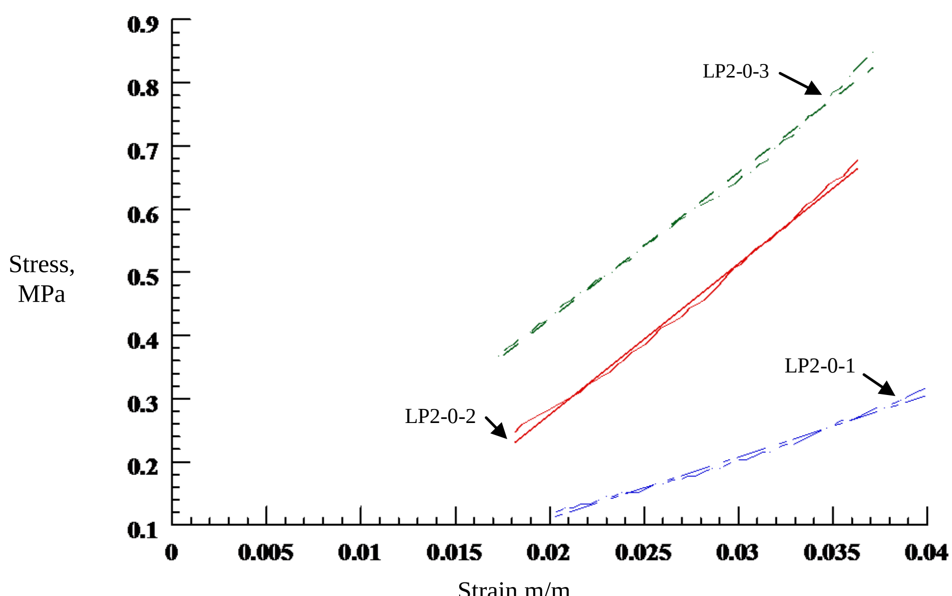

(b)

Figure 4.9 (a) Complete stress-strain, and (b) Bulk modulus response of base LP2 specimen

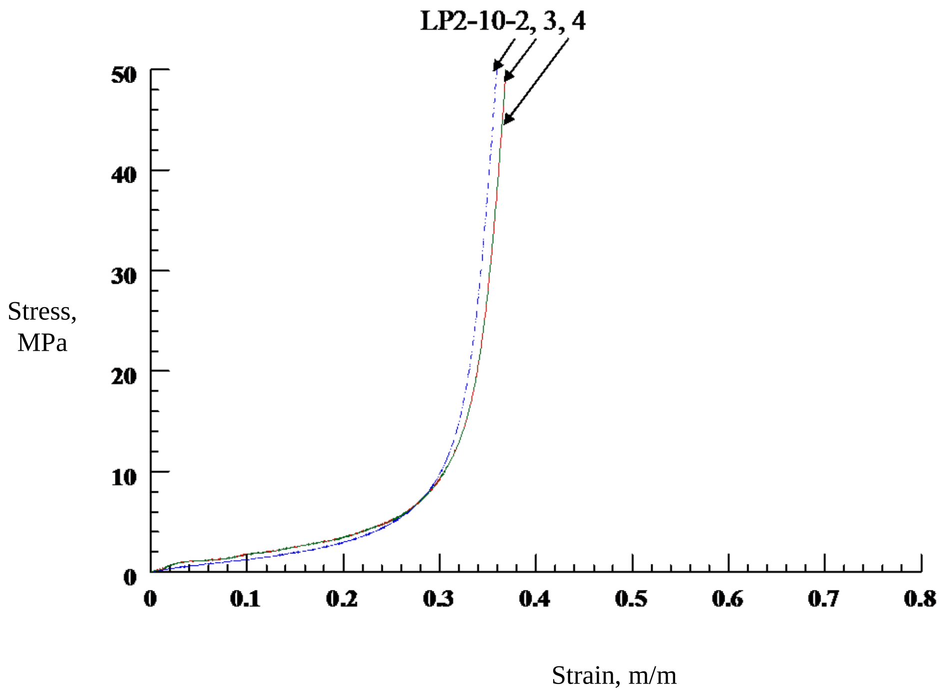

(a)

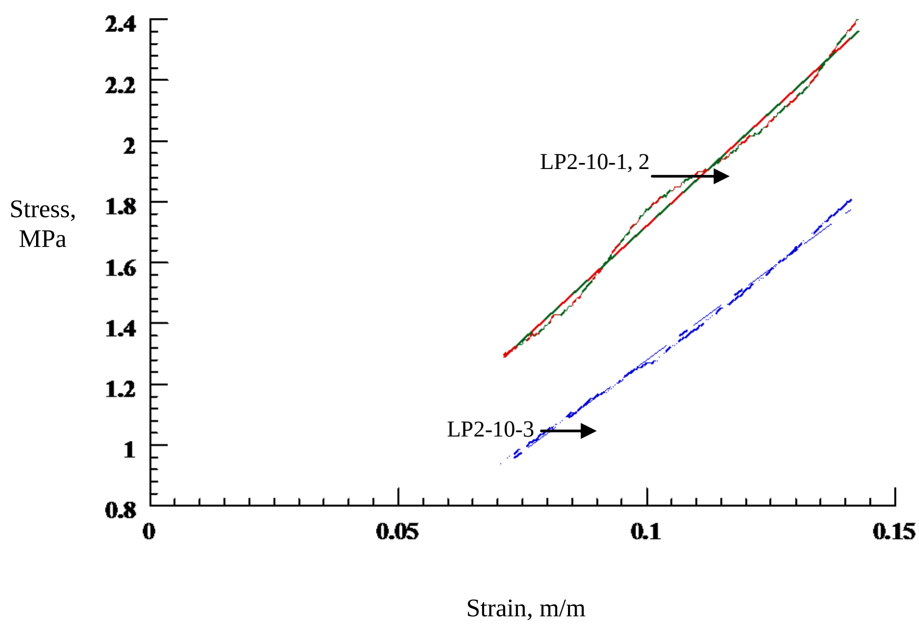

(b)

Figure 4.10 (a) Complete stress-strain, and (b) Bulk modulus response of 10% wt. Pμb specimen

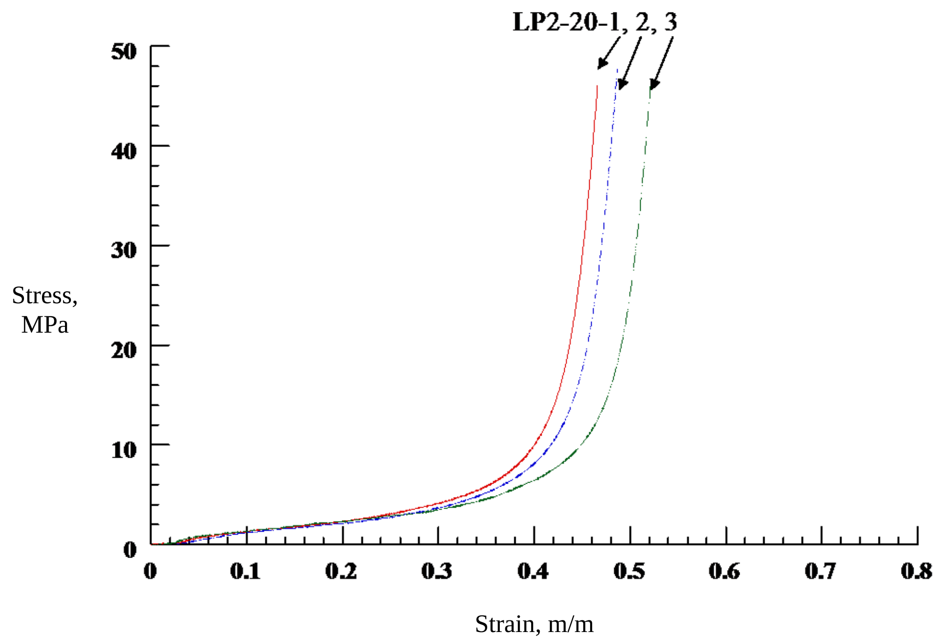

(a)

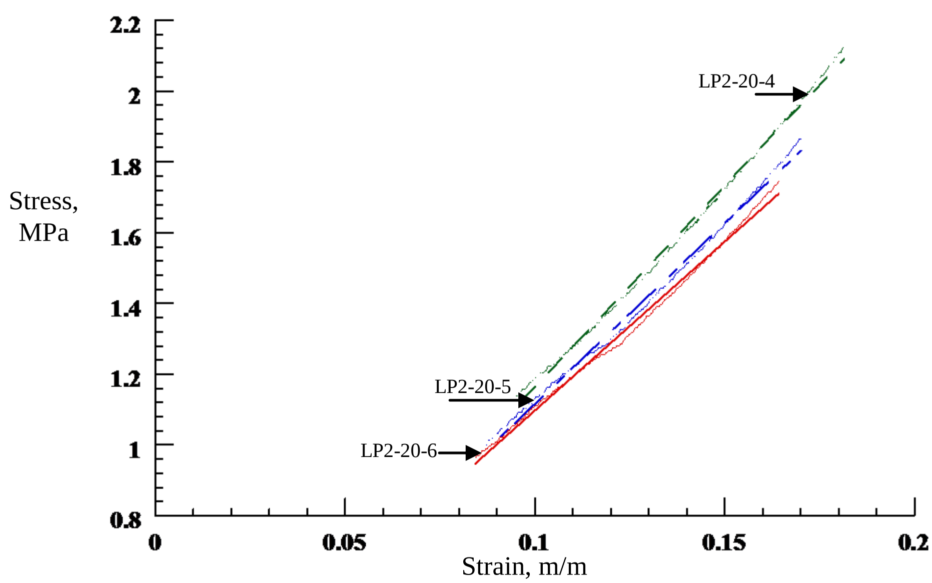

(b)

Figure 4.11 (a) Complete stress-strain, and (b) Bulk modulus response of 20% wt. Pμb specimen

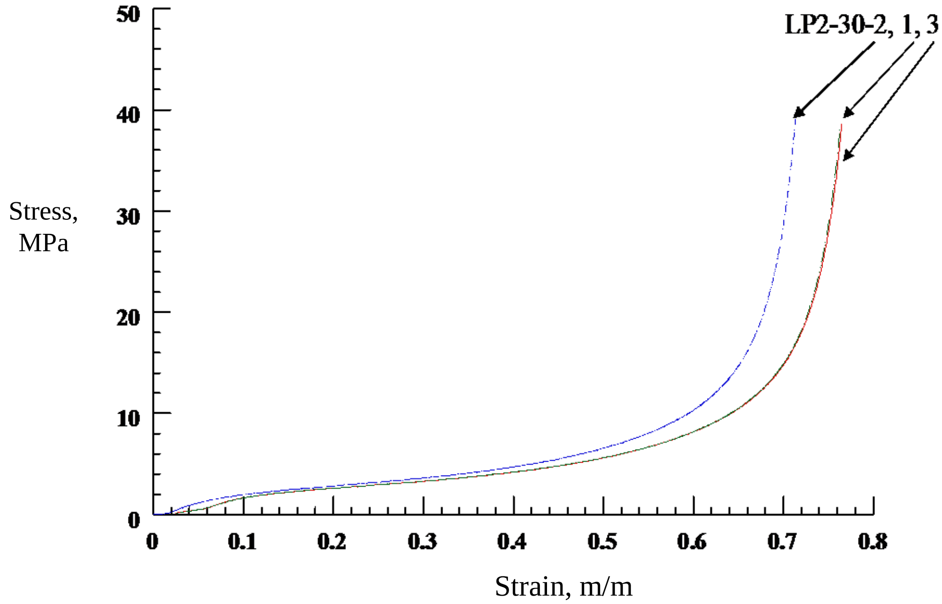

(a)

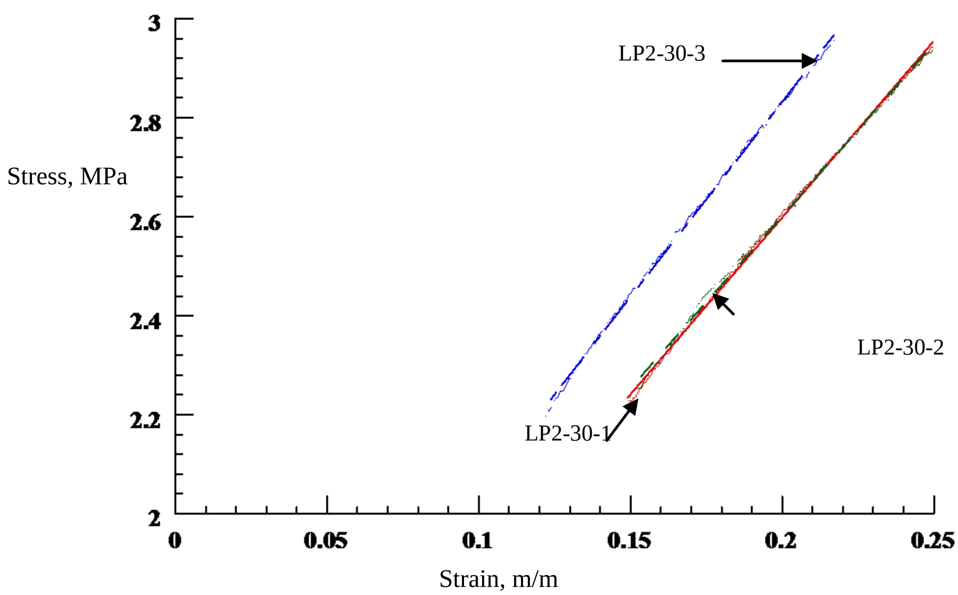

(b)

Figure 4.12 (a) Complete stress-strain, and (b) Bulk modulus response of 30% wt. Pμb specimen

The average curves of each test case are shown in Figure 4.13. This includes the data for 5%, 15%, and 25% weight percent filler content. Here all the curves shift almost parallel to each other depending on the filler content.

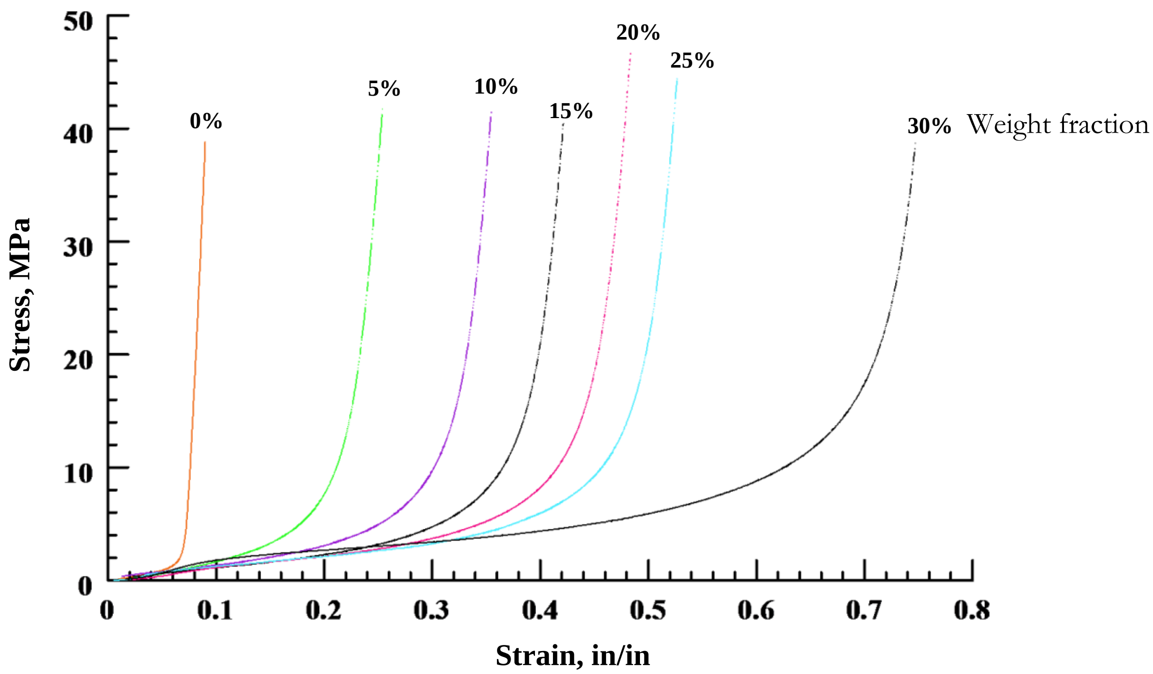

Figure 4.13 Average confined compression stress vs. strain for various Pμb contents

The table includes the data for 5, 15, and 15% filler content also. The compressibility increases with the filler content and reaches a limit of 68% for 30% weight filler content. Calculated bulk moduli are listed in the Table 4.4. At least three samples were tested for each case to confirm the repeatability of the test results.

Table 4.4 Summary of bulk modulus and compressibility of the specimens

Specimen No.	Strain Range, m/m	Initial Bulk Modulus (K), MPa	Compressibility, %
LP2-0-1	0.018 -0.036	23.9	0.07
LP2-0-2	0.018 -0.036	9.8	0.07
LP2-0-3	0.018 -0.036	23.4	0.07
Average	-	**19.0**	**0.07**
Std. Dev.	-	**8.0**	**0.00**
LP2-5-1	0.051-0.102	13.3	0.24
LP2-5-2	0.051-0.103	19.9	0.26
LP2-5-3	0.051-0.104	22.6	0.26
Average	-	**18.6**	**0.25**
Std. Dev.	-	**4.8**	**0.01**
LP2-10-1	0.071-0.142	15.0	0.32
LP2-10-2	0.071-0.143	12.1	0.14
LP2-10-3	0.071-0.144	15.0	0.32
Average	-	**14.0**	**0.26**
Std. Dev.	-	**1.7**	**0.11**
LP2-15-1	0.084-0.168	9.0	0.33
LP2-15-2	0.084-0.169	10.2	0.38
LP2-15-3	0.084-0.170	11.4	0.37
Average	-	**10.2**	**0.36**
Std. Dev.	-	**1.2**	**0.02**
LP2-20-6	0.097-0.189	9.2	0.42
LP2-20-5	0.097-0.190	9.3	0.44
LP2-20-4	0.097-0.191	10.4	0.44
Average	-	**9.6**	**0.43**
Std. Dev.	-	**0.7**	**0.01**
LP2-25-1	0.104-0.208	8.6	0.48
LP2-25-2	0.104-0.209	8.4	0.49
LP2-25-3	0.104-0.210	10.3	0.48
Average	-	**9.1**	**0.48**
Std. Dev.	-	**1.0**	**0.01**
LP2-30-2	0.149-0.249	8.6	0.72
LP2-30-1	0.149-0.250	8.4	0.69
LP2-30-3	0.149-0.251	10.2	0.63
Average	-	**9.1**	**0.68**
Std. Dev.	-	**1.0**	**0.05**

The average compressibility agrees with the filler volume and void content of the material. The plot of bulk modulus versus weight percent of filler content is shown in the

Figure 4.14, it represents a linear relationship.

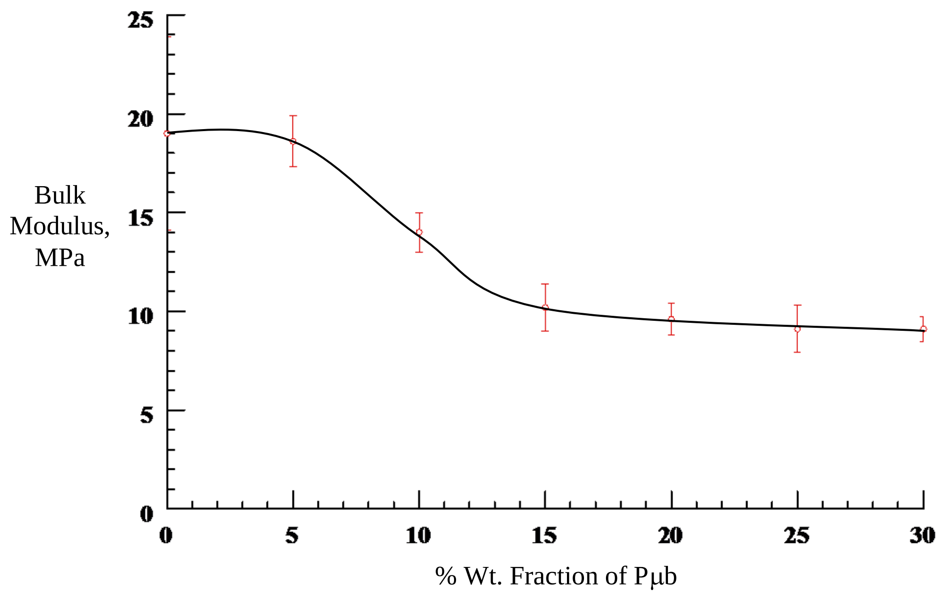

Figure 4.14 Polysulfide bulk modulus vs. percent wt. Pμb specimens

Figure 4.15 shows the variation of compressibility versus the percent weight fraction of Pμb. The bulk modulus drops from 19 MPa to about 9 MPa at about 15% Pμb loading then remains constant. This plateau in the curve may be due to counter acting combination of increased elastic modulus and flexibility with increase in weight fraction of filler [41].

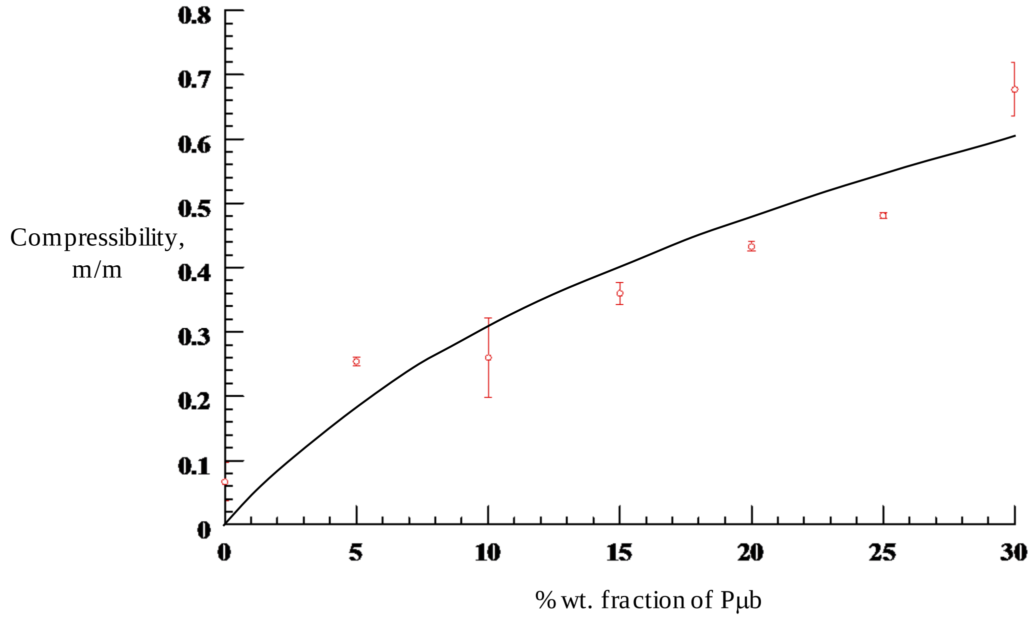

Figure 4.15 Polysulfide specimens compressibility vs. percent wt. Pμb

4.3.4 Comparison of Analysis with Experiment

Axial stress-strain response computed from the gas laws (Section 2.1.2) is compared with the experimental data for 0, 10, 20 and 30% weight of Pμb in the Figure 4.16. The broken lines represent the experiment and the solid lines represent the analysis. The analysis includes the microballoon wall deformation. The analysis assumes perfect fit condition and no initial adjustment of the test specimen and leakage of material. Therefore, the two results differ, however qualitatively they are similar. Furthermore, some polymer could also be compressible [44].

Alternatively, an empirical equation was fit to the base line data (0% Pμb) and modified to include the compressibility of the material by filler content (V_f). That equation is given by an exponential equation:

$$\sigma = B\left[1 - e^{(-\varepsilon - V_f)}\right] \tag{4.2}$$

where σ and ε are axial stress and strain, V_f is the volume content of the filler, and B is a constant. Comparison of the Equation 4.2 and the test data is shown in Figure 4.17 and the results agree very well.

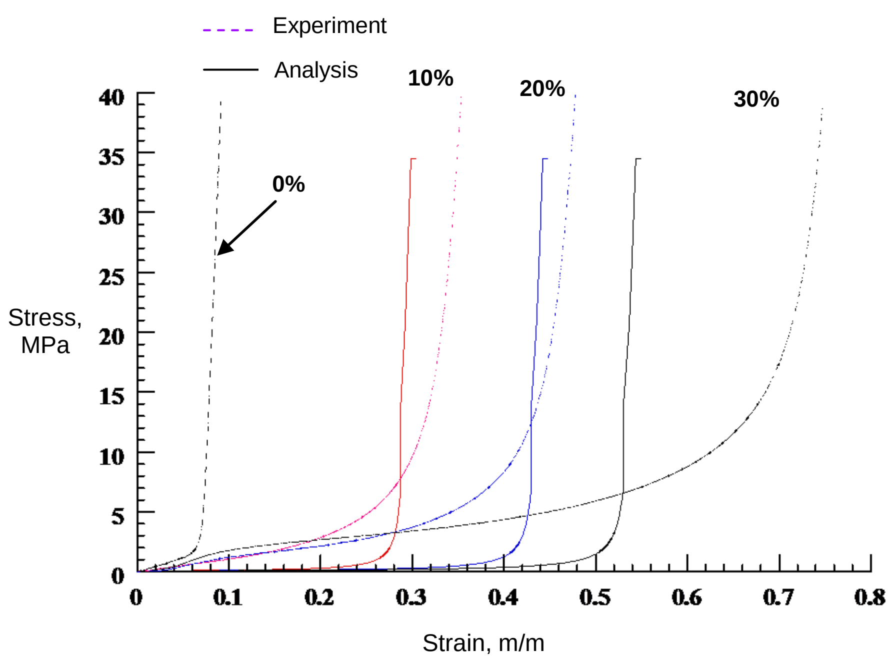

Figure 4.16 Comparison of analysis and experiment data

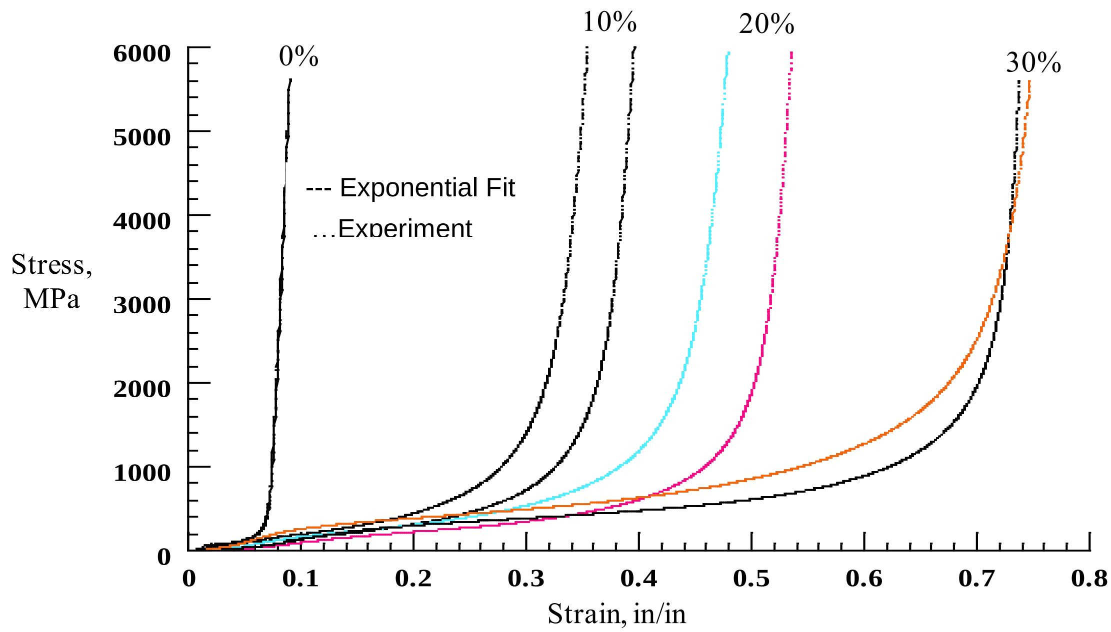

Figure 4.17 Comparison of experiment and exponential equation

4.4 Morphology of Microballoons at Different Stress Levels

One of the purposes of this flexible syntactic foam is to use it to develop an understanding of the survivability of the Pμb under multiple loading and unloading conditions. If the Pμb survives, then there is a potential of using this foam in multiple impact applications. To assess this performance, a 30% Pμb filled syntactic foam is subjected to confined compression and unloading. Stresses are taken to levels of 2.8, 4.2, 5.6 and 6.9 MPa and unloaded. The stress-strain responses of the material are shown in Figure 4.18. After the specimens are unloaded, the specimen is broken and the fractured surface is SEM imaged. The SEM images of specimens are shown in Figures 4.19 through 4.22 for 2.8, 4.2, 5.6 and 6.9 MPa loading, respectively.

Figure 4.19 is for 2.8 MPa loaded specimen and it shows nice spherical Pμbs, all are intact and there is no damage. In Figure 4.20, one of the Pμbs is collapsed, an indication of balloon failure. Number of Pμbs collapsing or breaking increases with increasing loading (see Figures 4.21 and 4.22). This study concludes that, although the BJO-93 Pμb is flexible and can take multiple loading and unloading but in a confined environment of elastomer, it does not survive the high loadings. Alternately, the present Pμbs are not suitable for multiple loadings.

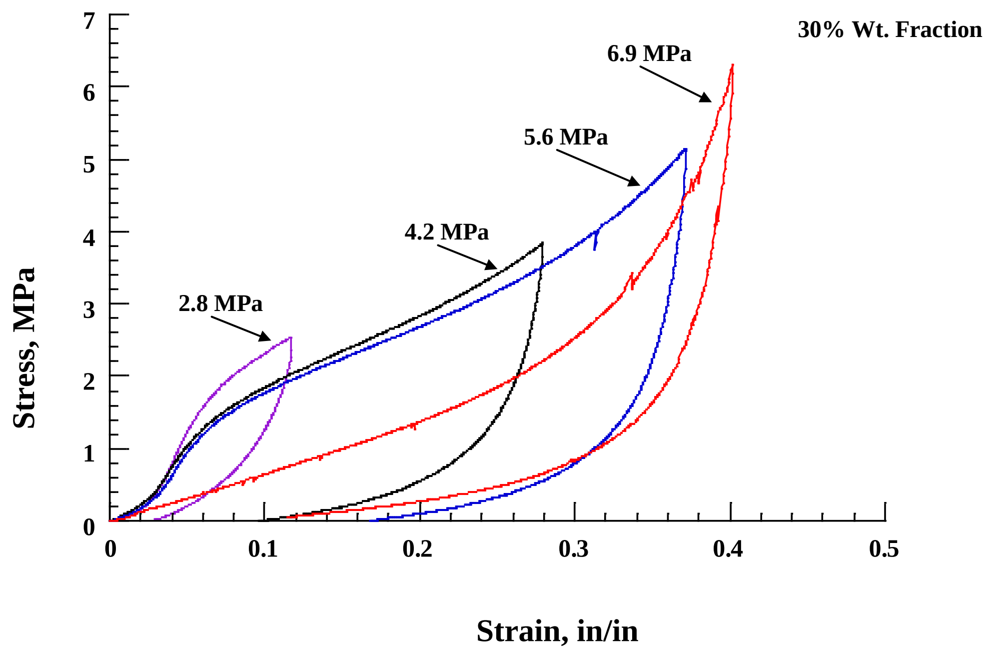

Figure 4.18 Confined compression-decompression at various stress level

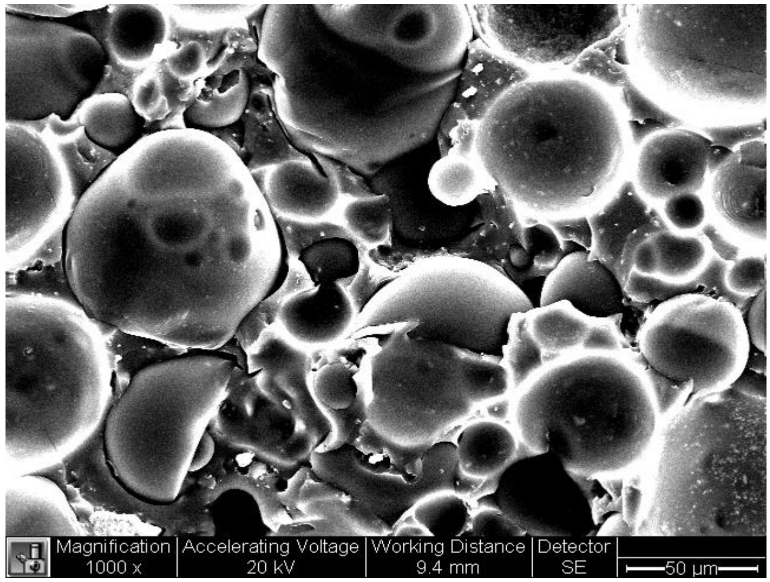

Figure 4.19 SEM morphology at 2.8 MPa stress level

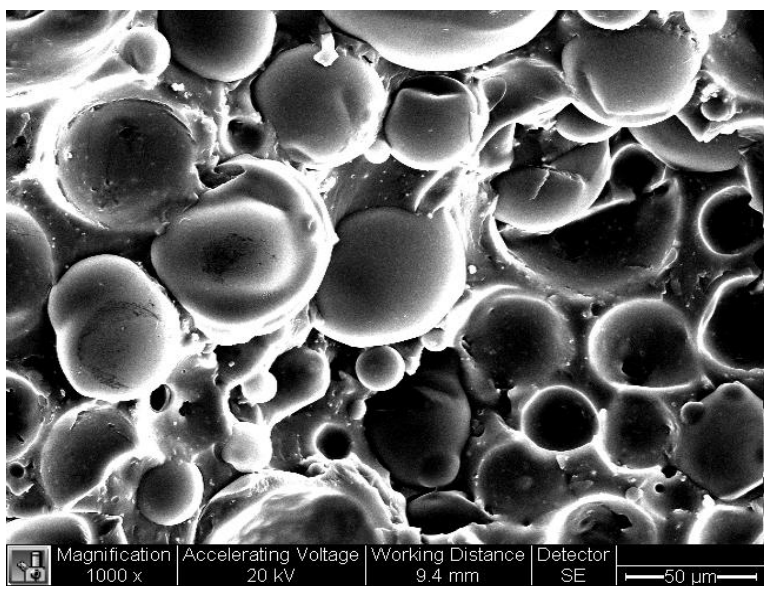

Figure 4.20 SEM morphology at 4.2 MPa stress level

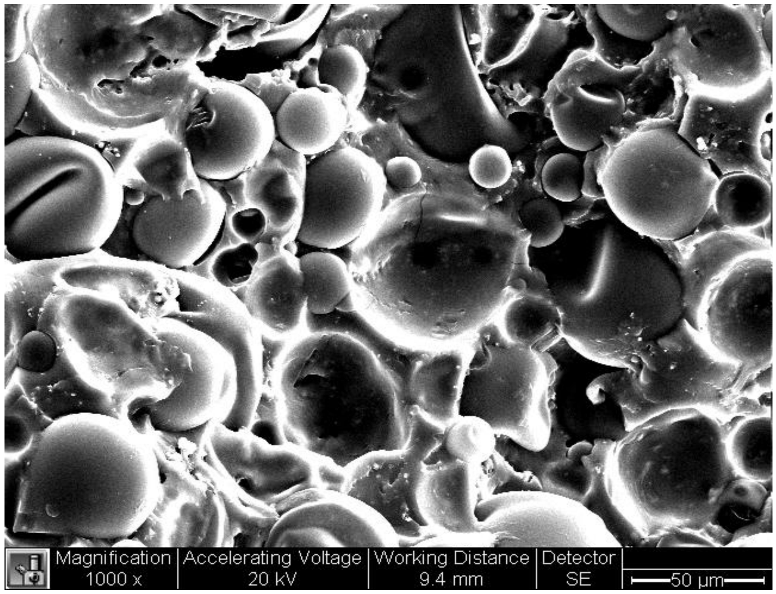

Figure 4.21 SEM morphology at 5.6 MPa stress level

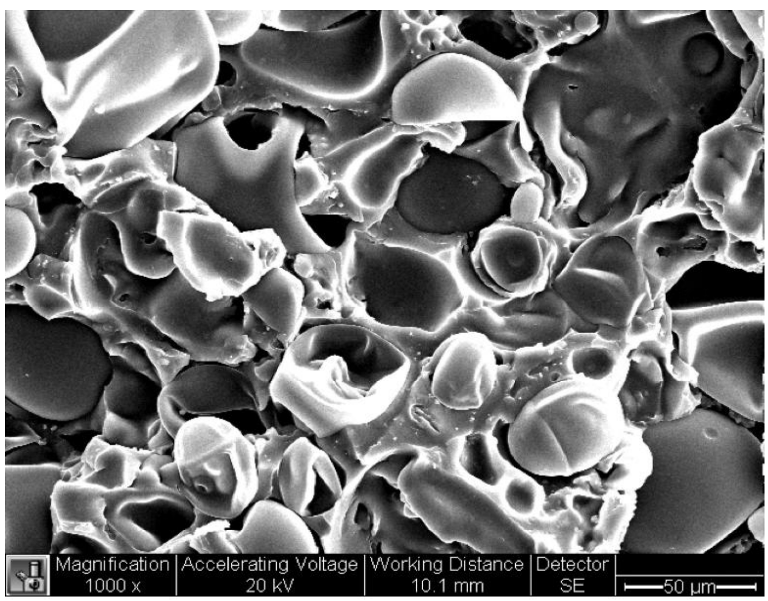

Figure 4.22 SEM morphology at 6.9 MPa stress level

4.5 Summary

This chapter presented a description and results of tensile modulus for base, 10, 20, and 30 % wt. Pμb. Further, it included the bulk modulus, and compressibility variations for base, 5, 10, 15, 20, 25, and 30 % wt. Pμb filled specimens under confined-compression subjected to various loads and a morphological study of Pμb structure was made using Scanning Electron Microscope. The results showed that the increase in tensile modulus with Pμb content was due to stiffening of the material due to the increased percent weight Pμbs. The initial bulk modulus and compressibility were impacted by the increased percent weight of Pμb. As shown, the initial bulk modulus decreased from 19 to 9 MPa from base to 20% filler content, while the compressibility of the specimens increased from 7% to 43% . Beyond 20% limit, the compressibility and decrease in bulk modulus was limited.

CHAPTER 5

HIGH STRAIN RATE CHARACTERIZATION OF POLYSULFIDE SYNTACTIC FOAMS

5.1 Introduction

This chapter describes high strain rate testing of base polysulfide and Pμb filled polysulfide specimens using the Split Hopkinson Pressure Bar (SHPB) apparatus. First, the base polysulfide specimen is characterized and then the test analysis is extended to Pμb filled polysulfide compositions. The properties such as shock pulse mitigation and strain rate sensitivity are of primary interest. Stress versus time, strain versus time, and stress versus strain data are analyzed and compared for polysulfide syntactic foams filled with various amounts of microballoons.

5.2 Sample Preparation

Samples with L/D ratio of 0.25 were selected based on the guidelines of Chen et al. [42] and Panduranga [43] in order to minimize wave attenuation. This L/D ratio accommodated the reduced wave speed (proportional to $(E/\rho)^{1/2}$) in the softer materials. Due to the viscoelastic nature of polysulfide elastomer and its compositions at ambient temperatures, a special molding method was developed. This molding method was capable of producing specimen of thickness 3.2 mm (0.125 in) with 0.025 mm (0.001 in) tolerance. The diameter of the specimen was 12.7 mm (0.5 in) with a tolerance of 0.25 mm (0.01 in). Figure 5.1 shows photographs of the polysulfide and Pμb filled polysulfide samples used in this research. The polysulfide specimens without any modification were termed as base. The specimens' numbers and sizes shown in Table 5.1 were as follows:

- LP2-0-x : Liquid Polysulfide 2 (Polysulfide with 0 wt.% Pμb)
- LP2-10-x : Liquid Polysulfide 2 with 10 wt.% of Pμb
- LP2-20-x : Liquid Polysulfide 2 with 20 wt.% of Pμb
- LP2-30-x : Liquid Polysulfide 2 with 30 wt.% of Pμb

Note, -x : Represent the specimen number

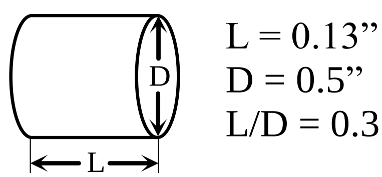

(a)

(b)

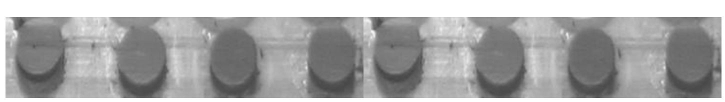

(c)

Figure 5.1 (a) Specimen schematic, (b) base polysulfide, and (c) Pμb filled polysulfide

Table 5.1 Specimen Number, Avg. Diameter, and Avg. Length

Spn.No/%PmB	Avg. Diameter, cm	Avg. Length, cm
LP2-0-4	1.20	0.33
LP2-0-6	1.20	0.33
LP2-0-7	1.22	0.36
LP2-0-8	1.22	0.34
LP2-0-9	1.23	0.34
LP2-0-10	1.22	0.36
LP2-0-11	1.22	0.35
LP2-0-13	1.22	0.34
LP2-0-15	1.24	0.33
LP2-10-1	1.25	0.35
LP2-10-3	1.25	0.35
LP2-10-4	1.23	0.35
LP2-10-5	1.25	0.33
LP2-10-6	1.27	0.32
LP2-10-7	1.26	0.31
LP2-10-8	1.28	0.32
LP2-10-11	1.25	0.32
LP2-10-12	1.24	0.35
LP2-10-13	1.26	0.33
LP2-10-14	1.24	0.33
LP2-10-16	1.24	0.33
LP2-20-2	1.27	0.33
LP2-20-4	1.27	0.34
LP2-20-5	1.27	0.36
LP2-20-6	1.27	0.32
LP2-20-7	1.25	0.33
LP2-20-8	1.25	0.33
LP2-20-9	1.26	0.38
LP2-20-10	1.24	0.33
LP2-20-11	1.27	0.36
LP2-20-12	1.27	0.35
LP2-20-13	1.26	0.36
LP2-20-14	1.26	0.35
LP2-30-2	1.26	0.34
LP2-30-3	1.24	0.35
LP2-30-5	1.24	0.34
LP2-30-6	1.26	0.40
LP2-30-7	1.26	0.35
LP2-30-8	1.25	0.40
LP2-30-11	1.25	0.41
LP2-30-12	1.25	0.35
LP2-30-13	1.24	0.35
LP2-30-14	1.24	0.35
LP2-30-15	1.24	0.35
LP2-30-17	1.24	0.35

The length of the specimens was also measured at three locations separated by 120° apart circumferentially. The average values of diameter and length of all specimens are listed in Table 5.1. All high strain rate testing was performed in the unconfined state of the specimen. The assumption was that due to high rate of loading, the unconfined and confined tests would be the same. However, this assumption needs to be verified by an independent study.

5.3 High Strain Rate Testing

5.3.1 Test Apparatus and Procedure

The SHPB apparatus was used for testing materials at high strain rate ranging from 100 to 10,000/s. This equipment was used to test polysulfide syntactic foams at one strain rate of about 3,000/s. The photograph of SHPB test apparatus and its critical components are shown in Figure 5.2 and 5.3, respectively. In the SHPB test, a right-cylindrical solid specimen with suitable dimensional tolerance was placed between the incident/input bar (I_{bar}) and the transmitter/output bar (T_{bar}) as shown in Figure 5.3b, also see the schematic Figure 5.4. The impact of a striker bar (S_{bar}) on the impact end of the incident bar (see Figure 5.3c) produced a compressive stress/strain pulse of geometric length twice that of the striker bar length . The striker bar length was 0.76m. The shape of the pulse in stress-time coordinates was almost rectangular. The strain pulse, $\varepsilon_I(t)$, in the incident bar was measured by the strain gauge on the bar and its amplitude was proportional to the impact velocity (energy) of the striker bar.

The pulse propagated toward the incident bar-specimen (I_{bar}-S) interface, while a part of the pulse transmits through the specimen and a part reflected back. The reflected pulse, $\varepsilon_R(t)$, was tensile (opposite to the incident pulse) and was measured by the strain gage on the incident bar. The transmitted pulse, $\varepsilon_T(t)$ was measured by the strain gage mounted on the transmitter bar. During the period of stress wave propagation through the specimen, the specimen underwent deformation until its dynamic limit was reached. The properties of the bars such as the density (ρ_b) elastic modulus (E_b) longitudinal wave speed in the bar (c_b) diameter (D_b) and the specimen dimensions (L_s, D_s) were determined prior to the data analysis from a SHPB test. The detailed test procedure and the data analysis of the SHPB test are given in [43].

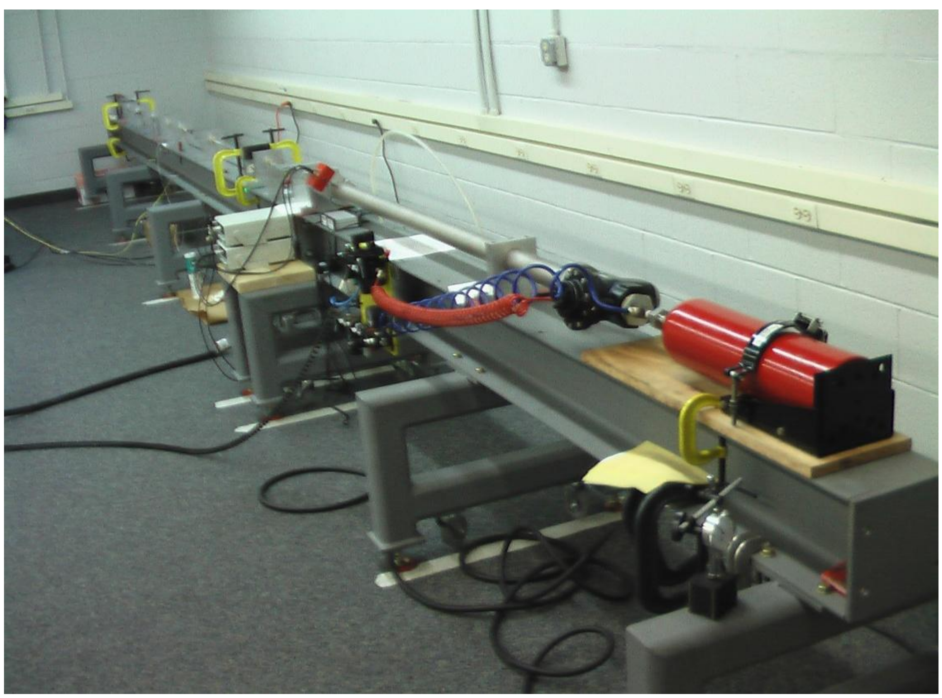

Figure 5.2 Photograph of main SHPB test apparatus

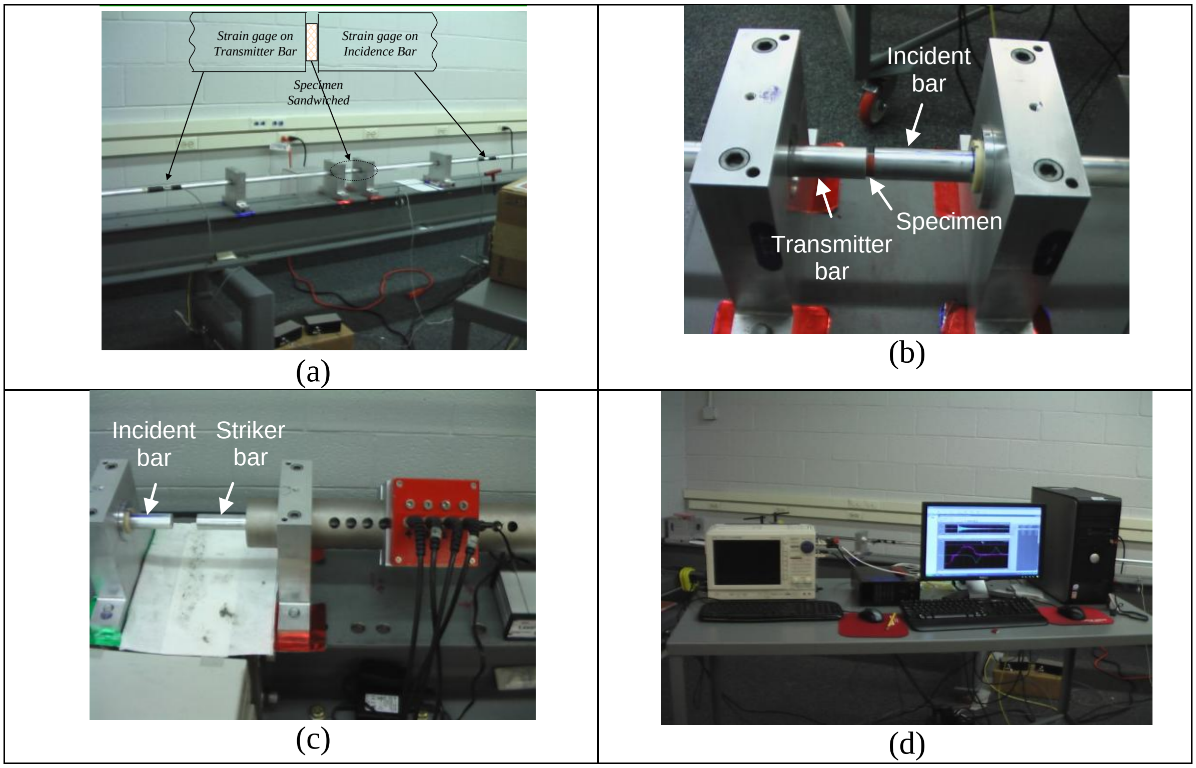

Figure 5.3 (a) Transmitter-Specimen-Incident bars, (b) Specimen bars assembly, (c) Striker hitting incident bar, and (d) Display of wave forms

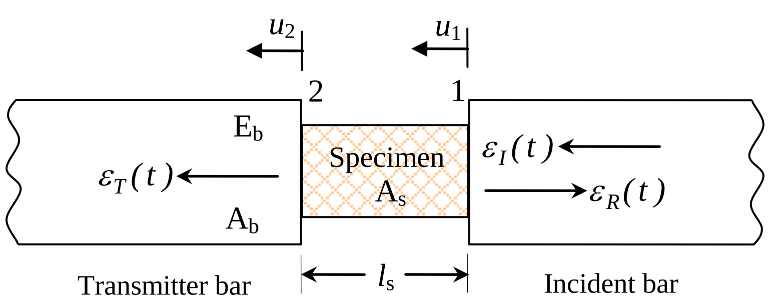

Figure 5.4 Specimen deformation state and strain waves in incident and transmitter bars

The polysulfide samples were tested in uniaxial compression strain waves at strain rates in the range of 2,861/s to 4,787/s using the Split Hopkinson Pressure Bar (SHPB) apparatus. Testing at strain rates below 2,861/s was not carried out due to insufficient momentum generated at breech pressure below 16psi. A striker bar of length 0.76 m (2.5 ft), and incident and transmitted bars of length 3.66 m (12 ft), 1.83 m (6 ft) respectively were used. All bars were made from 19 mm (0.75 in) diameter 7075 T6 aluminum alloy. The aluminum alloy was chosen to reduce the impedance mismatch with the elastomers and other non-metallic samples to attain a high sensitivity in the stress measurement from the transmission signal. In some tests a Photron FASTCAM high-speed digital camera was used to obtain high-speed images of specimens during the dynamic deformation. Figure 5.5 shows a typical incident, reflected and transmitted strain signals from the incident and transmitted bars for polysulfide specimen LP2-0-9.

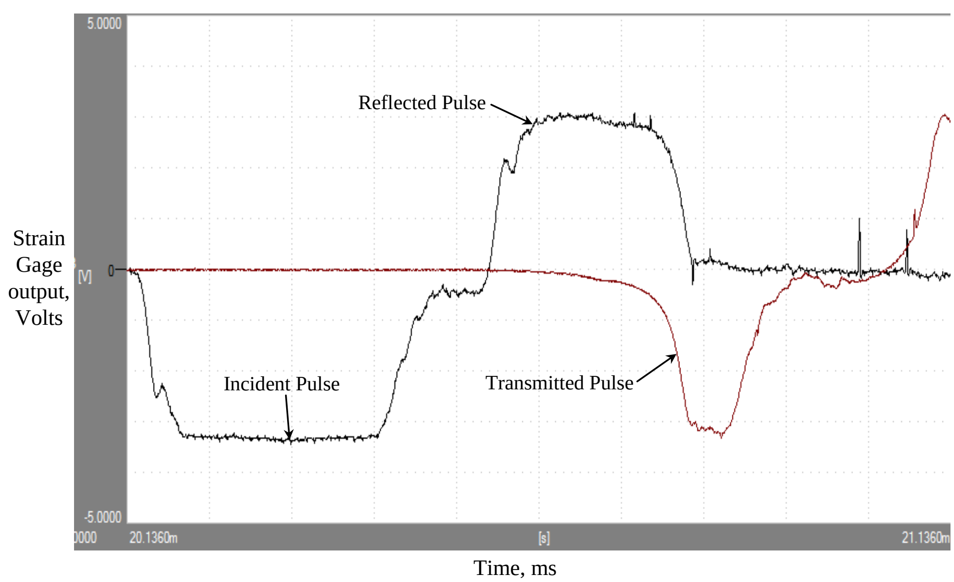

Figure 5.5 Typical strain pulses measured from the strain gages mounted on the incident and transmission bars (LP2-0-9)

The following steps were used in testing the samples:

- Ensure alignment of Bars
- Measure specimen dimensions carefully and apply lubricant on its ends
- Place the sample between the incident and transmitter bar with a thin layer of molycoat grease on each of the bar faces
- Set the pressure valves in appropriate position
- Adjust oscilloscope and strain gauge conditioner parameters
- Set pressure parameters in the gun
- Fire the striker bar by quickly opening the pressure valve
- Transfer data from oscilloscope to PC
- Reduce raw waveform data in Microsoft Excel sheet named “SHPB master”
- Plot strain vs. time, stress vs. time and stress vs. strain curves

5.3.2 Data Collection and Analysis

The data processing procedure to generate dynamic stress-strain relations of the specimen are explained with a block diagram in Figure 5.6.

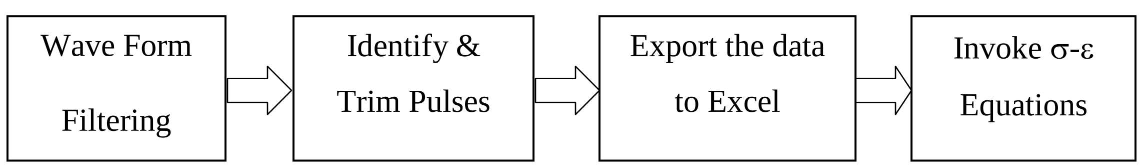

Figure 5.6 Block diagram of typical data processing procedure

An example of the typical axial strain signal in the incident and transmitted bars for base polysulfide specimen LP2-0-9 is shown in Figure 5.5. The plateau in the reflected pulse shown in Figure 5.5 indicates that the polysulfide specimen was deformed at a nearly constant strain rate for most of the time. The strain rate for a given test varied as a function of time. Typically, it increased from zero to a maximum value in a short period of time, then fluctuated about a constant value and finally dropped to zero. This constant value of the strain rate was accounted for and was defined by an average strain rate and was used to characterize the specific experiment.

A high-speed data acquisition card of Digital Storage Oscilloscope (DSO) at a sampling rate of 2 MHz was used to acquire the waveform data. The waveform file stored in DSO was converted into ASCII files and read by another signal processing software (Xviewer) for further analysis of the data. The raw waveform signals were oscillatory in nature due to noise. The waveforms were smoothened in Xviewer software using built-in mathematical filtering functions.

The start of each pulse had to be identified properly and the two pulses needed to be synchronized correctly to enable an accurate construction of the dynamic stress-strain curve. Therefore, the transit time through the greased joint and sample could interfere with the precise identification of the pulse start and end. The starting time was selected from the transmitted pulse at the instant when it began deviating from zero and the ending time was selected as the time when the transmitted pulse flattened out. The portion of the reflected pulse was chosen for the corresponding time range.

The identified and trimmed pulses were converted to reflected $\varepsilon_R(t)$ and transmitted

$\varepsilon_T(t)$ strains in the pressure bars using the following formula to compute the strain:

$$\varepsilon = \left(\frac{-R_G}{F_G N (R_G + R_C)} \right) \frac{V}{V_{ex}} \tag{5.1}$$

where, V was output voltage from signal-conditioning amplifier, V_{ex} was bridge excitation voltage (10V), F_G was the gage factor and ε was the strain (compressive) simulated by shunting R_G with R_C, R_G was the nominal resistance of the strain gage (1000 ohms), R_C was the shunt calibration resistance (49,000 ohms), and N was the number of active gages (N = 2 for half-bridge configuration).

The specimen stress, strain, and strain rate were calculated from the pressure bar strain pulses. The strain rate and strain in the specimen were determined from the reflected pulse, and the specimen stress was determined from the transmitted pulse. A trapezoidal rule was used to integrate the strain rate to calculate the specimen strain. The equations (5.2), (5.3), and (5.4) were used for calculating specimen strain rate, strain, and stress, respectively. The stress vs. time and strain vs. time plots were superimposed to get dynamic stress vs. strain curve. All the data analysis was performed using the MS Excel spreadsheet.

$$\dot{\varepsilon}_s(t) = \frac{2c_b \varepsilon_R(t)}{l_s} \tag{5.2}$$

$$\varepsilon_s(t) = \frac{2c_b}{l_s} \int_0^t \varepsilon_R(t)\, dt \tag{5.3}$$

$$\sigma_s(t) = \frac{A_b E_b}{A_s} \varepsilon_T(t) \tag{5.4}$$

where, A_s and A_b is the cross-sectional area of the specimen and the bars, respectively. l_s was the specimen length, E_b was the elastic modulus of the bars, c_b was the wave speed in the bars, and $\varepsilon_I(t)$, $\varepsilon_R(t)$, $\varepsilon_T(t)$, were the measured incident, reflected and transmitted strain pulses, respectively.

The calculated strain rate, strain and stress versus time using equations 5.2, 5.3 and 5.4, are shown in Figures 5.7 to 5.9, respectively for the base polysulfide specimen LP2-0-9 tested at a breech pressure of 23 psi. Parameters used in the calculation were l_s, c_b, A_b, A_s, and E_b are 3.2 mm, 5,051 m/s, 285.02 mm^2, 63.34 mm^2, and 71.7 GPa, respectively. The $\varepsilon_R(t)$ and $\varepsilon_T(t)$ were responses from reflected and transmitted wave signals collected from the data acquisition system. The superposition of data in Figures 5.8 and 5.9 gave the transient stress-strain curve shown in Figure 5.10. From the Figures 5.8 and 5.9 it was observed that the slope of the strain-time and stress-time curve is continuously changing from the onset of testing till the end of the testing. Therefore, the strain rate (slope of the strain-time curve) and stress rise rate (slope of the stress-time curve) were computed at 10%, 25%, and 70% (half power bandwidth of stress vs. time response, σ = $\sigma_{peak}/\sqrt{2}$) of peak values of base polysulfide specimens. The calculation of strain rate and stress rise rate is illustrated in Figures 5.11 and 5.12, respectively. The half power bandwidth (difference between the lower and upper half power points) is a measure of broadening of the curve which also a measure of shock attenuation.

For the polysulfide specimen LP2-0-9, the strain rates calculated at 10%, 25%, and 70% of peak values were 3,461/s, 4,111/s, and 4,099/s whereas the stress rise rates calculated at 10%, 25%, and 70% of peak values were 488 GPa/s, 2,033 GPa/s, and 8,012

GPa/s. Note that strain rate at 25% and 70% of peak strains were nearly same. However, the corresponding stress rates were different. Stress and strain rates at 70% of peak values or half-power bandwidth location were considered to be the rates experienced by the samples and was used for assessing the shock mitigation property of the material.

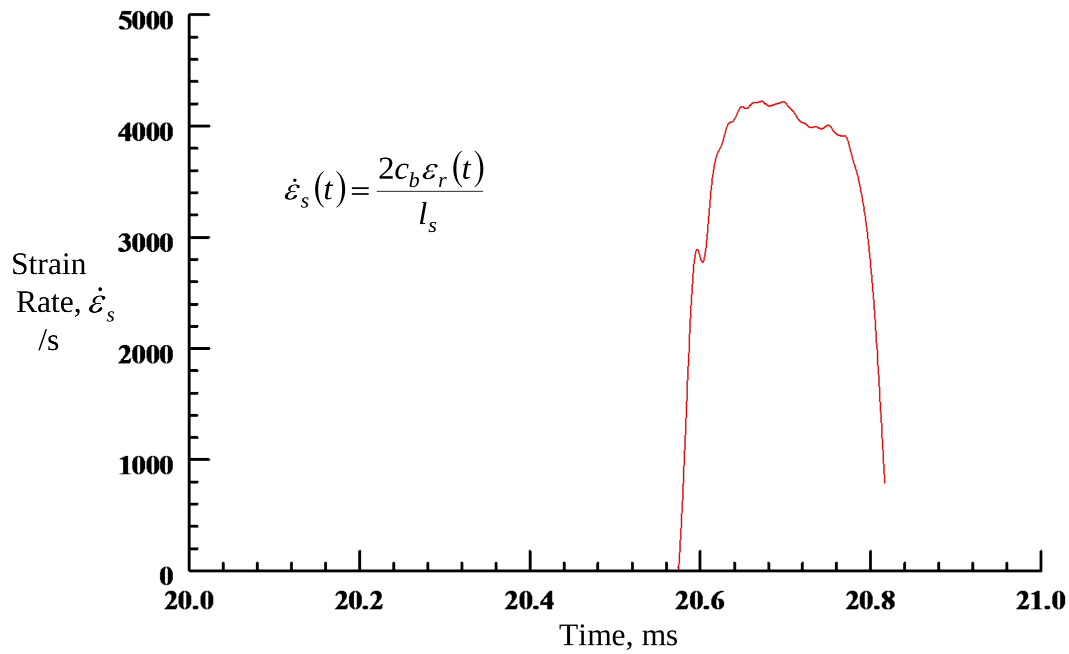

Figure 5.7 Strain Rate vs. Time plot for base polysulfide specimen LP2-0-9

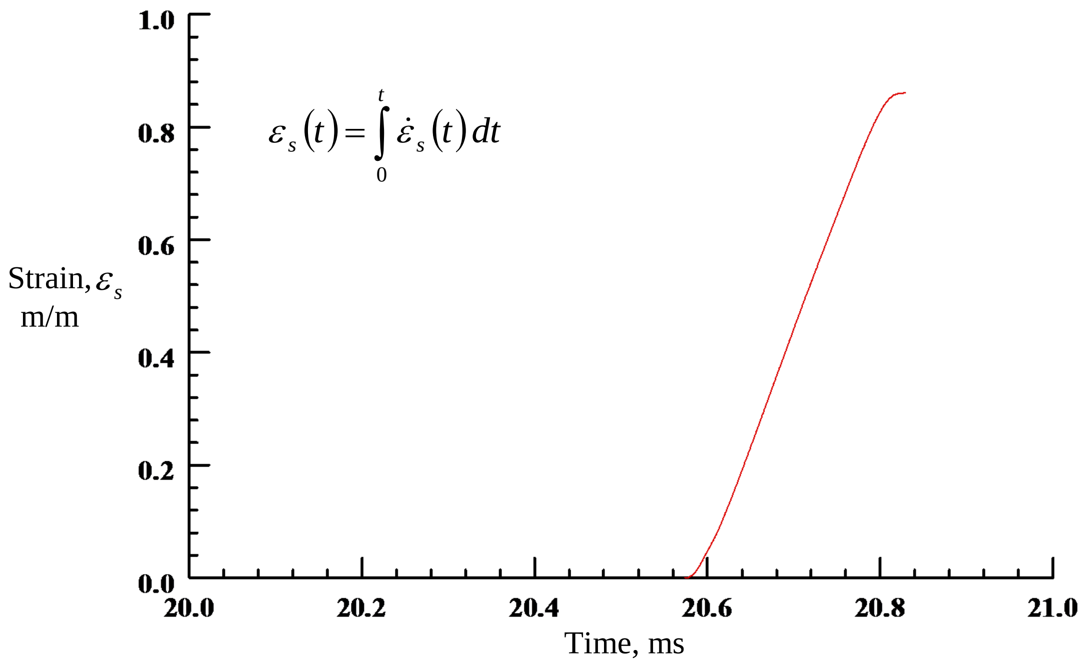

Figure 5.8 Strain vs. Time plot for base polysulfide specimen LP2-0-9

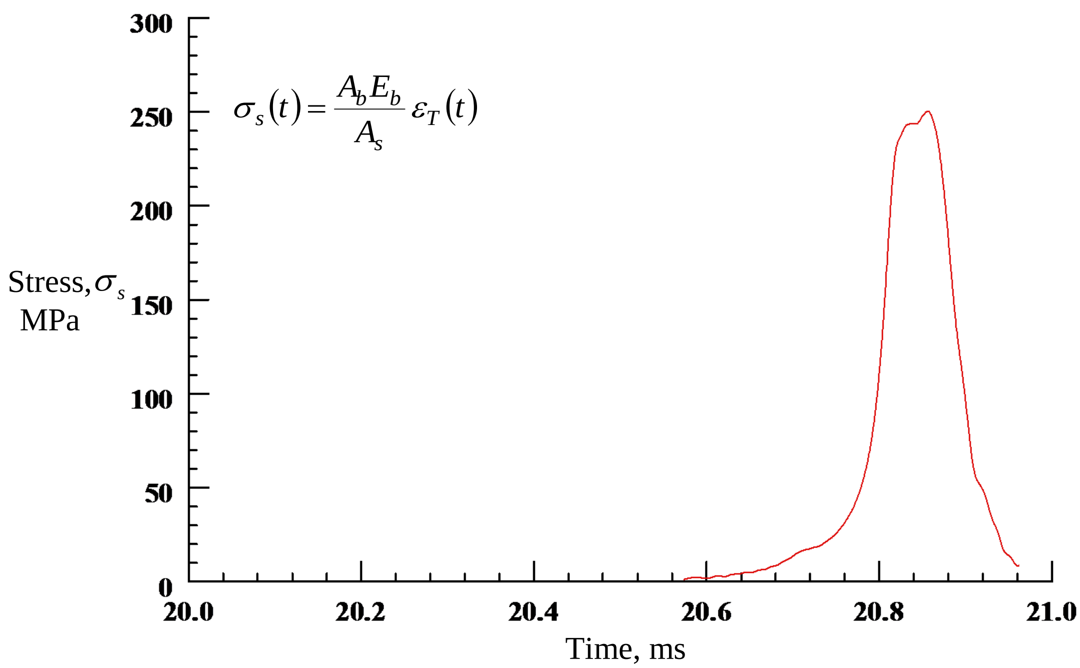

Figure 5.9 Stress vs. Time plot for base polysulfide specimen LP2-0-9

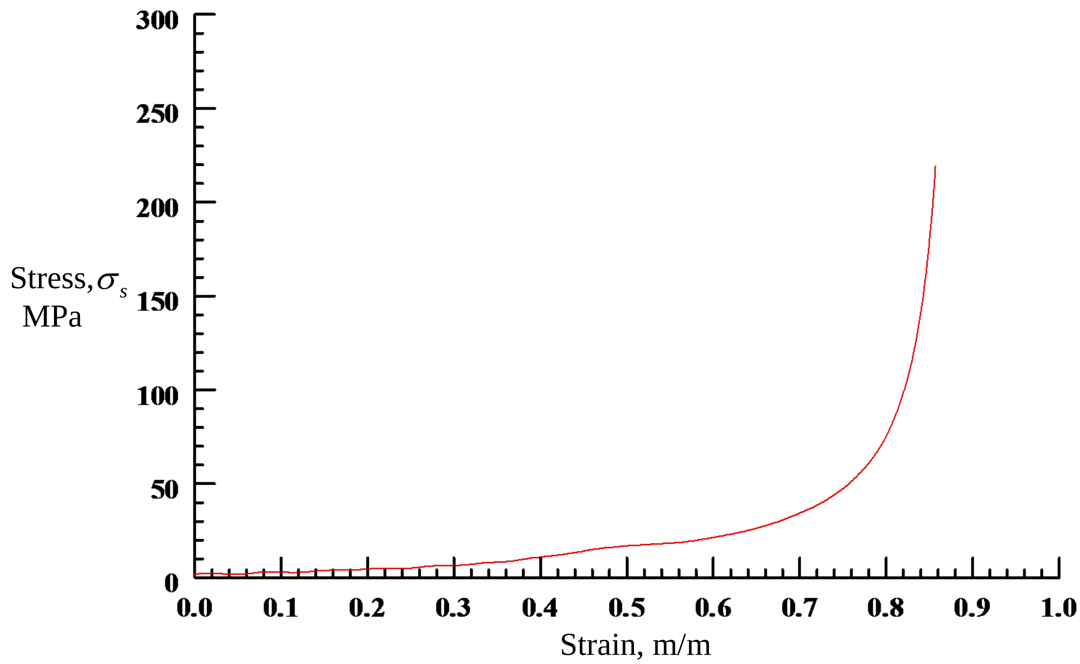

Figure 5.10 Stress vs. Strain plot for base polysulfide specimen LP2-0-9

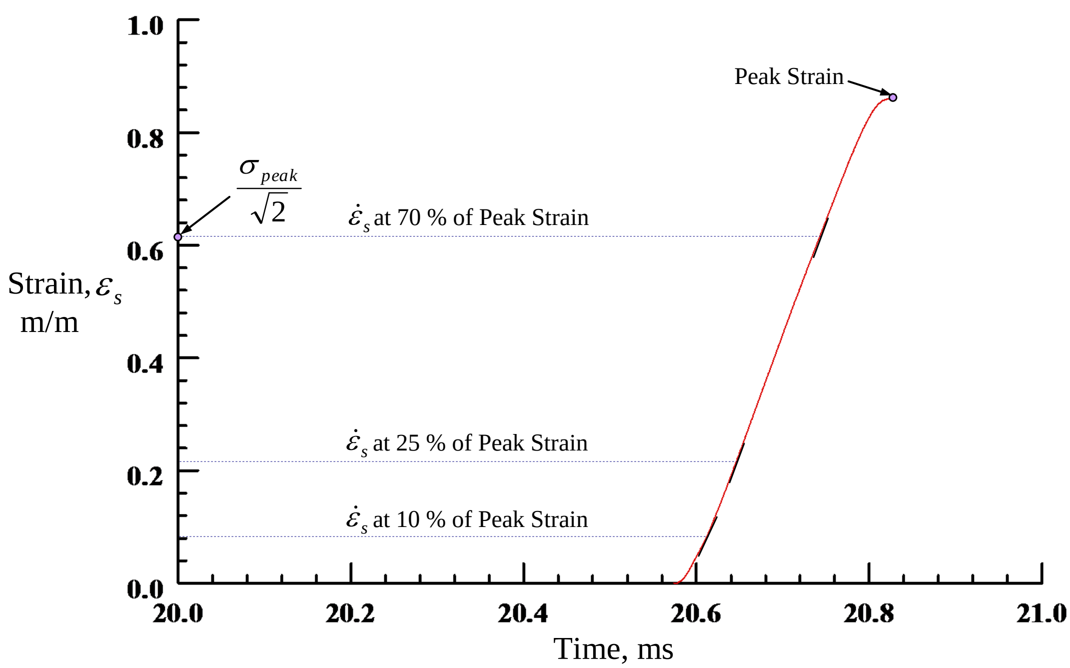

Figure 5.11 Illustration of computing Strain Rate at 10%, 25%, and at 70% (Half Power Point) of peak strain

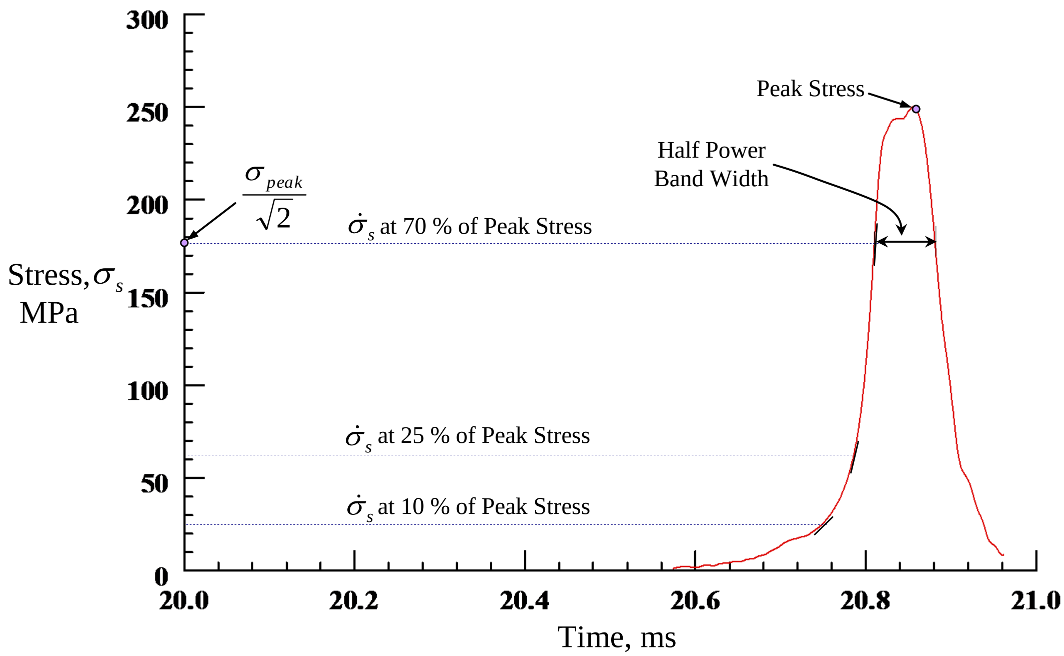

Figure 5.12 Illustration of computing Stress Rise Rate at 10%, 25%, and at 70% (Half Power Point) of peak stress

5.3.3 Test Matrix

Dynamic characterization of base and Pµb filled polysulfide samples were performed using a Split Hopkinson Pressure Bar set up (SHPB). The effect of strain rate on the compressive stress-strain response of base and PµB filled polysulfide samples was studied. Changing the breech pressure, this in turn changed the striker velocity and varied the strain rate. A range of strain rates (2,500/s to 5,000/s) were obtained by changing the breech pressure from 0.11MPa to 0.19 MPa during SHPB tests. The lowest strain rate achievable in SHPB was around 100/s. The lowest possible strain rate achievable at the CCMR SHPB facility was approximately 1,000/s.

At breech pressure of less than 0.11MPa (corresponding to strain rates less than 1,000/s), the striker bar did not generate enough momentum required to deform the specimen. This situation may have been due to the heavy mass of the striker bar and the friction between the bore riders and the internal surface of the gun barrel. The achievable high strain rate was limited by the elastic strain limit of the incident bar material. The breech pressure was limited to 0.19 MPa (corresponds to a strain rate of about 5,000/s) in order to ensure that the aluminum alloy did not yield during testing. The experiments conducted at breech pressure beyond 0.19 MPa frequently caused breakage of the soldering junction of the strain gage bonding terminals.

Therefore, the SHPB experiments for polysulfide were conducted at breech pressures from 0.11 to 0.19 MPa. The Table 5.2 lists test matrix used. All tests were conducted in the ambient conditions. Four specimens were tested for each case. One test data for base specimen is not listed because of malfunctioning of the system. All the other specimens test data have been listed.

Table 5.2 Dynamic Test Matrix for Base & Pμb-filled Polysulfide

Test Case	Breech Pressure, MPa		
Base Polysulfide	0.11	0.16	0.19
10 wt.% Pμb filled Polysulfide	0.11	0.16	0.19
20 wt.% Pμb filled Polysulfide	0.11	0.16	0.19
30 wt.% Pμb filled Polysulfide	0.11	0.16	0.19

5.4 Results and Discussions

5.4.1 Effect of % wt. of Pμbs on Materials Dynamic Response

Table 5.3 lists the peak strain, strain rate, pak stress and stress rise rate obtained from a high strain rate testing for base and microballoon filled polysulfide at a breech pressure of 23 psi. It can be observed from that Table 5.3 that the results are consistent and showed the repeatability of results from the replicated tests. The tested parameters of all the samples were within co-efficient of variation of 10% except for the case of 30 wt.% Pμb-filled polysulfide. The polysulfide samples with 30 wt.% microballoons showed co-efficient of variation up to 25%. The reason may be due to the difficulty in mixing at higher loading of Pμbs in polysulfide. The plot of stress vs. time and strain vs. time for all the base and microballoon filled polysulfide are given in appendix 1.

Table 5.4 summarizes the average values of peak stress, strain and their rate at 70% of the peak value and stress pulses half-power bandwidths. The values in the parenthesis represent the standard deviation. As noted in the Table 5.4, the average peak strain for base polysulfide is about 0.87 m/m and Pμb filled polysulfide ranges from 0.81 to 0.88 m/m. The average strain rates also remained same for all cases and it ranges from 3,977/s to 4,191/s. However, the average peak stress and stress raise rate decreases with increased filler content. The peak stress for base polysulfide is 258 MPa and it reduces to 246, 227, and 194 MPa at 10, 20, and 30 wt. % of Pμb, respectively. The stress rise rate decreases more significantly with increasing percent of microballoon.

The stress rate reduction is 51, 65, and 73% for 10, 20, and 30% filler content. The Table also contains the half-power bandwidth, which is nearly the same for both filled polysulfide elastomer. The normalized peak stress and normalized stress rise rate as a function of weight percent of Pμbs are shown in Figures 5.13 and 5.14. The first point in the Figures 5.13 represents base polysulfide values. It is observed that both peak stress and stress rise rate decrease with increasing amount of Pμbs. This indicates that the incorporation of Pμb to polysulfide is beneficial in attenuating the peak and stress rise rate.

Table 5.3 Summary of High Strain Rate Test Results for Base & Microballoon Filled Polysulfide Tested at Breech Pressure of 0.16 MPa

Specimen No.	Peak Strain, ε_{peak}, m/m	Strain Rate, /s	Peak Stress, σ_{peak}, MPa	Stress Rate @ HPB, GPa/s
LP2-0-4	0.87	4,099	264	8,021
LP2-0-7	0.86	4,030	258	7,371
LP2-0-9	0.87	4,111	250	8,012
LP2-10-1	0.76	3,918	250	4,054
LP2-10-3	0.88	4,026	234	3,872
LP2-10-4	0.79	3,990	257	4,066
LP2-10-5	0.81	4,189	246	3,404
LP2-20-2	0.87	4,186	227	2,344
LP2-20-4	0.88	4,157	227	2,369
LP2-20-5	0.82	3,938	229	3,356
LP2-20-6	0.92	4,483	227	2,951
LP2-30-2	0.81	4,139	238	2,700
LP2-30-3	0.91	4,066	210	2,063
LP2-30-5	0.88	4,032	203	1,998
LP2-30-6	0.91	3,670	125	1,666

Table 5.4 Summary of Peak Strain, Strain Rate, Peak Stress, and Stress Raise Rate at Breech Pressure of 0.16 MPa

Filler Content wt%	Peak Strain, ε_{peak}, m/m	Strain Rate, /s	Peak Stress, σ_{peak}, MPa	Stress Rate @ HPB, GPa/s	Half Power Bandwidth,μs
0 (Base)	0.87 (0.01)*	4,080 (44)	258 (7)	7,802 (373)	62 (7)
10% μb	0.81 (0.05)	4,031 (114)	246 (10)	3,849 (310)	53 (6)
20% μb	0.87 (0.04)	4,191 (224)	227 (1)	2,755 (489)	57 (12)
30% μb	0.88 (0.05)	3,977 (210)	194 (48)	2,107 (432)	63 (15)

* The values given in parenthesis are the standard deviation

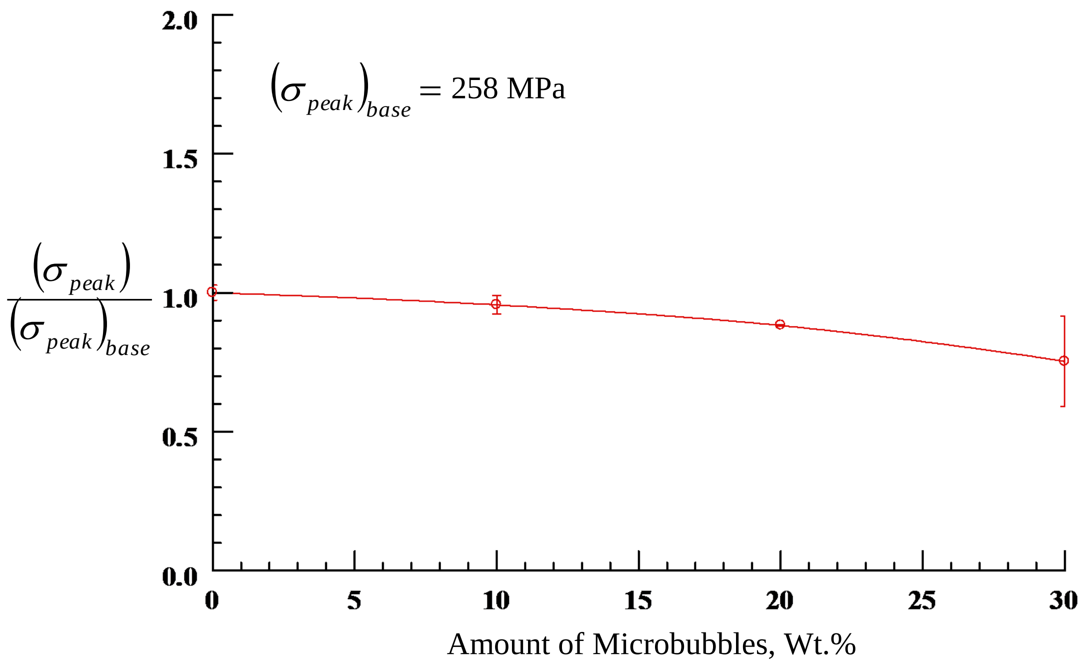

Figure 5.13 Plot of normalized Peak Stress vs. Amount of Pμbs at breech pressure of 0.16 MPa

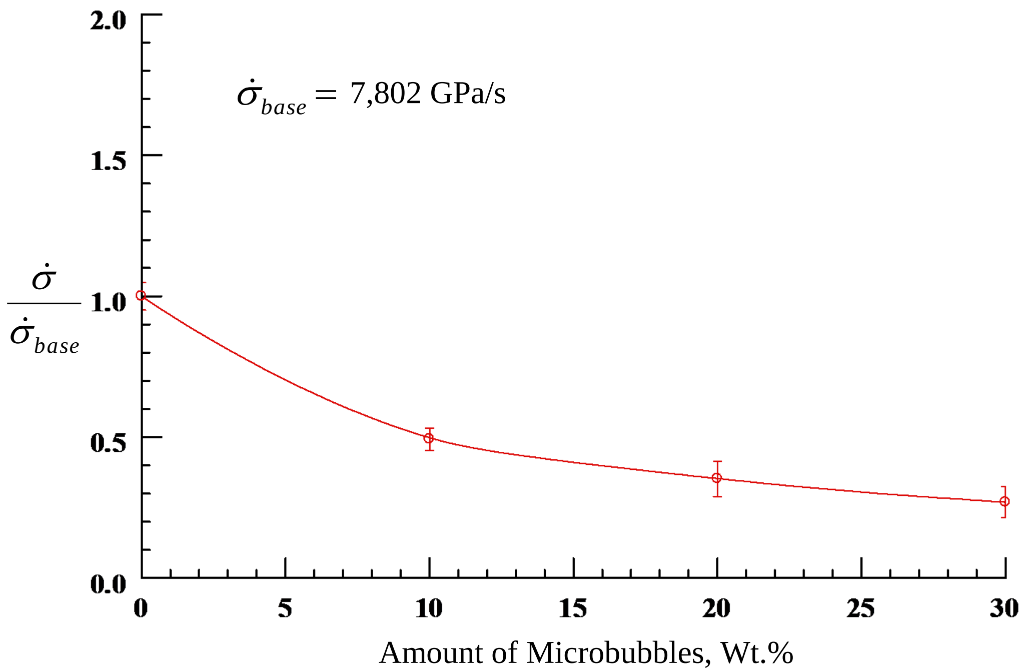

Figure 5.14 Plot of normalized Stress Rise Rate vs. Amount of Pμbs at breech pressure of 0.16 MPa

5.4.2 Effect of % wt. of Pμbs on Stress-Strain Response

Figure 5.15 illustrates the dynamic compressive stress-strain response of base polysulfide specimens at strain rates near 4,100/s. The stress-strain curves are plotted in engineering stress and engineering strain. The stress-strain curves for all those test specimens show very similar response, therefore the results are repeatable. All specimens show linearly elastic region at low strains, followed by the middle nonlinear region, which may be due to the collapse of voids, then the densification zone where the stress rises steeply. The first region shows a linear elastic response and the third region shows the solid behavior of the elastomer. The second region, which joins the two, shows a period where the microballoons collapse and the elastomer flows plastically.

Figure 5.16 presents the dynamic compressive stress-strain response of polysulfide with 10 wt.% of Pμbs at strain rates near 4,000/s. The strain rate ranges from 3,918/s to 4,189/s. Dynamic compressive experiments on 10 wt.% Pμbs filled polysulfide shows constitutive behaviors very similar to the stress-strain curves shown in Figure 5.15, except for the strain levels. All the stress–strain curves are close to each other regardless of strain rates except one specimen, which show more elongated stress-strain curve. The reason may be due to the presence of more voids, unfilled spaces and early cracks in the matrix.

Figure 5.17 shows the dynamic compressive stress-strain response of polysulfide with 20 wt.% of Pμbs at strain rates near 4,200/s. The strain rate ranges from 3,938/s to 4,483/s. The shape of the stress-strain curves of all the four specimens' are similar but they are spread out in the densification region. All the specimens showed a kink in the stress-strain curve at strain of around 0.63. This can be attributed to one or all of the following deviations; presence of more voids, collapse of Pμb and early cracks in the matrix. For all specimens, the dynamic stress-strain curves overlap each other at linear elastic region. Furthermore, densification begins at a strain of around 67% where new and denser structures are being formed in the specimen.

Figure 5.18 illustrates the dynamic compressive stress-strain response of polysulfide with 30 wt.% of Pμbs at strain rates near 4,000/s. The strain rate ranges from 3,670/s to 4,139/s

Figure 5.18 again shows similar stress-strain curves as that of the 20 wt.% Pμb filled polysulfide specimens. All the dynamic compressive stress-strain curves show similar responses but they are spread out in the densification region.

All the specimens show a kink in the stress-strain curve at a strain of around 0.63 except one of the specimen, which show a kink near strain of 0.72. For all specimens, the dynamic stress-strain curves overlap each other at linear elastic region and the densification phenomenon begin at a strain of around 64%.

Figure 5.19 summarizes the dynamic compressive stress-strain curves for both base and Pμb filled polysulfide at strain rates near 4,000/s. The stress-strain curves presented in Figure 5.19 are average curves of each types of specimens tested. At strain below 0.4, both base and Pμb filled polysulfide show similar linear elastic response. The Pμb filled polysulfide show early onset of densification than the base polysulfide.

All the samples exhibits an initial elastic regime, a plastic phase which is followed by a densification region. The polysulfide samples with 20 and 30 wt.% Pμbs show a kink in stress-strain curve at a strain of around 0.63. This can be attributed to one or all of the following deviations; presence of more voids, collapse of Pμb and shear flow of the matrix (see specimens before and after the test).

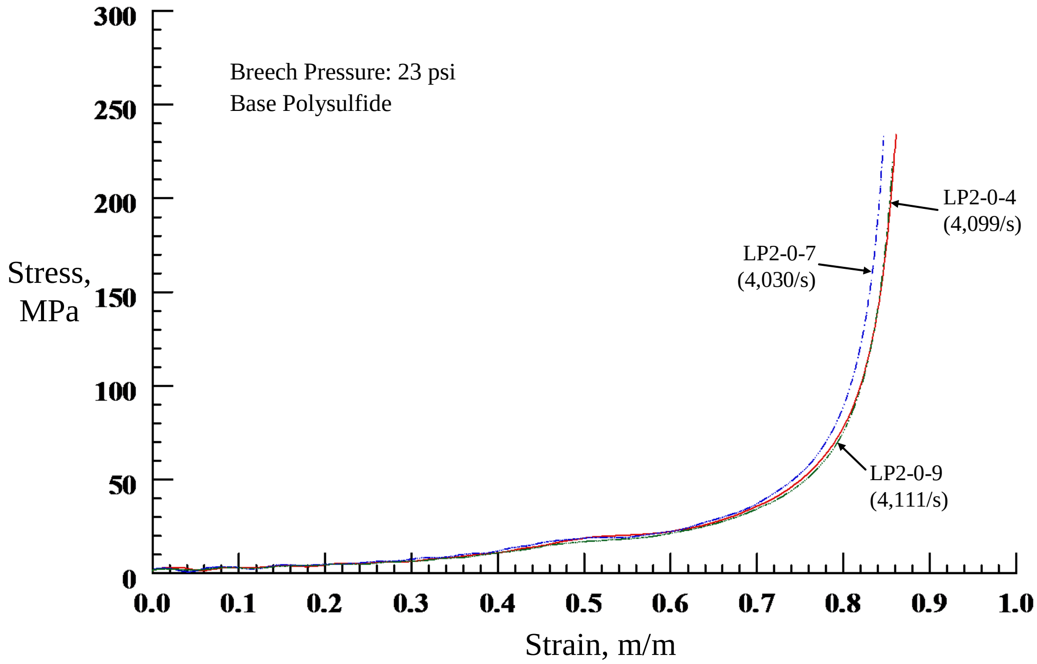

Figure 5.15 Stress-Strain response of base LP2 at breech pressure of 0.16 MPa

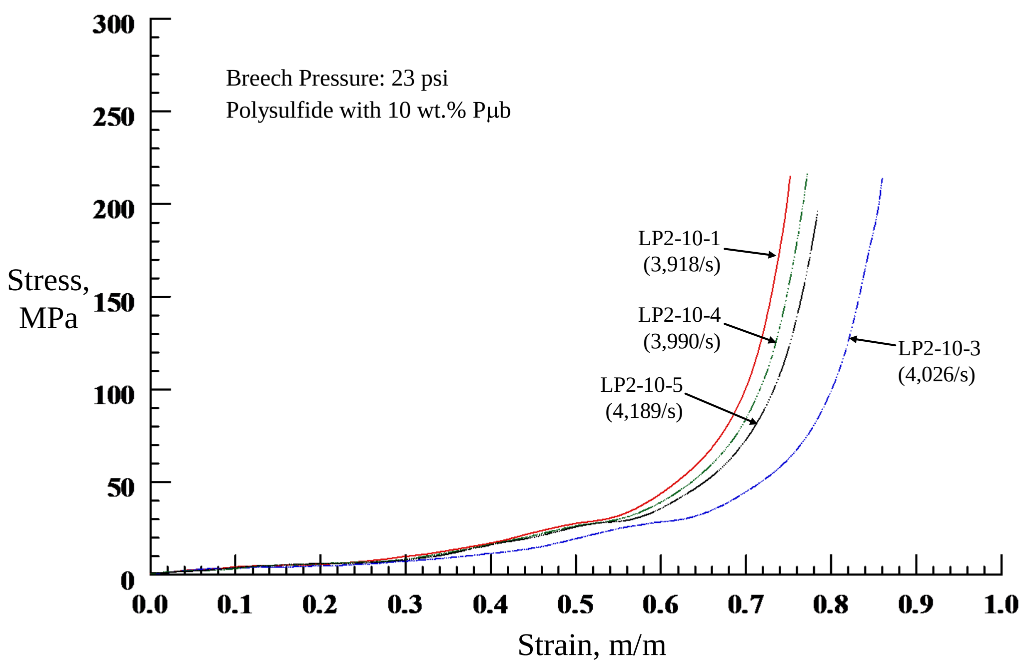

Figure 5.16 Stress-Strain response of 10 wt.% Pμb-filled LP2 at breech pressure of 0.16 MPa

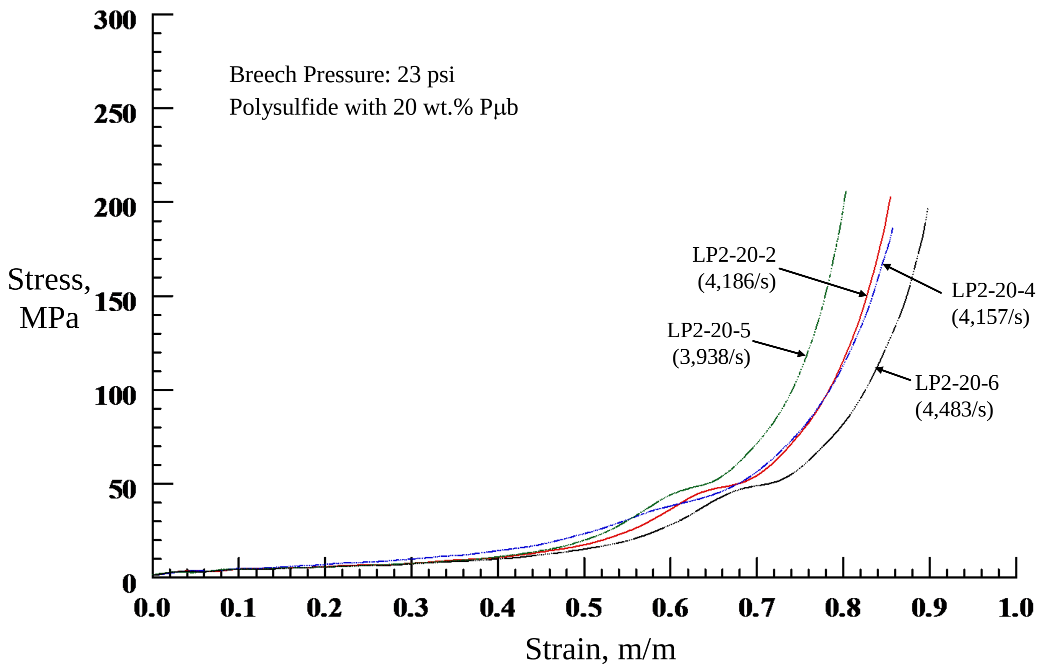

Figure 5.17 Stress-Strain response of 20 wt.% Pμb-filled LP2 at breech pressure of 0.16 MPa

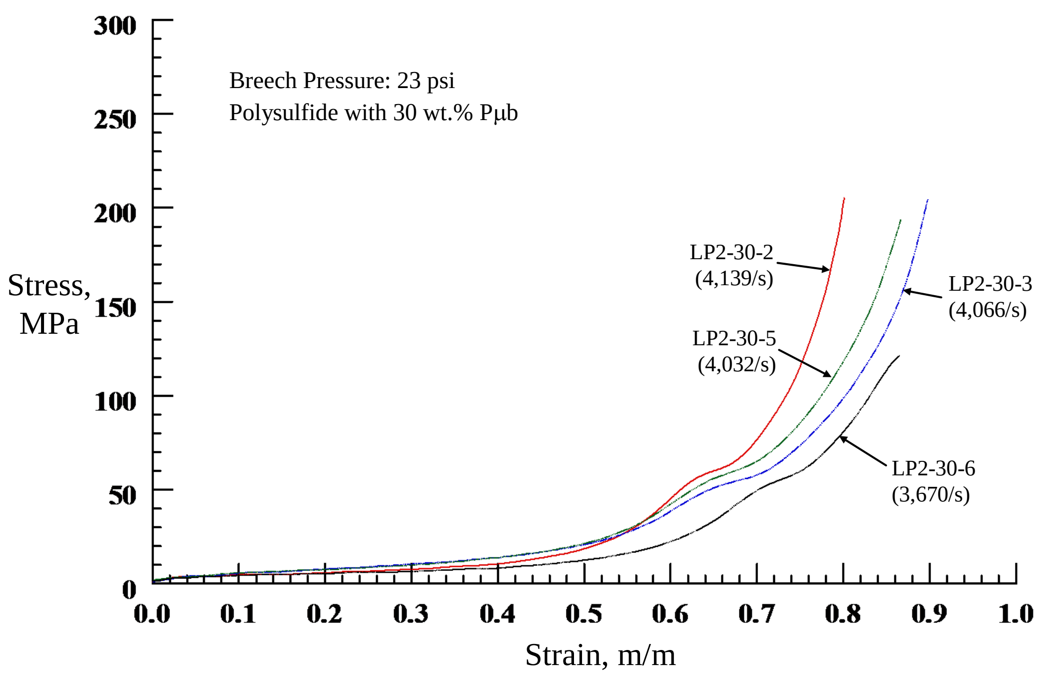

Figure 5.18 Stress-Strain response of 30 wt.% Pμb-filled LP2 at breech pressure of 0.16 MPa

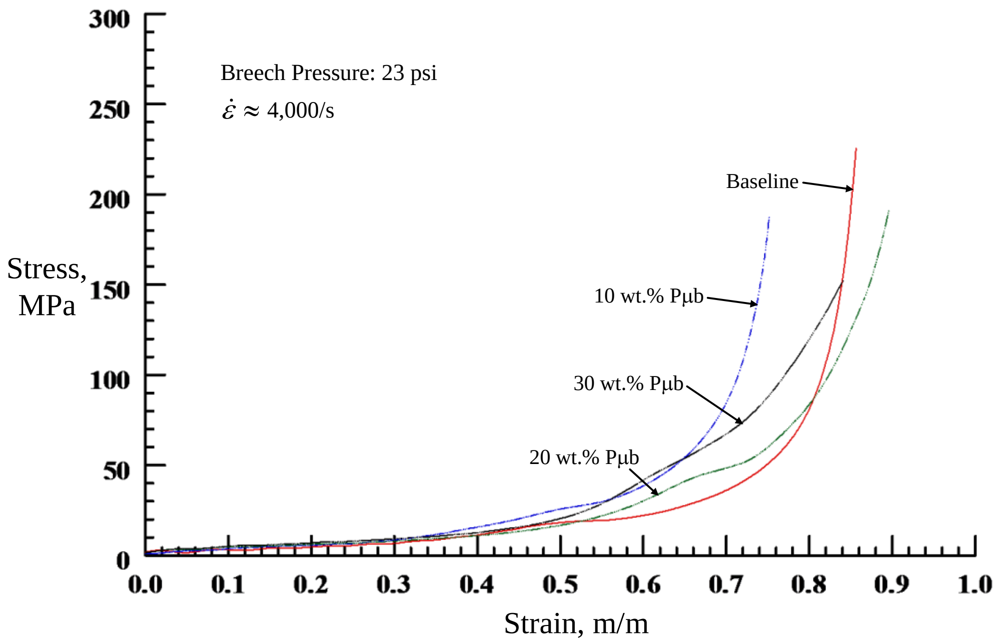

Figure 5.19 Average Stress-Strain Response of Pμb-filled LP2 at breech pressure of 0.16 MPa

5.4.3 High Strain Test Results for 0.11MPa Breech Pressure

Table 5.5 lists the peak strain, strain rate, peak stress and stress rise rate obtained from a high strain rate testing for base and microballoon filled polysulfide at a breech pressure of 0.11 MPa. It can be observed from Table 5.5 that the results are consistent and show the repeatability. The tested parameters of all the samples are within co-efficient of variation of 13% except for the case of base and 30 wt.% Pμb-filled polysulfide. The polysulfide samples with 30 wt.% microballoons show co-efficient of variation up to 30%. The reason may be due to difficulty in mixing higher loading of Pμbs in polysulfide. The plots of stress vs. time and strain vs. time for all the base and microballoon filled polysulfide are provide in appendix.

Table 5.5 Summary of High Strain Rate Test Results for Base & Pμb-filled Polysulfide Tested at Breech Pressure of 0.11 MPa

Specimen No.	Peak Strain, ε_{peak}, m/m	Strain Rate, /s	Peak Stress, σ_{peak}, MPa	Stress Rate @ HPB, GPa/s
LP2-0-6	0.87	2,985	68	1,399
LP2-0-10	0.86	2,996	52	688
LP2-0-11	0.87	3,070	43	414
LP2-10-6	0.86	3,386	93	905
LP2-10-7	0.89	3,464	97	*
LP2-10-8	0.87	3,317	77	837
LP2-10-11	0.88	3,338	75	764
LP2-20-7	0.84	3,213	72	903
LP2-20-8	0.85	3,224	67	726
LP2-20-9	0.74	2,856	70	685
LP2-20-10	0.85	3,232	68	756
LP2-30-7	0.82	3,041	54	547
LP2-30-8	0.78	2,734	35	520
LP2-30-11	0.75	2,610	30	342
LP2-30-12	0.82	3,059	56	567

* Data Dropped

Table 5.6 summarizes the average values of peak strain, strain rate, peak stress, stress rise rate and half-power bandwidth of stress pulse for unfilled and filled polysulfide at a breech pressure of 0.11MPa. As noted previously, both peak strain and strain rate almost remain unchanged with Pμb filler content. The average strain rates range from 2,861/s to 3,376/s. The average peak stress for base polysulfide is 54 MPa and for the filled polysulfide are 86, 69, and 44 MPa for 10, 20, and 30 wt. % of Pμb, respectively. The rise in the peak stress for 10% filler content is an anomaly.

The average stress rise rate is also reduced with the Pμb-filler content except for 10% filler content. The normalized peak stress and normalized stress rise rate as a function of amount of Pμbs are given in Figures 5.19 and 5.20.

Table 5.6 Summary of Peak Strain, Strain Rate, Peak Stress, and Stress Raise Rate at Breech Pressure of 0.11 MPa

Sample	Peak Strain, ε_{peak}, m/m	Strain Rate, /s	Peak Stress, σ_{peak}, MPa	Stress Rate @ HPB, GPa/s
Baseline	0.87 (0.01)*	3,017 (46)	54 (13)	834 (509)
LP2_10pmb	0.88 (0.01)	3,376 (65)	86 (11)	835 (71)
LP2_20pmb	0.82 (0.05)	3,131 (184)	69 (2)	768 (95)
LP2_30pmb	0.79 (0.03)	2,861 (224)	44 (13)	494 (103)

* The values given in parenthesis are the standard deviation

The first point in the Figures 5.20 and 5.21 represents base polysulfide values. It is observed that the effect of % wt. of microballoons on the peak stress and stress rise rate appeared puzzling because both peak stress and stress rise rate are increasing nonlinearly till 10 wt. % of Pμb and then it shows a decreasing trend.

An important note that the standard deviation of strain rate between specimens is lower in base line category compared to significantly higher with 30% wt. of Pμb where as the stress rise rate is quite the opposite. This clearly shows the effect of microballoons in the reduction of stress rise rates.

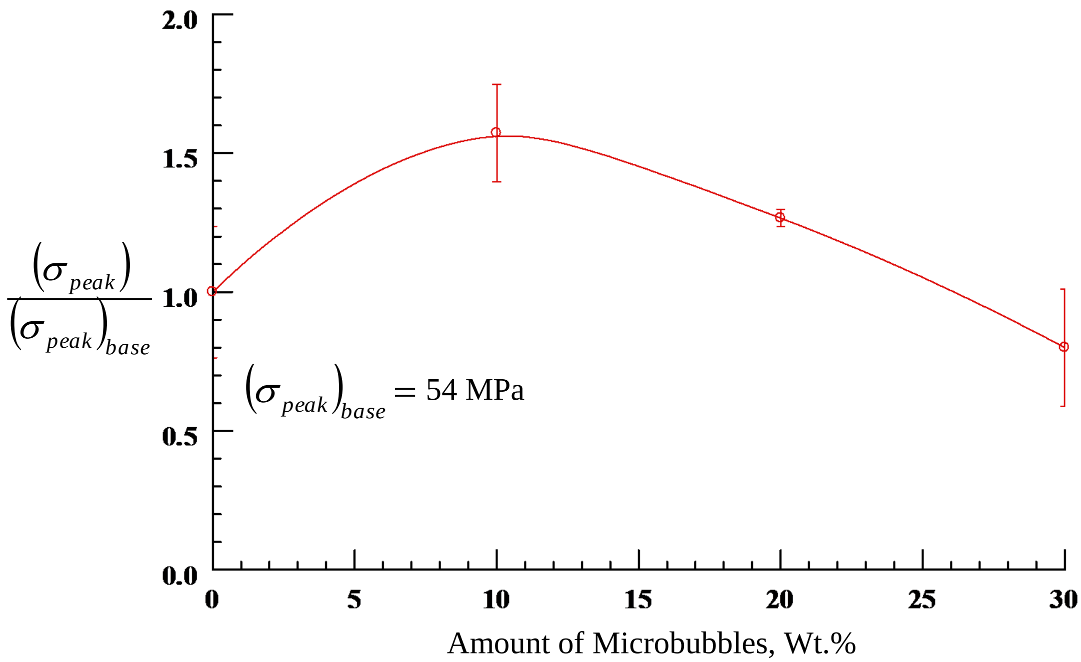

Figure 5.20 Plot of normalized Peak Stress vs. Amount of Pµbs at breech pressure of 0.11 MPa

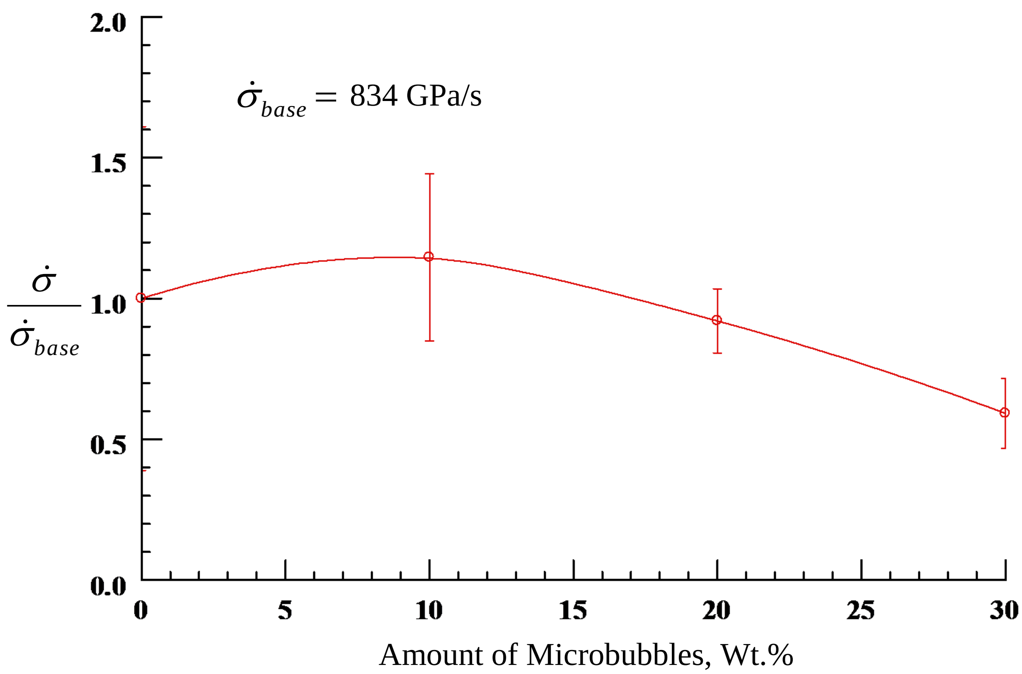

Figure 5.21 Plot of normalized Stress Rise Rate vs. Amount of Pµbs at breech pressure of 0.11 MPa

Figure 5.22 illustrates the dynamic compressive stress-strain response of base polysulfide specimens at strain rates near 3,000/s. The stress-strain curves are plotted in measures of engineering stress and engineering strain. The inset in the plot is the exaggerated graph of stress vs. strain. All the dynamic compressive stress-strain curves show very similar response, proving the results are repeatable. All specimens show linearly elastic region at strains up to 0.4, followed by the nonlinear region till strains of 0.8. The non-linear region may be due to the collapse of voids.

Figure 5.23 presents the dynamic compressive stress-strain response of polysulfide with 10 wt.% of Pµbs at strain rates near 3,376/s. The strain rate ranges from 3,317/s to 3,464/s. Dynamic compressive experiments on 10 wt.% Pµbs filled polysulfide show constitutive behaviors very similar to the stress-strain curves shown in Figure 5.22, except for the strain levels. All the stress–strain curves are close to each other regardless of strain rates. All the stress-strain curves showed onset of densification in addition to initial linear elastic region and nonlinear region. The reason may due to the higher strain rates at which these specimens are tested.

Figure 5.24 shows the dynamic compressive stress-strain response of polysulfide with 20 wt.% of Pµbs at strain rates near 3,131/s. The strain rate ranges from 2,856/s to 3,232/s. The shape of the stress-strain curves of all the specimens is similar but except for one of the specimens. All the specimens showed a kink in the stress-strain curve at strain of around 0.66 except for the one of the specimen, which showed a kink near 0.50.

All the stress-strain curves show onset of densification in addition to initial linear elastic region and nonlinear region. The reason may due to the higher strain rates at which these specimens are tested.

Figure 5.25 illustrates the dynamic compressive stress-strain response of polysulfide with 30 wt.% of Pμbs at strain rates near 2,861/s. The strain rate ranges from 2,610/s to 3,059/s. Figure 5.25 show similar stress-strain curves as that of base polysulfide specimens. All the dynamic compressive stress-strain curves show similar response. For all specimens, the dynamic stress-strain curves overlap each other at initial linear elastic region.

Figure 5.26 summarizes the dynamic compressive stress-strain curves for both base and Pμb filled polysulfide at strain rates near 3,000/s. The stress-strain curves presented in Figure 5.19 are average curves of the repeatable data. At strain below 0.44, both base and Pμb filled polysulfide show similar linear elastic response. All the samples exhibited an initial elastic regime followed by a nonlinear region. The nonlinear region of all the Pμb filled polysulfide lies above that of the base polysulfide. The polysulfide samples with 20 wt.% Pμbs show a kink in stress-strain curve at a strain of around 0.66. This can be attributed to one or all of the following deviations: presence of more voids, collapse of Pμb and early cracks in the matrix.

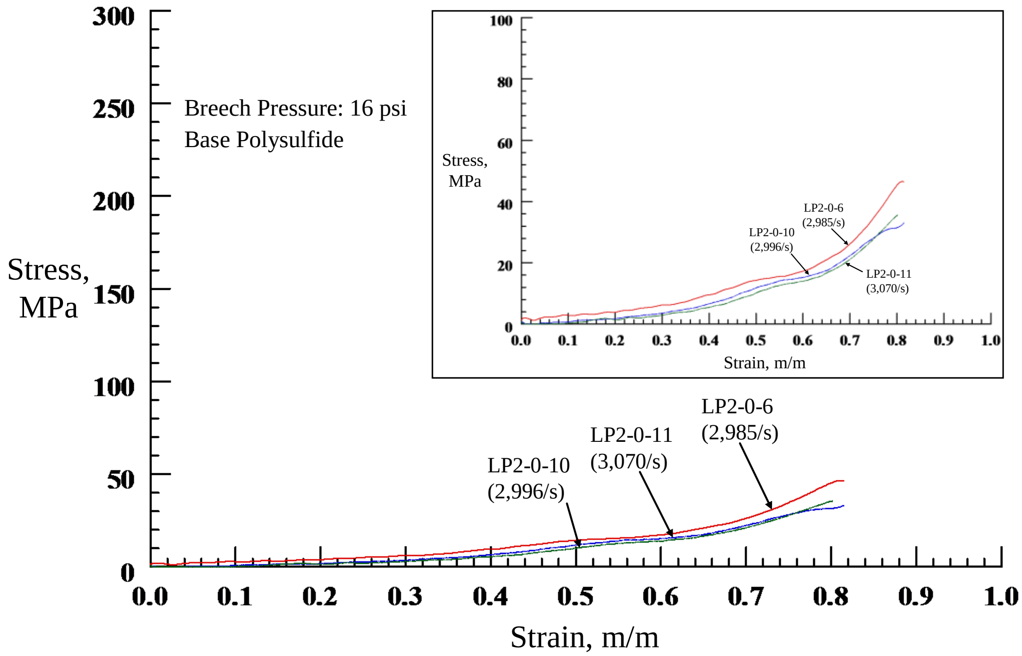

Figure 5.22 Stress-Strain response of base LP2 at breech pressure of 0.11 MPa

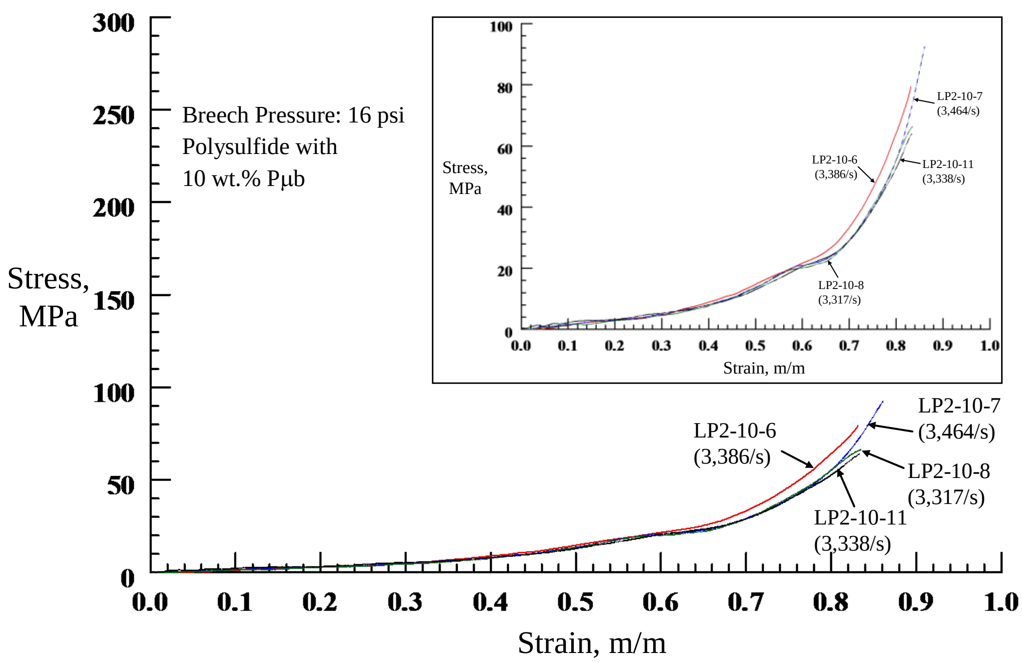

Figure 5.23 Stress-Strain response of 10 wt.% Pµb-filled at breech pressure of 0.11 MPa

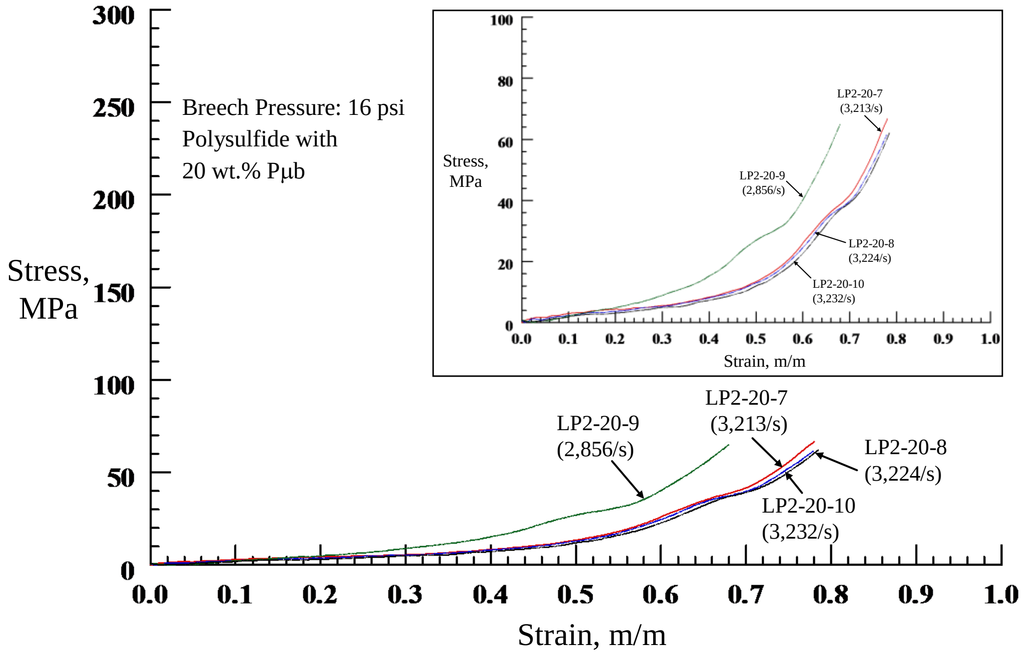

Figure 5.24 Stress-Strain response of 20 wt.% Pμb-filled at breech pressure of 0.11 MPa

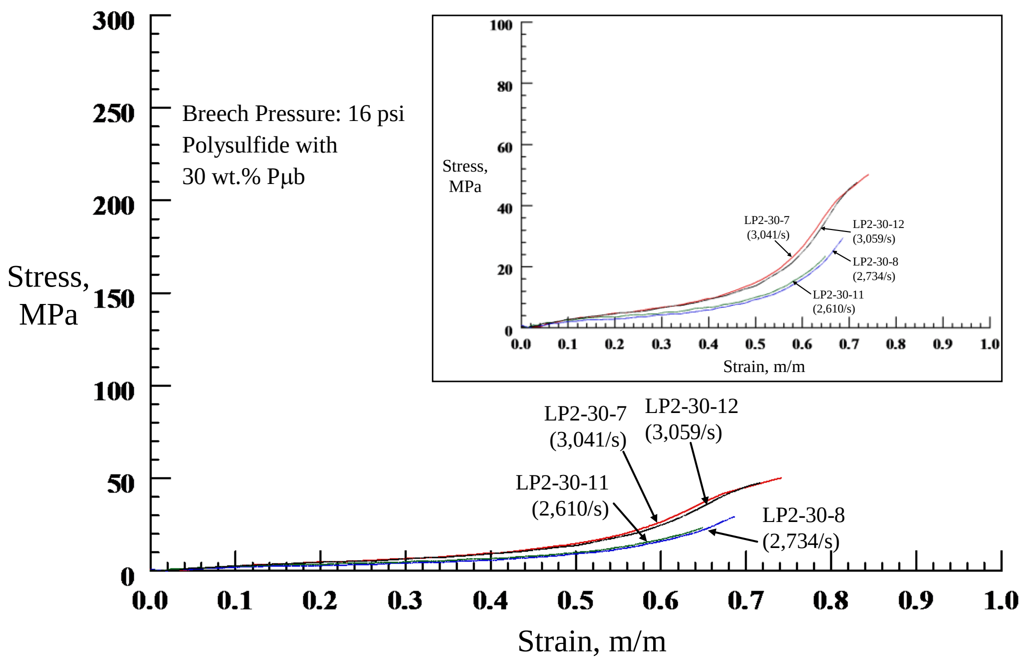

Figure 5.25 Stress-Strain response of 30 wt.% Pμb-filled at breech pressure of 0.11 MPa

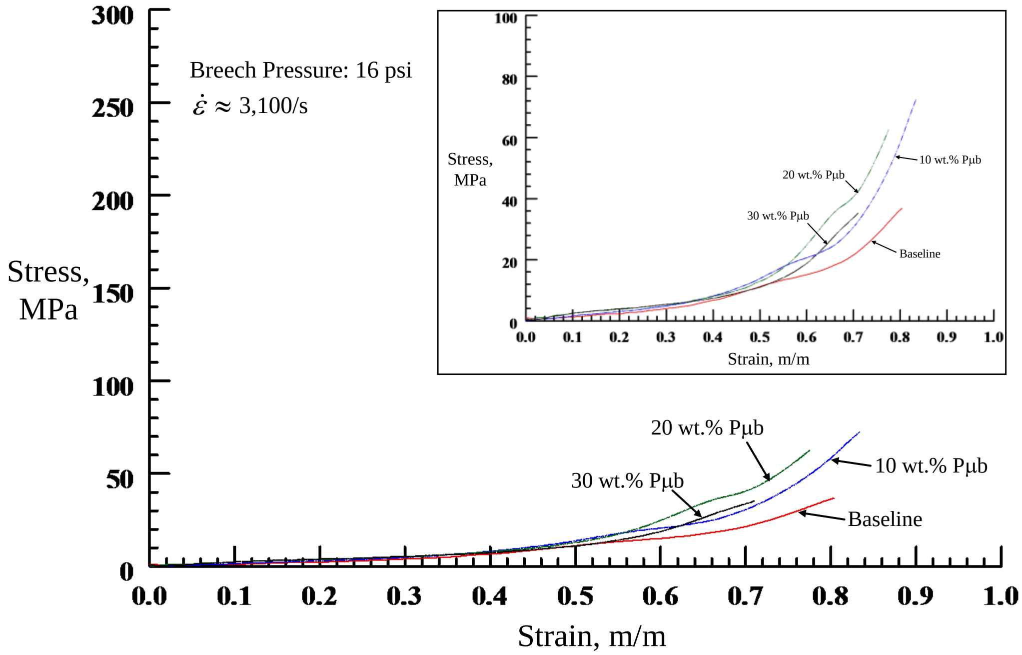

Figure 5.26 Average Stress-Strain response of Pμb-filled LP2 at breech pressure of 0.11 MPa

5.4.4 High Strain Test Results for 0.19 MPa Breech Pressure

Table 5.7 lists the peak strain, strain rate, peak stress and stress rise rate obtained from a high strain rate testing for base and microballoon filled polysulfide at a breech pressure of 27 psi. It can be observed from that Table 5.7 that the results are consistent and showed repeatability. The tested parameters of all the samples are within co-efficient of variation of 10% except for the case of 10 wt.% Pμb-filled polysulfide. The plot of stress versus time and strain versus time for all the base and microballoon filled polysulfide is given in Appendix.

Table 5.7 High Strain Rate Test Results for Base & Microballoon Filled Polysulfide Tested at Breech Pressure of 0.19 MPa

Specimen No.	Peak Strain, ε_{peak}, m/m	Strain Rate, /s	Peak Stress, σ_{peak}, MPa	Stress Rate @ HPB, GPa/s
LP2-0-8	0.91	4,516	284	7,706
LP2-0-13	0.89	4,500	281	7,154
LP2-0-15	0.91	4,691	283	8,687
LP2-10-12	0.92	4,601	269	*
LP2-10-13	0.92	4,841	279	4,951
LP2-10-14	0.92	4,845	288	4,767
LP2-10-16	0.92	4,861	288	5,125
LP2-20-11	0.92	4,460	266	3,458
LP2-20-12	0.94	4,568	266	3,246
LP2-20-13	0.92	4,452	271	3,510
LP2-20-14	0.93	4,639	278	4,022
LP2-30-13	0.91	4,421	279	4,020
LP2-30-14	0.93	4,538	279	3,735
LP2-30-15	0.93	4,530	276	3,801
LP2-30-17	0.90	4,497	280	3,931

* Data dropped

Table 5.8 summarizes the average values of peak strain, strain rate, peak stress, stress rise rate for filled and unfilled polysulfide at a breech pressure of 0.19 MPa. The value within the parenthesis is the standard deviation. As expected, both peak strains and strain rates almost remain unchanged. Also noted is that the reduction in peak stress rate is limited to 5%. This result indicates that higher breech pressures, the peak stress reduction is limited or none. Also note the very high strain rates 4,487/s to 4,787/s. On the other hand the stress rise rate does not reduce with filler content [44]. The reduction is about 35, 55, and 51% for Pμb contents of 10, 20, and 30% by weight, respectively. The normalized peak stress and normalized stress rise rate as a function of amount of Pμbs are given in Figures 5.19 and 5.20. The first point in these figures represents base polysulfide values. It is observed that the peak stress is almost same irrespective of the amount of Pμbs. The stress rise rate is decreasing nonlinearly with increasing amount of Pμbs. This indicates that the incorporation of Pμbs to polysulfide is beneficial in attenuating the stress, which is important for shock mitigation of structures.

Table 5.8. Summary of Peak Strain, Strain Rate, Peak Stress, and Stress Raise Rate at Breech Pressure of 0.19 MPa

Sample	Peak Strain, ε_{peak}, m/m	Strain Rate, /s	Peak Stress, σ_{peak}, MPa	Stress Rate @ HPB, GPa/s
Baseline	0.90 (0.01)*	4,569 (106)	283 (1)	7,849 (776)
LP2_10pmb	0.92 (0.01)	4,787 (124)	281 (9)	4,948 (179)
LP2_20pmb	0.93 (0.01)	4,530 (90)	270 (5)	3,559 (329)
LP2_30pmb	0.92 (0.02)	4,497 (53)	279 (2)	3,872 (128)

* The values given in parenthesis are the standard deviation

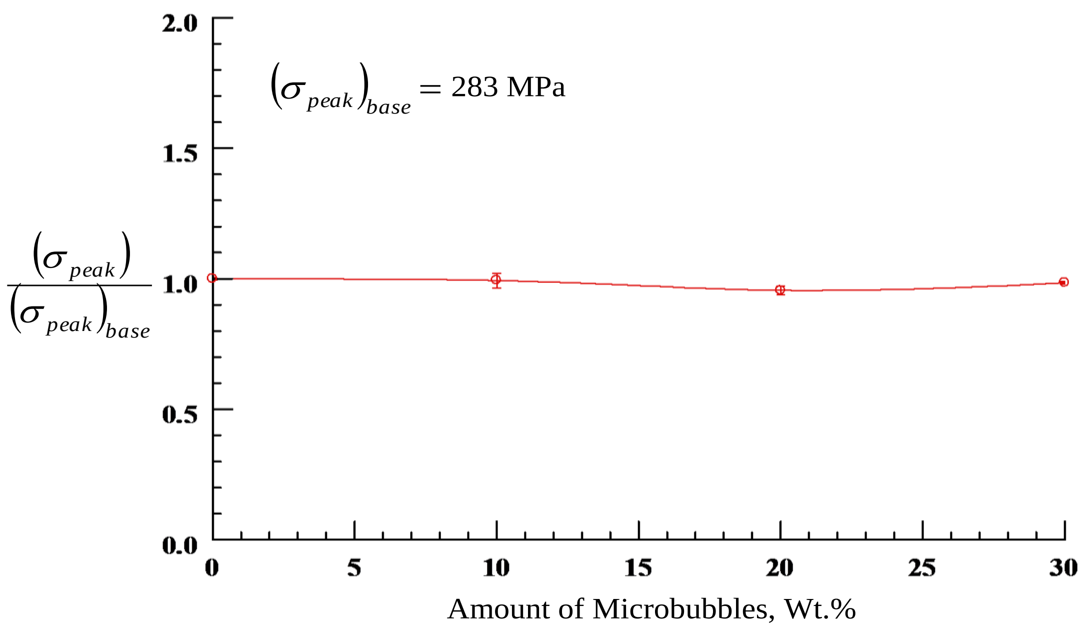

Figure 5.27 Plot of normalized Peak Stress vs. Amount of Pμbs at breech pressure of 0.19 MPa

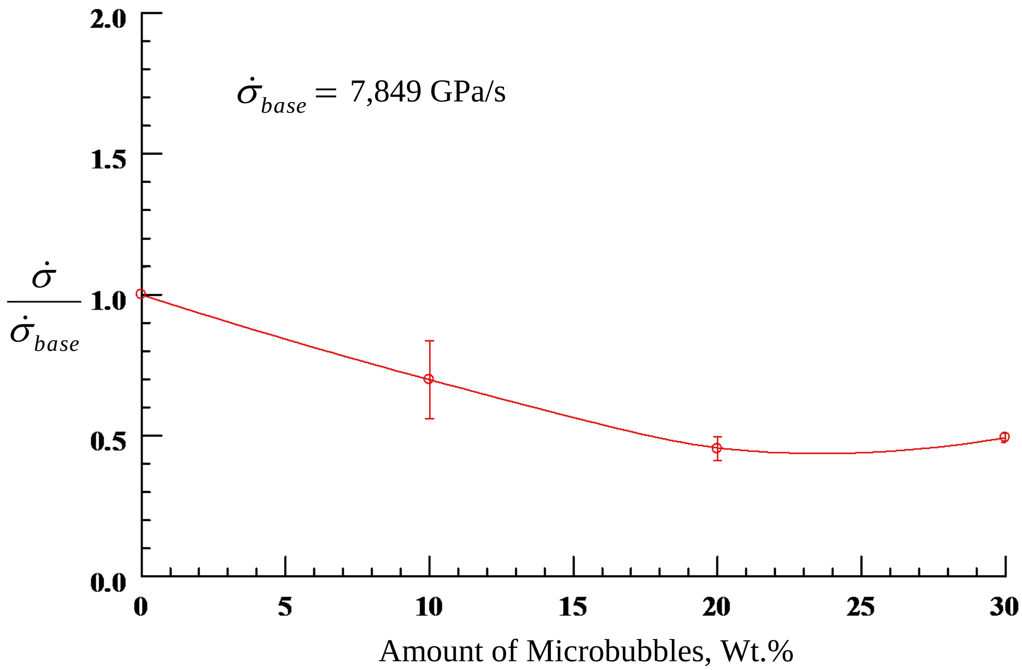

Figure 5.28 Plot of normalized Stress Rise Rate vs. Amount of Pμbs at breech pressure of 0.19 MPa

Figure 5.29 illustrates the dynamic compressive stress-strain response of base polysulfide specimens at strain rates near 4,569/s. The stress-strain curves are plotted in measures of engineering stress and engineering strain. The shapes of the stress-strain curves of all three specimens were similar but they are spread out in the densification region, therefore the results were repeatable. All specimens show linearly elastic region at low strains, followed by the middle nonlinear region, which may be due to the collapse of voids, then the densification zone where the stress rises steeply. The first and third regions show linear elasticity of elastomer. The second region that joins the two shows a period where the elastomer flows like a plastic, which can be attributed to increased load-carrying capacity. The densification phenomenon begins at a strain of approximately

0.65.

Figure 5.30 presents the dynamic compressive stress-strain response of polysulfide with 10 wt.% of Pμbs at strain rates near 4,787/s. The strain rate ranged from 4,601/s to 4,861/s. Dynamic compressive experiments on 10wt.% Pμbs filled polysulfide show constitutive behaviors similar to the stress-strain curves as shown in Figure 5.29. All the stress–strain curves are close to each other regardless of strain rates. Three of the specimens showed kink in the stress-strain curve near a strain of 0.64. The reason may be due to the presence of more voids, unfilled spaces and early cracks in the matrix.

Figure 5.31 shows the dynamic compressive stress-strain response of polysulfide with 20 wt.% of Pμbs at strain rates near 4,530/s. The strain rate ranged from 4,452/s to 4,639/s.

The shape of the stress-strain curves of all the four specimens' is similar but they are spread out in the densification region. All the specimens show a kink in the stress-strain curve at strain of around 0.66. This can be attributed to one or all of the following deviations; presence of more voids, collapse of Pμb and early cracks in the matrix. For all specimens, the dynamic stress-strain curves overlapped each other at linear elastic region. Furthermore, densification began at a strain of around 70% where new and denser structures are being formed in the specimen.

Figure 5.32 illustrates the dynamic compressive stress-strain response of polysulfide with 30 wt.% of Pμbs at strain rates near 4,500/s. The strain rate ranged from 4,421/s to 4,538/s. Figure 5.32 again shows similar stress-strain curves as that of the 20 wt.% Pμb filled polysulfide specimens. All the dynamic compressive stress-strain curves show similar responses but they are spread out in the densification region.

All the specimens show a kink in the stress-strain curve at a strain of around 0.69 except one, which showed a kink near a strain of 0.65. For all specimens, the dynamic stress-strain curves overlap each other at the linear elastic region and the densification phenomenon begins at a strain of around 72%. Figure 5.33 summarizes the dynamic compressive stress-strain curves for both base and Pμb filled polysulfide at strain rates near 4,600/s.

The stress-strain curves presented in Figure 5.33 are average curves of the repeatable data. At strain below 0.4, both base and Pμb filled polysulfide show similar linear elastic response. The Pμb filled polysulfide show early onset of densification than the base polysulfide.

All the samples exhibited an initial elastic regime, a plastic phase which is followed by a densification region. The Pμb filled polysulfide samples show a kink in stress-strain curve at a strain of approximately 0.66. This can be attributed to one or more of the following deviations; presence of more voids, collapse of Pμb and early cracks in the matrix.

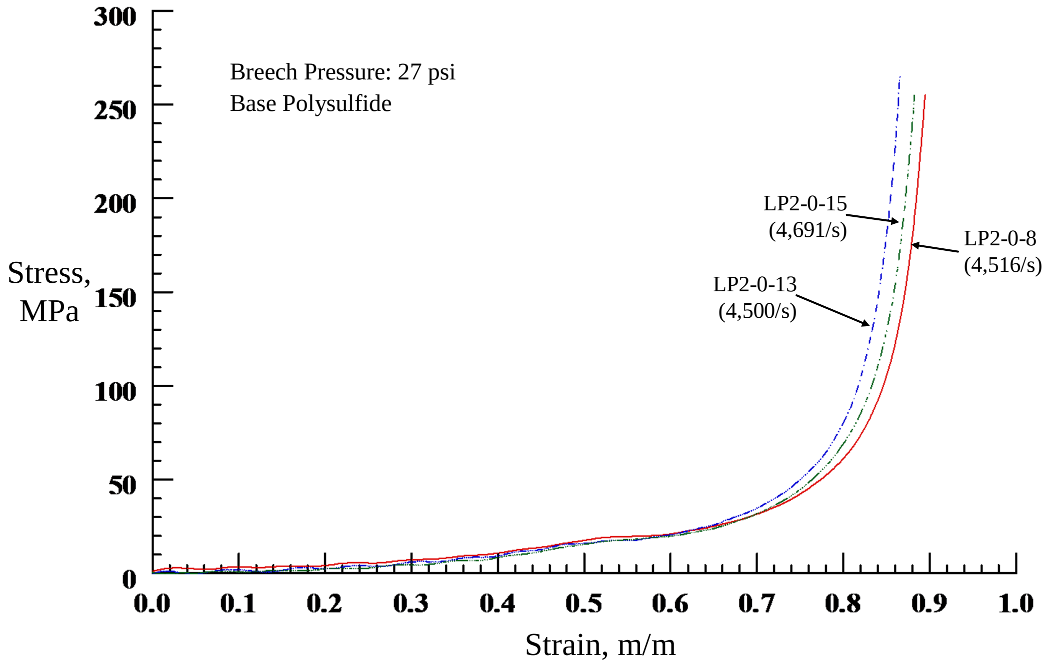

Figure 5.29 Stress-Strain response of base LP2 at Breech Pressure 0.19 MPa

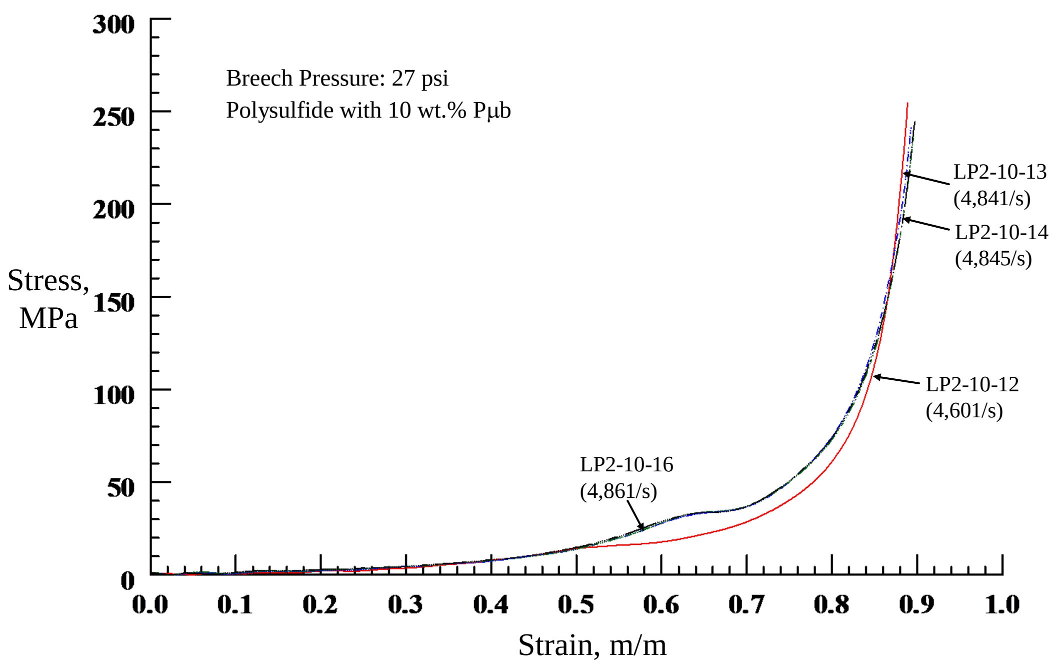

Figure 5.30 Stress-Strain response of 10 wt.% Pμb-filled LP2 at Breech Pressure 0.19 MPa

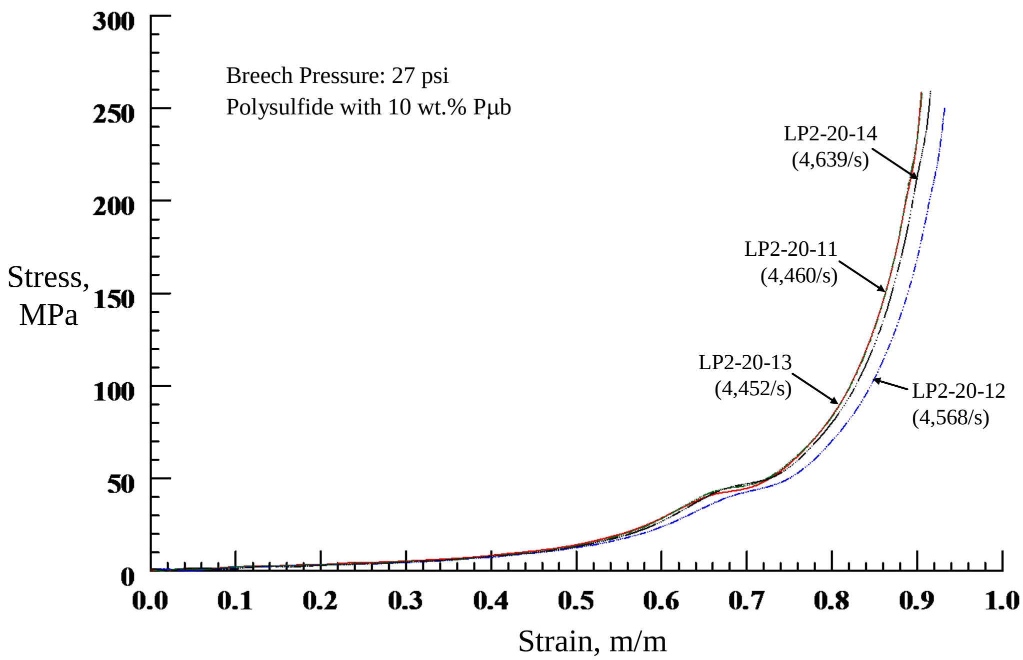

Figure 5.31 Stress-Strain response of 20 wt.% Pμb-filled LP2 at Breech Pressure 0.19 MPa

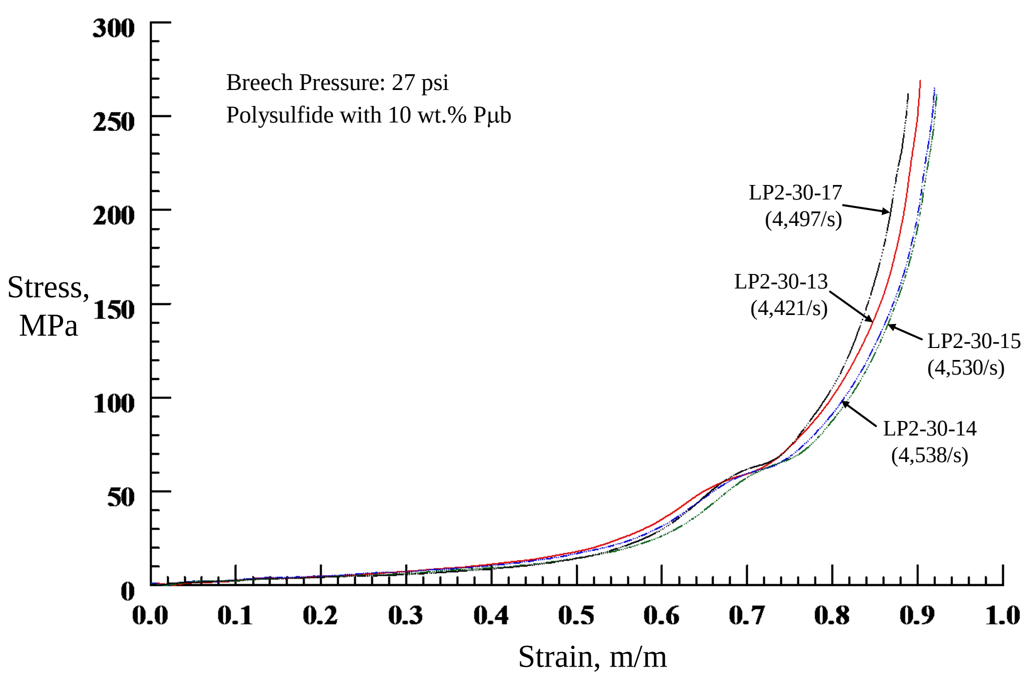

Figure 5.32 Stress-Strain response of 30 wt.% Pμb-filled LP2 at Breech Pressure 0.19 MPa

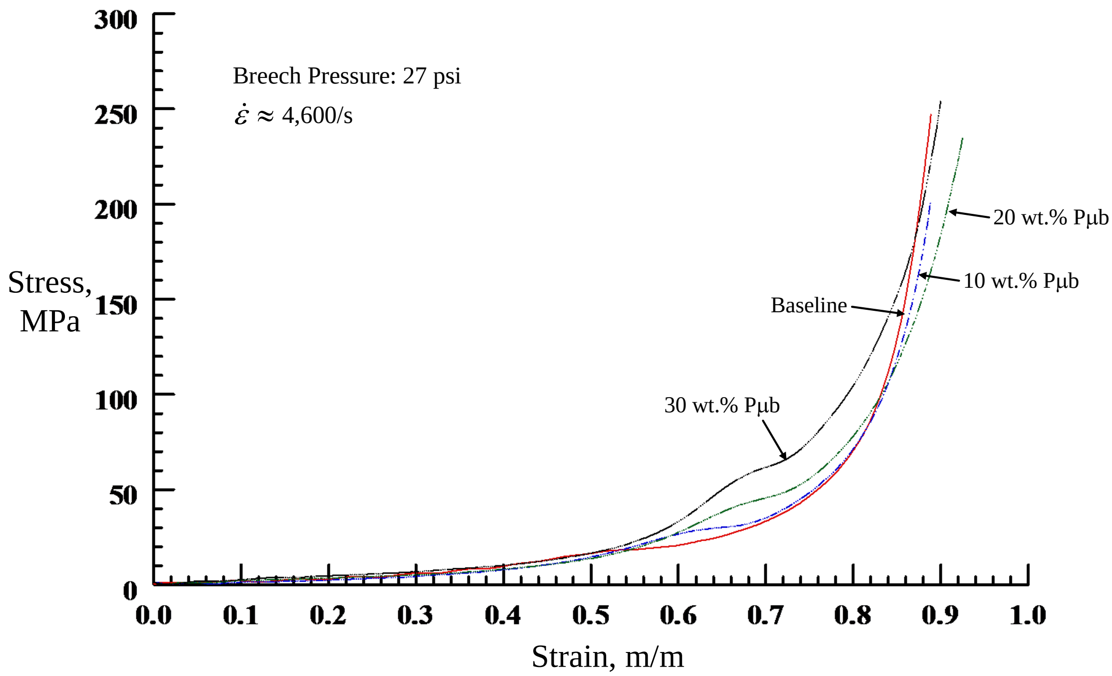

Figure 5.33 Average Stress-Strain response of Pμb-filled LP2 at Breech Pressure 0.19 MPa

5.4.5 Effect of Strain Rate on Base and Pμb Filled Polysulfide

The dynamic compressive stress-strain response of base polysulfide samples at strain rates between 3,017 and 4,569/s is summarized in Figure 5.34. The Figure clearly shows that all the dynamic stress-strain response at strain rates near 3,000/s did not showed the densification phenomenon. The uniaxial compressive stress-strain behavior is observed to be rate dependent and highly non-linear. Figure 5.34 reveals that there is an increase in the stress level with an increase in strain rate for a given strain: but the shape of the response is almost remains unaffected till the onset of densification. The trend is not monotonic.

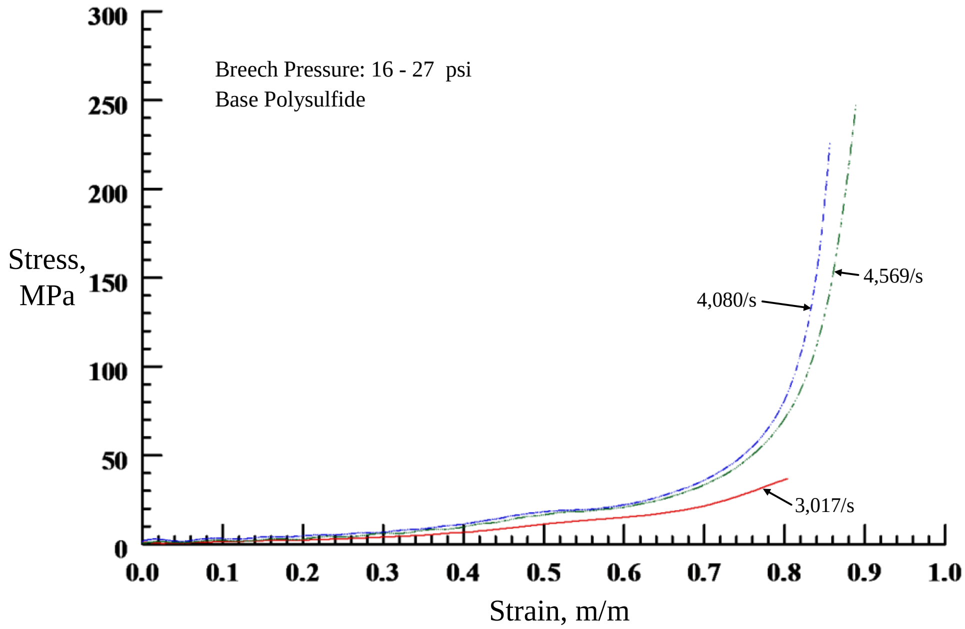

Figure 5.34 Average Stress-Strain response of base polysulfide at strain rates ranging from 3,017/s to 4,569/s

The dynamic compressive stress-strain response of polysulfide with 10 wt.% of Pμb over strain rates between 3,017 and 4,569/s is presented in Figure 5.35. It clearly shows that all the dynamic stress-strain response at strain rates near 3,376/s do not show the densification phenomenon. The specimens tested at strain rates 4,000/s and 4,800/s show prolonged densification region. The stress-strain behavior is observed to be rate dependent and highly non-linear. Figure 5.35 shows that there is an increase in the stress level with an increase in strain rate for a given strain. The trend is not monotonic. After a strain rate of 4,000/s, the adiabatic temperature rising in the specimen during dynamic tests was believed to cause the softening phenomenon which in turn might have reduced the stress levels.

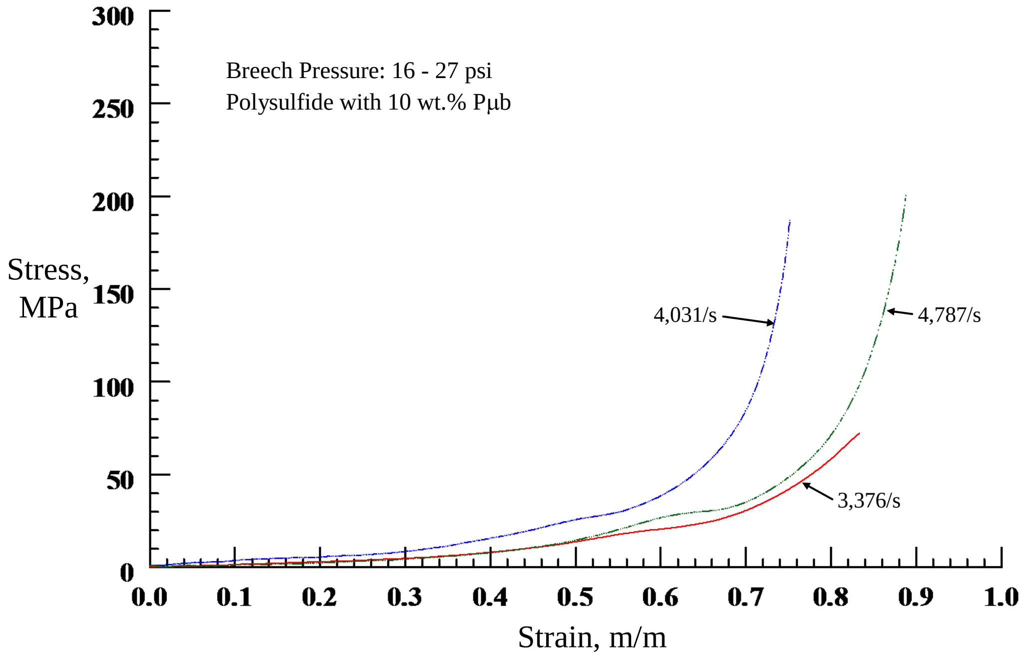

Figure 5.35 Average Stress-Strain response of 10 wt.% Pμb-filled polysulfide at strain rates ranging from 3,376/s to 4,787/s

The dynamic compressive stress-strain response of polysulfide with 20 wt.% of Pμb over strain rates between 3,131 and 4,530/s is summarized in Figure 5.36. It clearly shows that all the dynamic stress-strain response at strain rates near 3,131/s do not show the densification phenomenon. The uniaxial compressive stress-strain behavior is observed to be marginally rate dependent and highly non-linear. Figure 5.36 reveals that there is a marginal increase in the stress level with an increase in strain rate for a given strain: but the shape of the response remains unaffected. The trend is not monotonic.

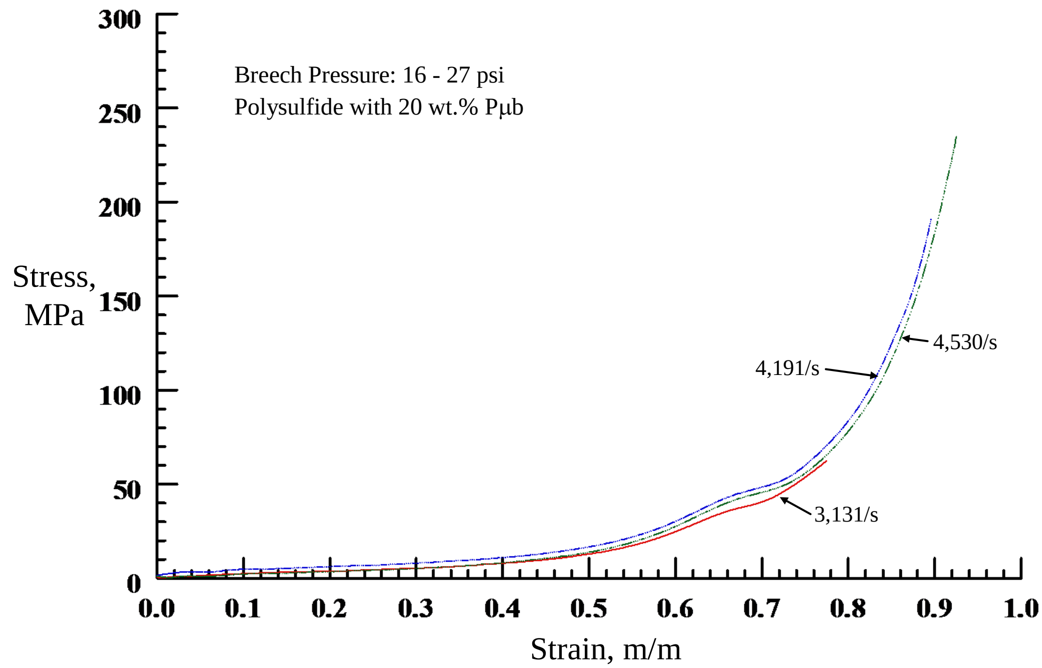

Figure 5.36 Average Stress-Strain response of 20 wt.% Pμb-filled polysulfide at strain rates ranging from 3,131/s to 4,530/s

The dynamic compressive stress-strain response of polysulfide with 30 wt.% of Pμb over strain rates between 2,861/s and 4,497/s is presented in Figure 5.37. It clearly shows that all the dynamic stress-strain response at strain rates near 2,861/s did not showed the densification phenomenon. The specimens tested at strain rates near 4,500/s show prolonged densification region than the specimen tested at strain rates near 4,000/s. The uniaxial compressive stress-strain behavior is observed to be rate dependent and highly non-linear.

Figure 5.37 reveals that there is an increase in the stress level with an increase in strain rate for a given strain: but the shape of the response remained unaffected till the onset of densification. As observed in all Pμb filled polysulfide foams, at strain rate of 4,000/s, or above the adiabatic temperature rise in the specimen during dynamic tests is believed to have cause the softening phenomenon, which in turn might have reduced the stress levels.

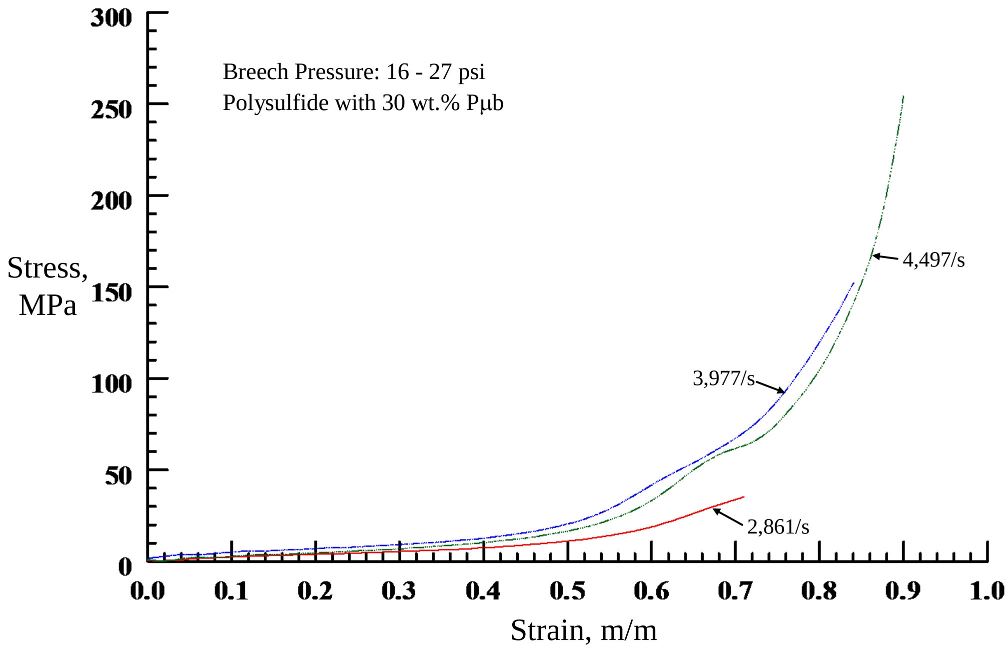

Figure 5.37 Average Stress-Strain response of 30 wt.% Pμb-filled polysulfide at strain rates ranging from 2,861o 4,497/s

5.5 Summary

The compressive high strain rate behavior of the base and Pμb-filled polysulfide is measured using the SHPB apparatus over strain rates between 3,000/s to 4,600/s. The weight percent of microballoons were 0, 10, 20, and 30% of base polysulfide. The peak strain values remain unaffected irrespective of the amount of Pμbs. Both peak stress and stress rise rate decrease and half-power bandwidth of the stress pulse increased as the weight fraction of the Pμb increase thereby indicating that the incorporation of Pμbs in polysulfide does attenuate the stress pulse which is important for shock mitigation of structures.

The peak stress reduction range from 25% to 5% for breech impact pressures of 0.11-0.19 MPa. The higher the impact pressure, the lower will be the reduction in peak stress. The stress rise rate reduces with filler content and it does not alter much with the breech pressure. The reduction in stress rise rate is of the order of 50% for many cases tested. The half-power bandwidth of the stress pulse does not show any clear trend for these experimental analyses.

The dynamic stress-strain response of both base and Pμb-filled polysulfide exhibited initial linear elastic region, a middle nonlinear region followed by a densification region. Polysulfide with 20 and 30 wt.% of microballoon show a kink in the stress-strain curve near a strain of about 0.63 - 0.66. The SHPB experiments revealed that both base and Pμb-filled polysulfide are sensitive to strain rates over the range of strain rates studied. In all Pμb filled polysulfide, the adiabatic temperature rise in the specimen at high strain rates (greater or equal to 4,000/s) causes material softening.

CHAPTER 6

CONCLUDING REMARKS AND FUTURE WORK

6.1 Concluding Remarks

Protection of soldiers and vehicles that carry men and material in combat or noncombat against an ever-increasing firepower of ammunitions and improvised ammunitions by the enemy is a challenging task for the US military. The lightweight and more agile armors are essential so that soldiers can handle attacks with no loss of their war fighting capability. A continuous development and improvement of materials (metals, ceramic and polymer composites) have been carried out for a number of years. Advancements of nanotechnology, computer power, and simulation models have provided an opportunities to develop materials by simulations. However, in the present research modification of elastomer by adding flexible microballoons through a syntactic process is proposed. Elastomer being purely plastic (Poisson's ratio 0.5), transmits a transverse impact or shock directly onto the supporting structure without any modifications. Furthermore, undesirable lateral stresses can cause unexpected failures. To control such stresses, a controlled bulk modulus material is needed. The preferred bulk modulus would be one-third the elastic modulus, which corresponds to zero Poisson's ratio. In this research, an idea of variable bulk modulus material and its impact on shock mitigation is evaluated. Such materials could also be used in packing sensitive instruments and protect structural components against shock and impact.

The goal of the research was to develop a variable bulk modulus elastomeric material using an elastomer and flexible microballoons so that the bulk modulus of the composite material can be varied by the microballoon content. The specific objectives included development of material, fabrication of test samples, and performing static and dynamic tests. The static testing consisted of tension and confined compression test to measure the bulk modulus. Material chosen was liquid polysulfide elastomer LP-2, uncured BJO-093 hollow Pμb (Pμb), and a solid manganese dioxide curing agent. The weight percentage range of Pμb was varied from 0 to 30% that worked out to be 0 to 60% volume percentage, respectively. The material was processed using hand mixing and pressure curing at room temperature. The specimen (tension and compression) were fabricated while allowing the compound to cure in the mold. The specimen materials were analyzed in Scanning Electronic Microscopy and were found to have good distribution of Pμb. Physical properties such as color, density, volume fraction of the constituents and void content were measured.

The concept of variable bulk modulus by using flexible Pμb was examined through simple gas laws. A simple relation between axial stress and axial strain was derived for a confined compression condition based on realistic assumptions. The equation is given by $\varepsilon_a = \left(1 - \frac{1}{(1+\sigma_a / P_1)}\right) V_f$ where σ_a and ε_a are the applied axial stress and calculated axial strains, respectively. The base pressure P_1 was assumed to be one atmosphere. The equation's limiting strain is V_f, which is the volume fraction of the fluid in microballoons and voids.

The equation was extended to include the elastic deformation of the elastomer and the microballoon wall materials and that showed it had a marginal effect. The slope of the axial stress and strain curve gave the bulk modulus. The bulk modulus and the limiting strain were dependent on the percent weight or volume of the Pμb.

Tension and confined compression tests were conducted on LP2- Pμb composite for Pμb content of 0 to 30% of LP2 polysulfide. The tensile modulus increased with increased weight percent of Pμb. The increased modulus was attributed to increased brittleness or stiffness of the matrix. On the other hand, the bulk modulus decreased with increasing Pμb content. The bulk modulus decreased from 19 MPa to 9 MPa from base (0%) to 30% Pμb content. Compressibility is a measure of energy absorption, before the material becomes solid or rigid-plastic. The compressibility was found to be directly proportional to the filler content. The compressibility increased to 43% when the Pμb content changed from 0 to 20% by weight. The data beyond 20% Pμb was not reliable because of processing difficulty of the composite. Tensile modulus determined by Halpin-Tsai's empirical equation agreed reasonably with the experimental data.

The compressive high strain rate behavior of the base and Pμb filled polysulfide was measured using the SHPB apparatus at strain rates ranged from about 3,000/s to 4,600/s. The peak strain and strain rate values remain unaffected irrespective of the amount of Pμb. Both peak stress and stress rise rate decreased with increasing weight fraction of the Pμb. This indicate a potential of mitigating a stress pulse by the use of flexible syntactic foam. The stress rise rate reduction was of the order of 50% for many filled test specimen.

However, the half-power bandwidth was measured only for few samples and the data was non-conclusive.

6.2 Future Work

The present study was the first attempt to understand the shock mitigation characteristics of flexible syntactic foam. The foam was made from LP2 polysulfide and Pμbs. The study showed the potential of using this material for shock mitigation. However, more detailed study needs to be conducted before one considers this material for application. The present study identified processing difficulties as the microballoon content increased; at high pressures the peak stresses did not reduce; and all high strain rate tests were done the unconfined stress state. These issues need to be revisited. Example, processing the material in a mechanical mixer like extruders; and performing high strain rate tests in a confined stress state like the confined compression test; and increasing the strain rate range from the current 2,800 to 4,900/s to a wider range so that the performance of the material at wide range of strain rate is clearly understood. In addition, the flexible Pμbs may be replaced by high performance balloons to increase the collapsed pressure wall as well as the peak stress tolerance. That apart, the whole system needs to be tested in a multilayer composite grouping if the material is chosen for armor applications.

REFERENCES

[1] Cornerstone Research Group. http://www.crgrp.net/technology/materialsportfolio/syntactics.shtml.

[2] Shivakumar, K.N., Argade, S.D., Sadler, R.L., Sharpe, M.M., Dunn, L., Swaminathan, G., and Sorathia, U., 2006, " *Processing and Properties of Lightweight Fire Resistant Core Material for Sandwich Structures*," Journal of Advanced Materials, Vol. 38, No. 1, pp. 32-38.

[3] Kudo, K., 2008, "*Overseas Trends in the Development of Human Occupied Deep Submersibles and a Proposal for Japan's Way to Take*." Science and Technology Trends Quarterly Review 26, pp. 104–123.

[4] Karst, G., 2002, "*Novel Processing of High-Performance Structural Syntactic Foams*." Society for the Advancement of Material and Process Engineering.

[5] Thim, J., 2005, "*Performing Plastics- Johann Thim examines how plastics set out to conquer the world of sports*." Chemistry & Industry, pp. 20-21.

[6] ASTM D7012-10 Standard Test Method for Compressive Strength and Elastic Moduli of Intact Rock Core Specimens under Varying States of Stress and Temperatures.

[7] Matsuka, S., and Maxwell, B.,1958, "*Response of Linear High Polymers to Hydrostatic Pressure*," Journal of Polymer Science., Vol. 32, pp.131 -159.

[8] Warfield R.W., 1966, "*Compressibility of Bulk Polymers*," Polymer Engineering and Science, pp. 176-180

[9] Burchett O.L. and Bert C.W., 1972, *"The Effect of Specimen Geometry and Lateral Constraint on the Isothermal Compressiblity of Low-Strength Polymeric Materials*," Experimental Mechanics, pp. 328-331.

[10] Hopkinson, J., 1901, "*On the rupture of iron wire by a blow*," Article 38, Original Papers-by the late John Hopkinson, Vol 2, Scientific Papers, B Hopkinson (ed.), Cambridge University Press, pp.316-320.

[11] Hopkinson, J.,1901, "*Further experiments on the rupture of iron wire*," Article 39, Original Papers-by the late John Hopkinson, Vol 2, Scientific Papers, B Hopkinson (ed.), Cambridge University Press, pp. 316-320.

[12] Hopkinson, B., 1914, "*A method of measuring the pressure produced in the detonation of high explosives or by the impact of bullets*," Philos. Trans. R. Soc. London, Ser. Article 213, pp. 437-456.

[13] Kolsky, H., 1949, "*An investigation of the mechanical properties of materials at very high rates of loading*," Proc. Phys. Soc. London, Sect. B 62 (II-B), pp. 676-700.

[14] Bancroft, D., 1941, "*The velocity of longitudinal wave in cylindrical bars*," Physical Review, Vol. 59, pp. 588-593.

[15] Davies, R. M.,1948, "*A critical study of the Hopkinson pressure bar*," Philos. Trans. R. Soc. London, Ser. Article 240 (821), pp. 375-457.

[16] ASM Int (2000): *ASM Handbook*, Mechanical Testing and Evaluation, edited by Howard Kuhn and Dana Medlin, Vol 8, ASM Int, Materials Park OH, pp. 436, 462-476.

[17] Nemat-Nasser S., 2000, ASM Handbook ,"Introduction to high strain rate testing, Vol. 8, Mechanical Testing and Evaluation," ASM Int, Materials Park OH, pp. 427.

[18] Chen, W. and Ravichandran, G., 1997, "*Dynamic Compressive Failure of a Glass Ceramic Under Lateral Confinement*," J. Mech. Phys. Solids, Vol. 45, pp. 1303-1328.

[19] Chen, W., Zhang, B., and Forrestal, M. J., 1999, "*A split Hopkinson bar technique for low impedance materials*," Exp. Mech. Vol. 39, pp. 1-5.

[20] Gary, G., Klepaczko, J. R., and Zhao, H., 1995, *"Generalization of split Hopkinson bar technique to use viscoelastic materials*," Int. J. Impact Eng. Vol. 16, pp. 529-530

[21] Pandurangha, PhD Thesis, 2010, "High Strain Rate Response of Eco-Core & its Modification, Department of Mechanical Engineering," CCMR, N.C. A&T State University, Greensboro,N.C.

[22] Bateman,V.I., Brown, F.I., and Hanson.N.R.,1998 "*A Study of Shock Mitigating Materials in a Split Hopkinson Bar Configuration Phase I*,", Sandia National Laboratory, California.

[23] Bateman,V.I., Brown, F.I., and Hanson, N.R., 1998 "*A Study of Shock Mitigating Materials in a Split Hopkinson Bar Configuration Phase II**," Sandia National Laboratory, California.

[24] Wasley, R.J., Nidick, V.J. Jr., Valentine,R.H., and Hoge, K.G.,1971, "*Shock Pulse Mitigation in Various Organic Foams*," Journal of Applied Polymer Science Vol. 15, pp. 2303-2315, Lawrence Radiation Laboratory, University of California, Livermore, California 94550

[25] Wouterson, E. M., Boey, F. Y. C., Hu, X., and Wong, S., 2005, "*Specific Properties and Fracture Toughness of Syntactic Foam: Effect of Foam Microstructure*," Composites Science and Technology, Vol. 65, pp.1840-1850.

[26] Expancel, Inc., Technical Bulletin 20, 2240 Northmont Parkway, Duluth, GA 30096.

[27] Daniel, I. M. and Ishai, O., 2005, Engineering Mechanics of Composite Materials, 2nd edition, Oxford Univ. Press, NY, USA.

[28] Timoshenko, S., 1970, Theory of Elasticity, McGraw-Hill Companies, NY.

[29] Toray Corp., 2003, Technical data sheet: Liquid Polysulfide LP2, Chicago, IL, USA.

[30] Polymeric materials encyclopedia: P, Volume 9, Edited by Joseph C. Salamone, CRC Press, 1996, pp.6857

[31] Castek, A Transpo Industries Company Inc., 2002, Technical data sheet: Polysulfide Epoxy Coat T-48 Chip Seal, New Rochelle, NY.

[32] The Flamemaster Corp., Chem Seal Industries, Inc., 2002, Technical data sheet: Polysulfide Rubber CS 3100 Electrical Potting and Sealing Compound, California 91352.

[33] PPG Aerospace PRC-DeSoto, Technical data sheet: PR-1422 Class A Fuel Tank Sealant,, California 91209.

[34] Lowe, G.B., 1997, "*The cure chemistry of polysulfides*", International Journal Adhesion & Adhesives, Vol. 17, No. 4, pp. 345-348.

[35] Asia Pacific Microspheres Malayan Adhesives & Chemicals Sdn Bhd, 2008, Technical data sheet: Phenoset Microspheres, www.phenoset.com.

[36] Chemical Structure of Phenolic Microballoon, University of Virginia, Department of Material Science and Engineering.

[37] Wouterson, E. M., Boey, F. Y. C., Hu, X., and Wong, S., 2005, "*Specific Properties and Fracture Toughness of Syntactic Foam: Effect of Foam*

Microstructure", Composites Science and Technology, Vol. 65, pp. 1840-1850.

[38] Expancel Inc., Microspheres, Technical Bulletin No. 40, www.expancel.com.

[39] Carlisle, K.B. and Chawla, K.K., 2006, "*Structure and Mechanical Properties of Micro and Macro Balloons: An Overview of Test Techniques*", Journal of Material Science, pp. 3961-3972.

[40] Halpin, J.C., and Tsai, S.W., 1969, "Effects of Environmental Factors on Composite Materials, Air Force Technical Report AFML-TR-67-423, Wright Aeronautical Labs, Dayton, OH.

[41] Ashby, M. F., 1983, "*The Mechanical Properties of Cellular Solids*," Metallurgical Transactions A, Vol. 14A, pp. 1755-1769.

[42] Chen, W., Zhang, B., and Forrestal, M.J., 1999, " *A Split Hopkinson Bar technique for low impedence materials*," Exp. Mech. Vol. 39, pp. 1-5.

[43] Pandurangha, R., PhD Thesis, 2010, "*High Strain Rate Response of Eco-Core & its Modification*," Department of Mechanical Engineering, CCMR, N.C. A&T State University.

[44] Woldesenbet, E., and Peter, S., 2009, "*Volume Fraction Effect on High Strain Rate Properties of Syntactic Foam Composites*," Journal of Materials Science, Vol. 44, pp. 1528-1539.

APPENDIX

STRESS VS. TIME AND STRAIN VS. TIME PLOTS

The appendix contains the stress vs. time and strain vs. time plots for base and Pμb-filled polysulfide specimens.

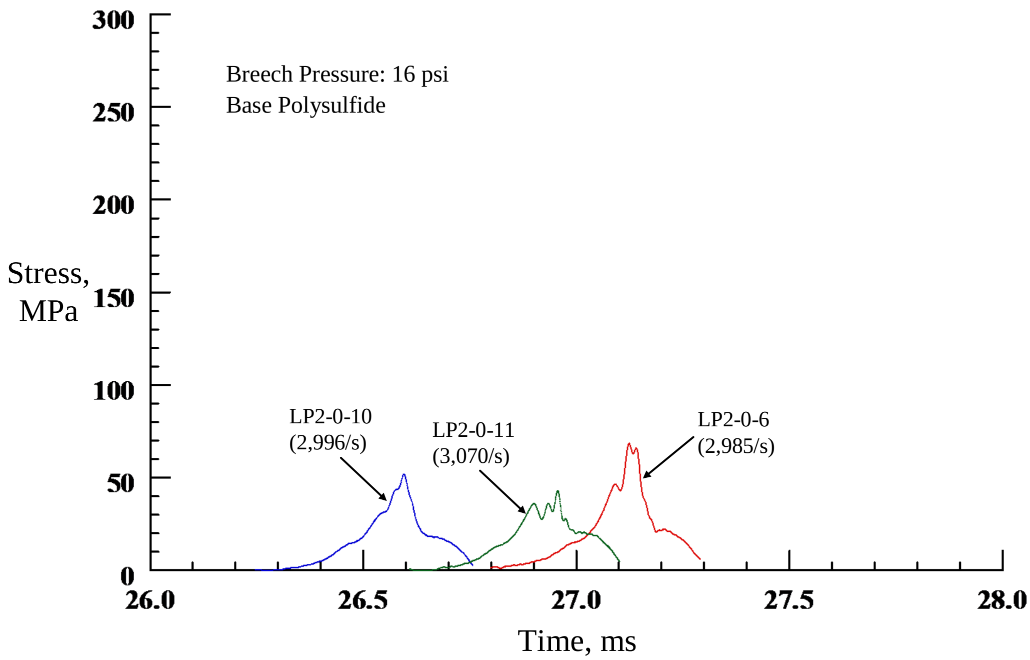

Figure A.1 Stress-Time response of base LP2 at breech pressure 0.11 MPa

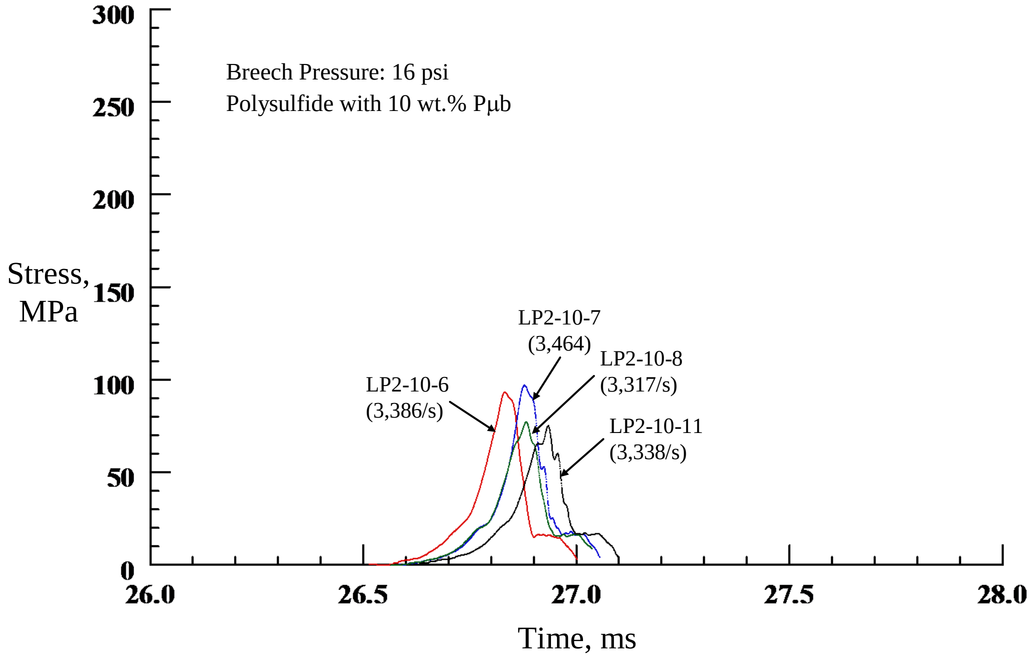

Figure A.2 Stress-Time response of 10 wt.% Pμb-filled LP2 at breech pressure 0.11 MPa

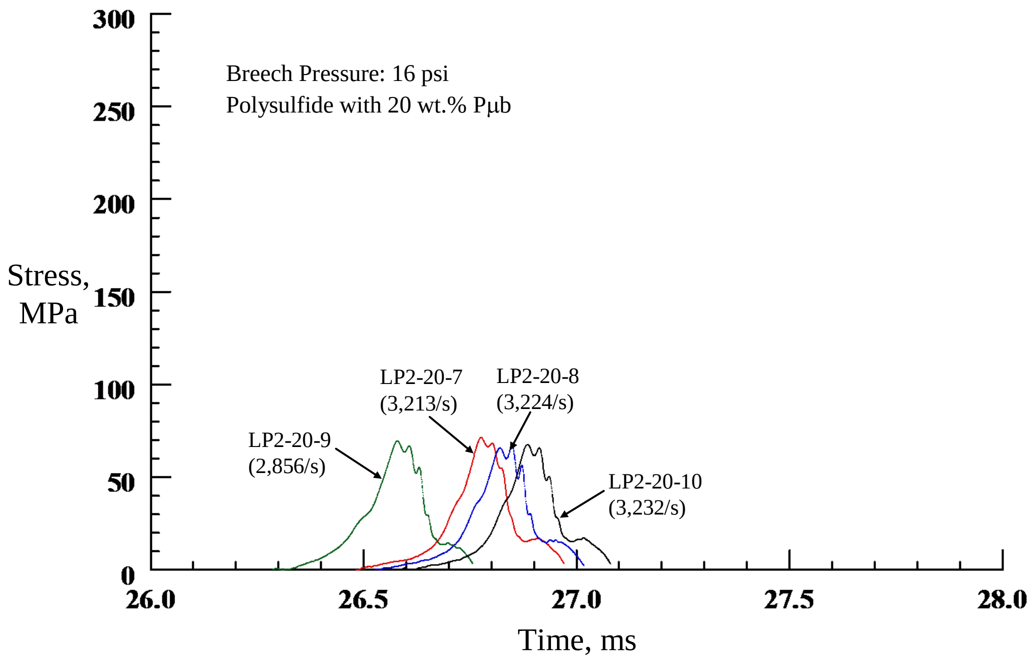

Figure A.3 Stress-Time Response of 20 wt.% Pμb-filled LP2 at Breech Pressure 0.11 MPa

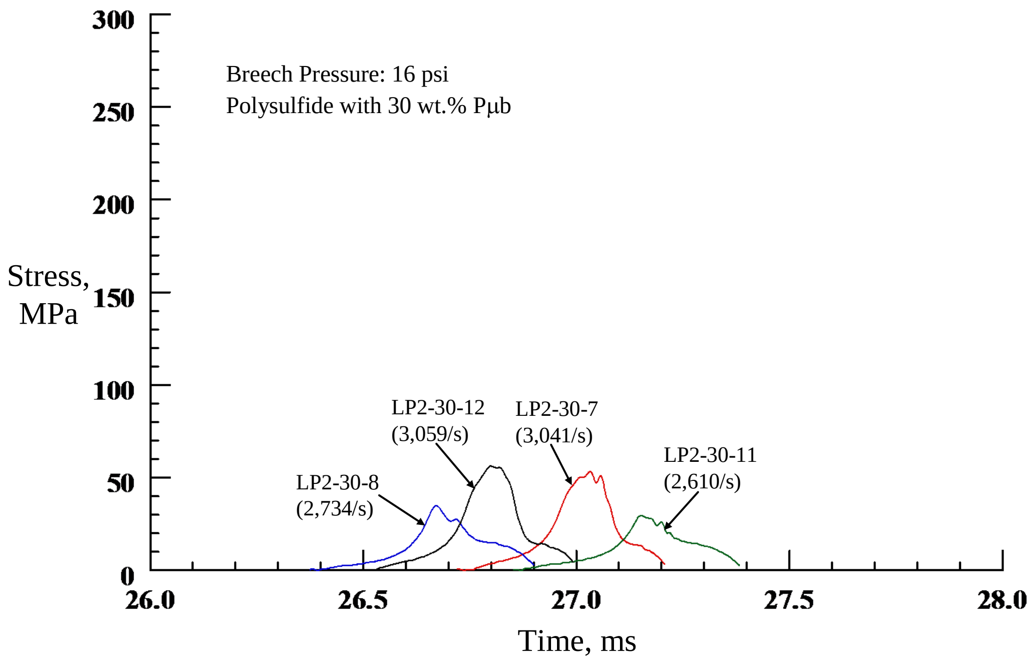

Figure A.4 Stress-Time response of 30 wt.% Pµb-filled LP2 at breech pressure 0.11 MPa

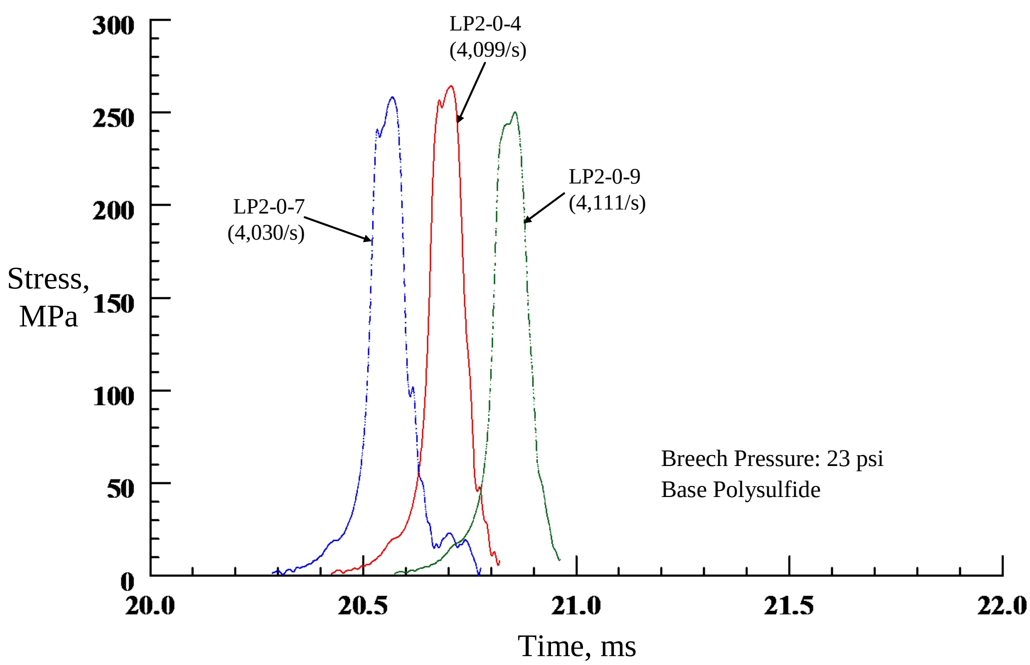

Figure A.5 Stress-Time Response of Base LP2 at Breech Pressure 0.16 MPa

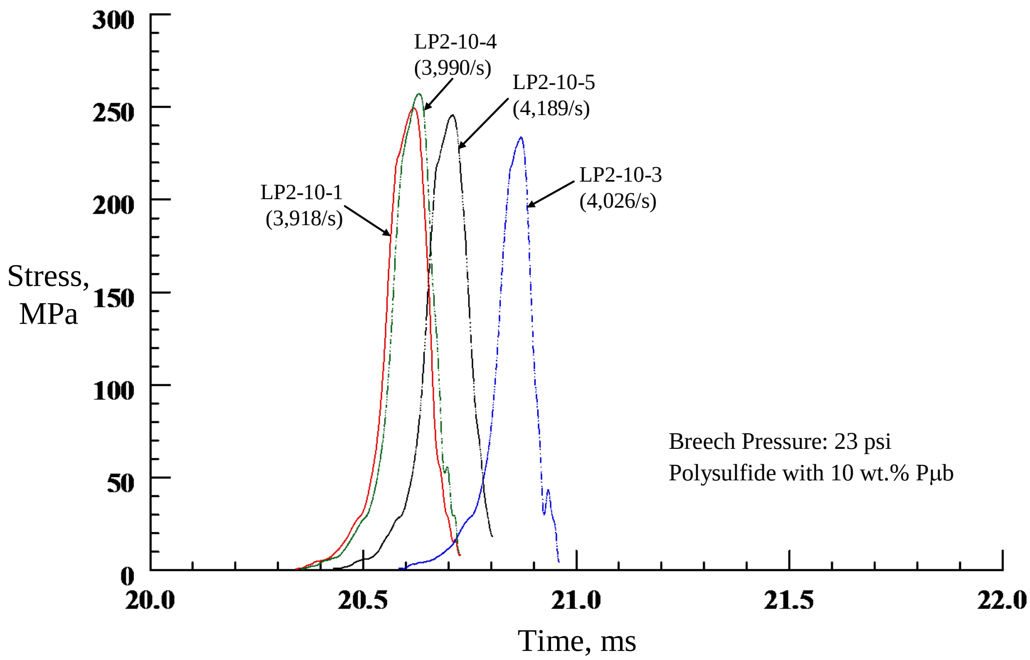

Figure A.6 Stress-Time response of 10 wt.% Pμb-filled LP2 at breech pressure 0.16 MPa

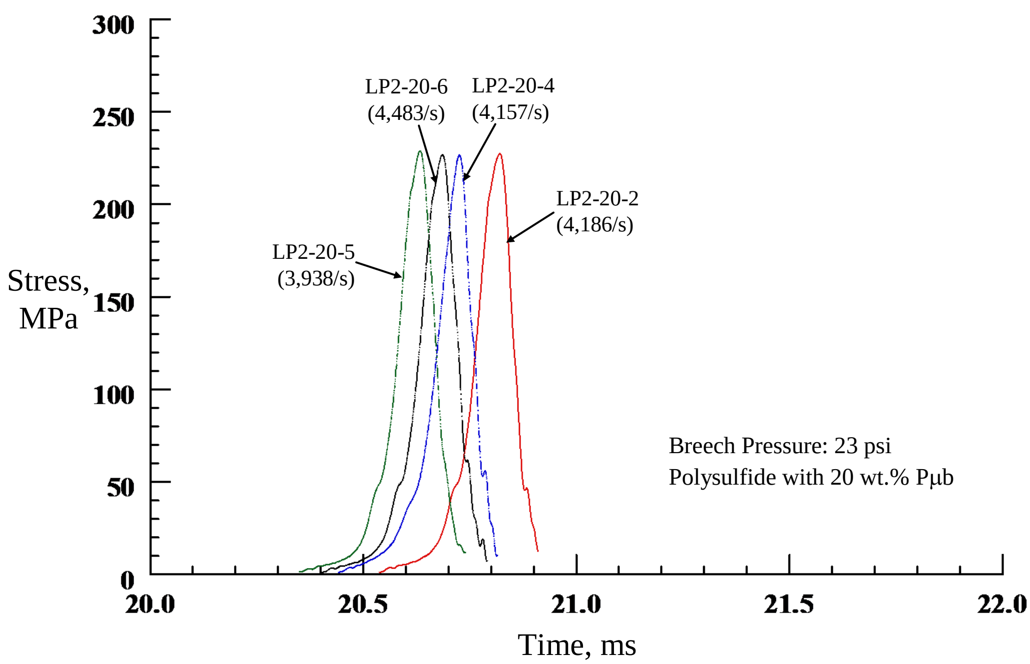

Figure A.7 Stress-Time Response of 20 wt.% Pμb-filled LP2 at Breech Pressure 0.16 MPa

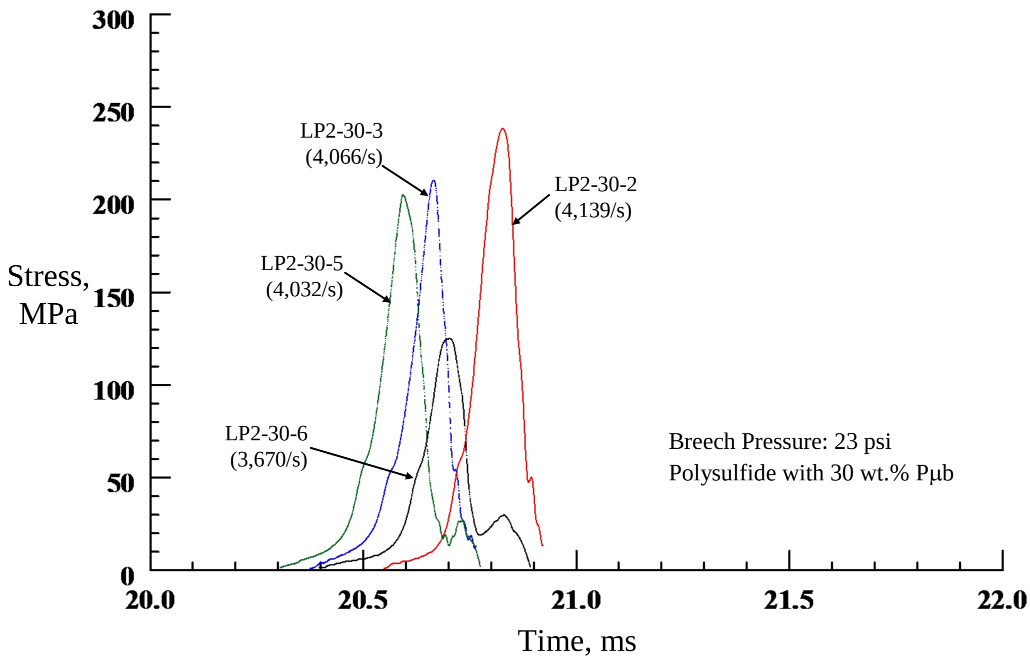

Figure A.8 Stress-Time response of 30 wt.% Pμb-filled LP2 at breech pressure 0.16 MPa

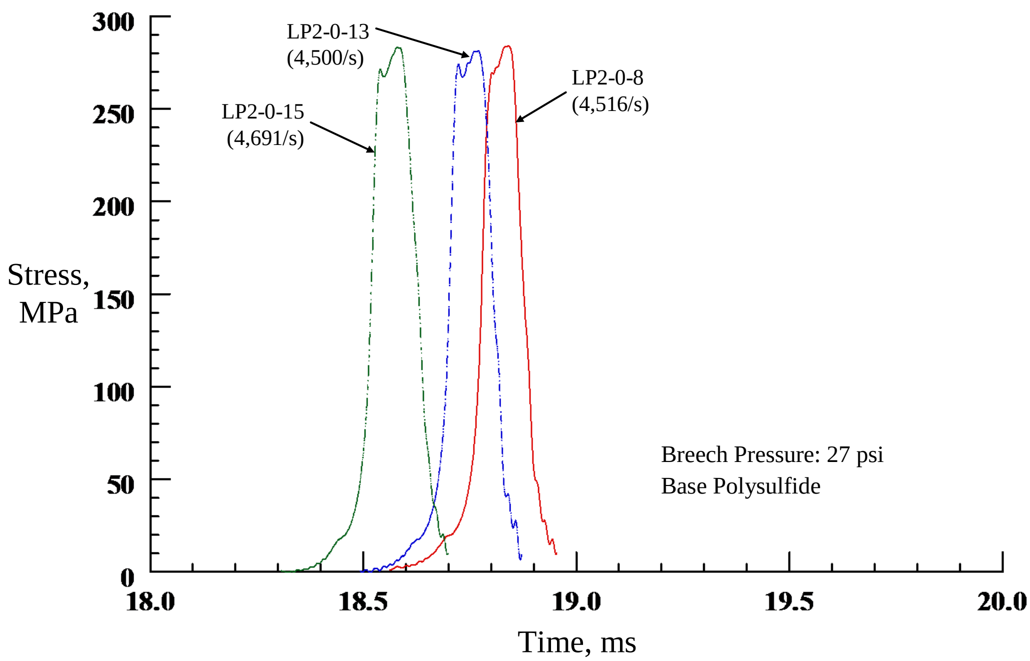

Figure A.9 Stress-Time response of base LP2 at breech pressure 0.19 MPa

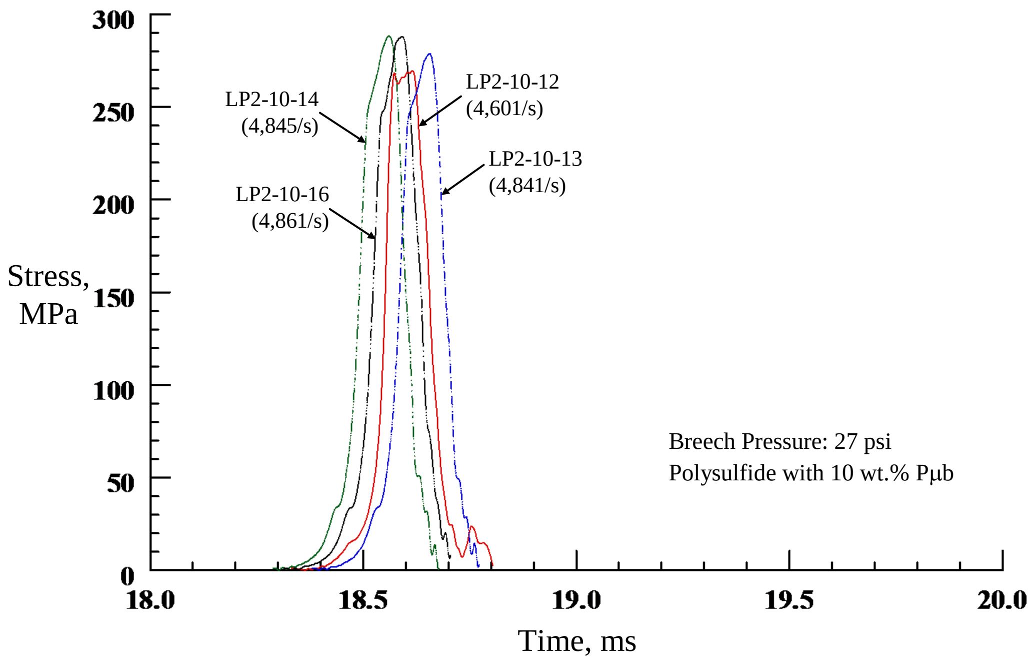

Figure A.10 Stress-Time response of 10 wt.% Pµb-filled LP2 at breech pressure 0.19 MPa

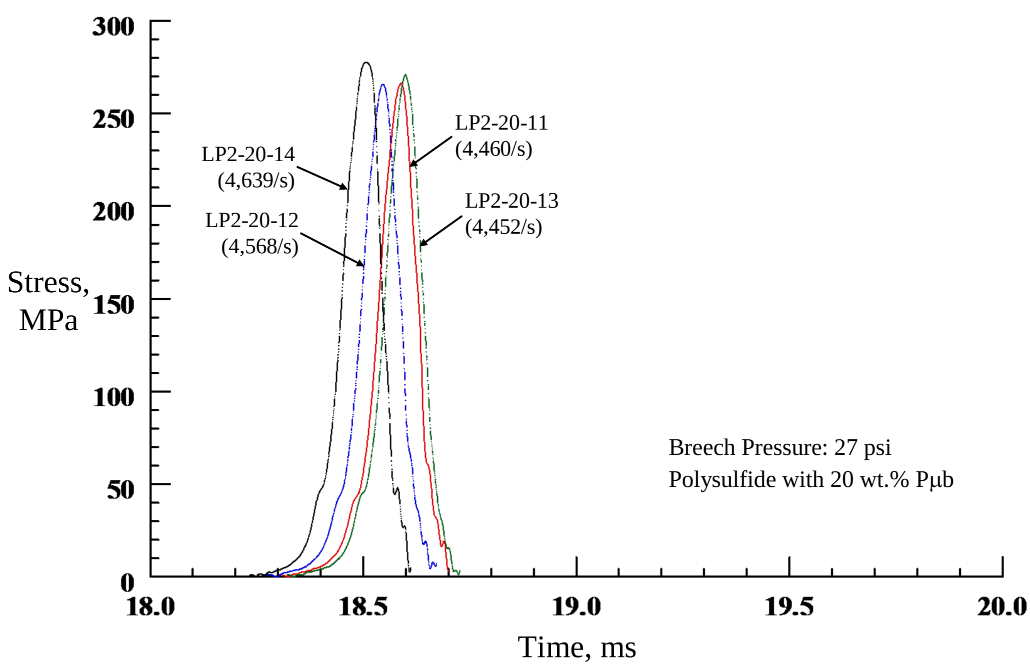

Figure A.11 Stress-Time response of 20 wt.% Pµb-filled LP2 at breech pressure 0.19 MPa

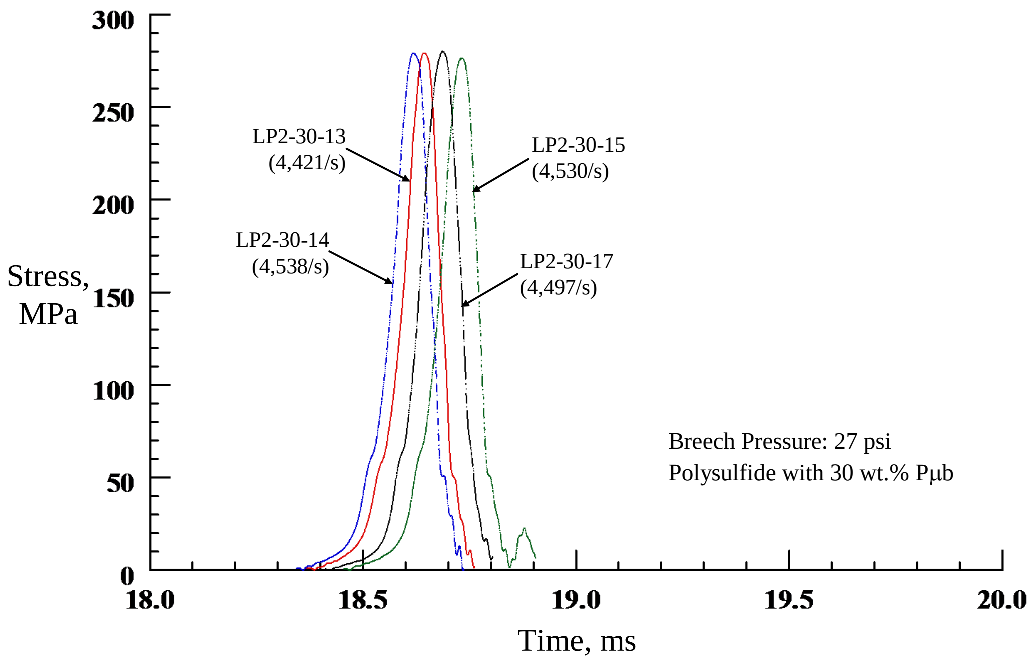

Figure A.12 Stress-Time response of 30 wt.% Pμb-filled LP2 at breech pressure 0.19 MPa

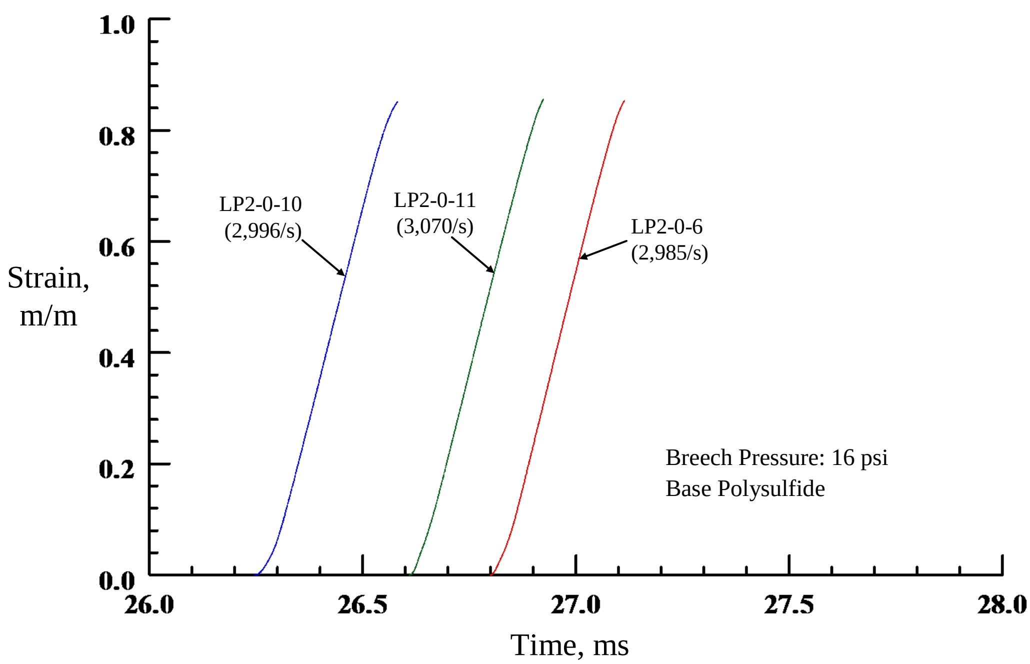

Figure A.13 Strain-Time response of base LP2 at breech pressure 0.11 MPa

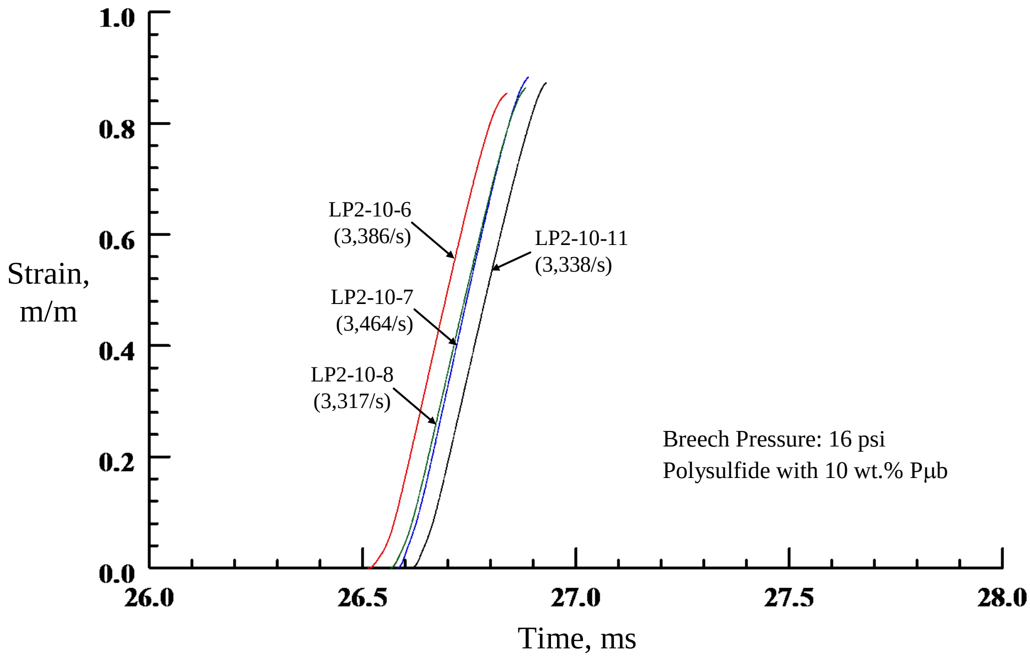

Figure A.14 Strain-Time response of 10 wt.% Pμb-filled LP2 at breech pressure 0.11 MPa

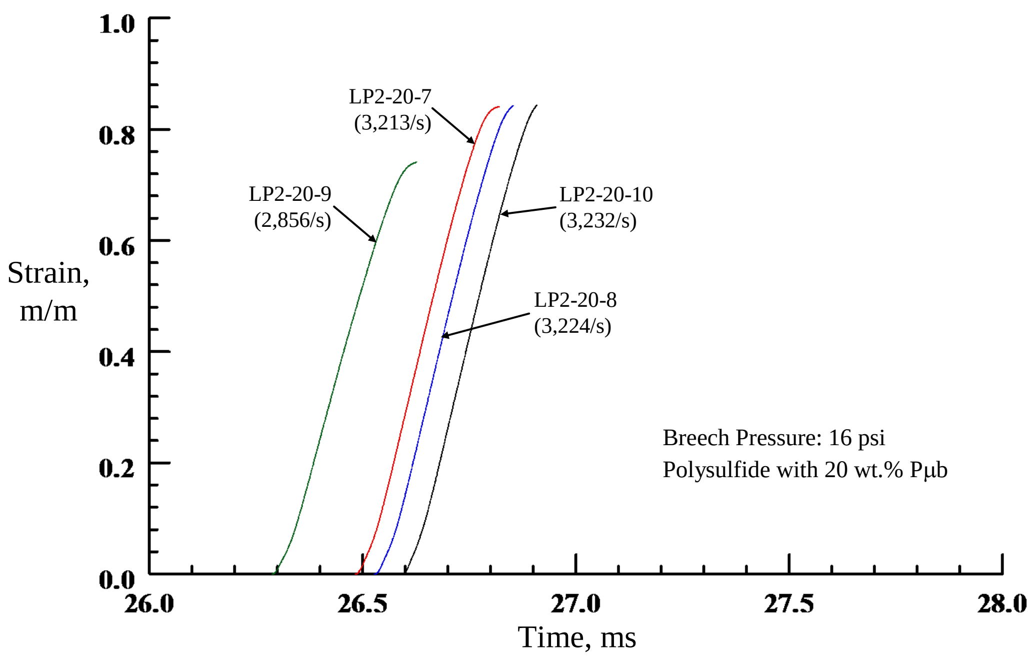

Figure A.15. Strain-Time response of 20 wt.% Pμb-filled LP2 at breech pressure 0.11 MPa

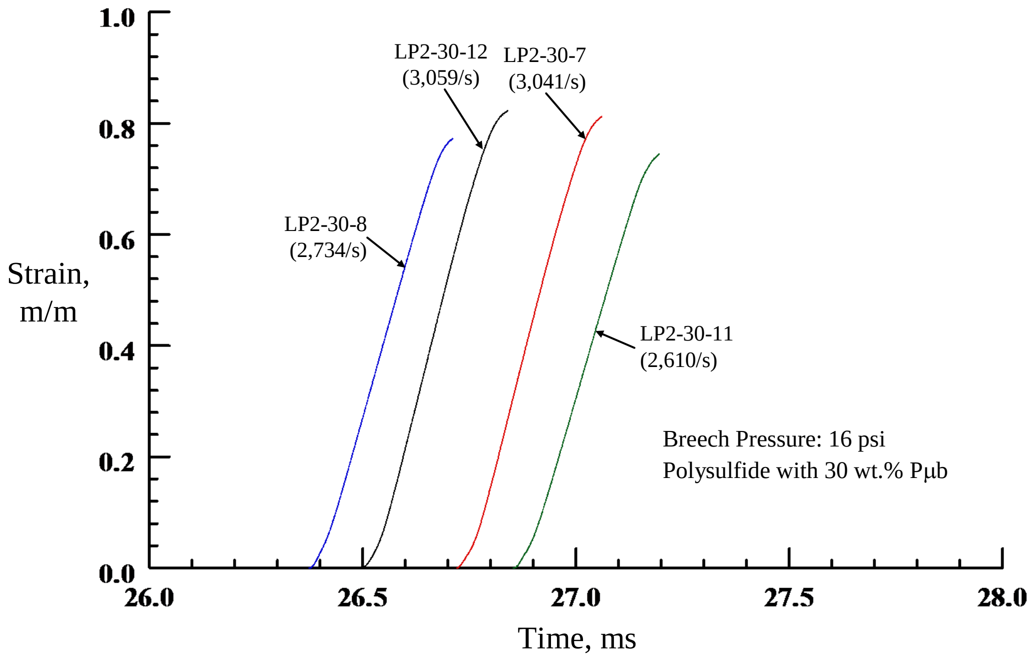

Figure A.16 Strain-Time response of 30 wt.% Pµb-filled LP2 at breech pressure 0.11 MPa

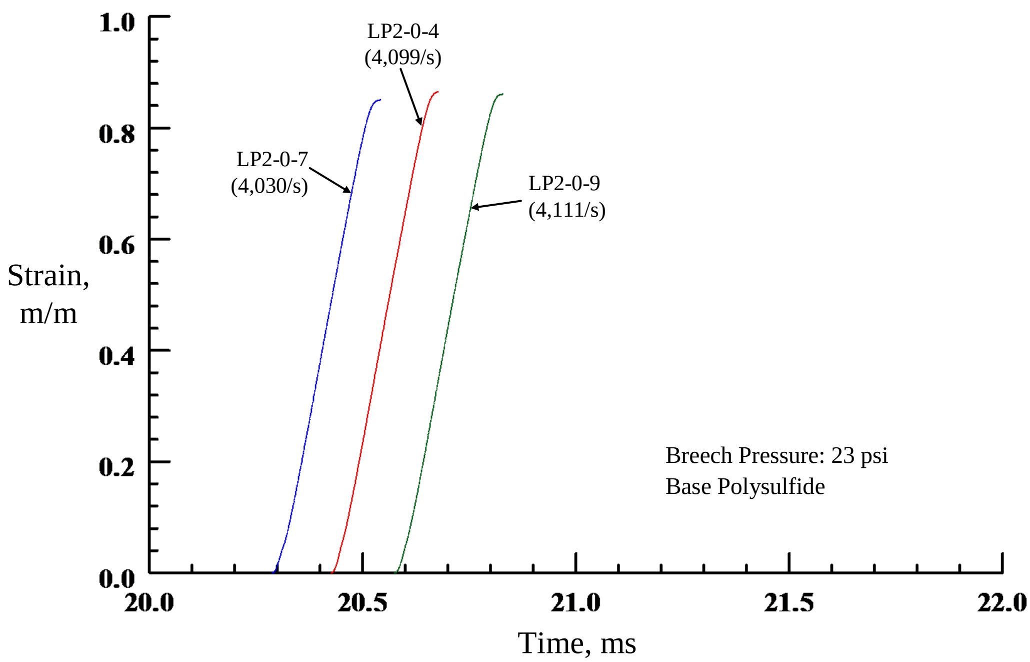

Figure A.17 Strain-Time response of base LP2 at breech pressure 0.16 MPa

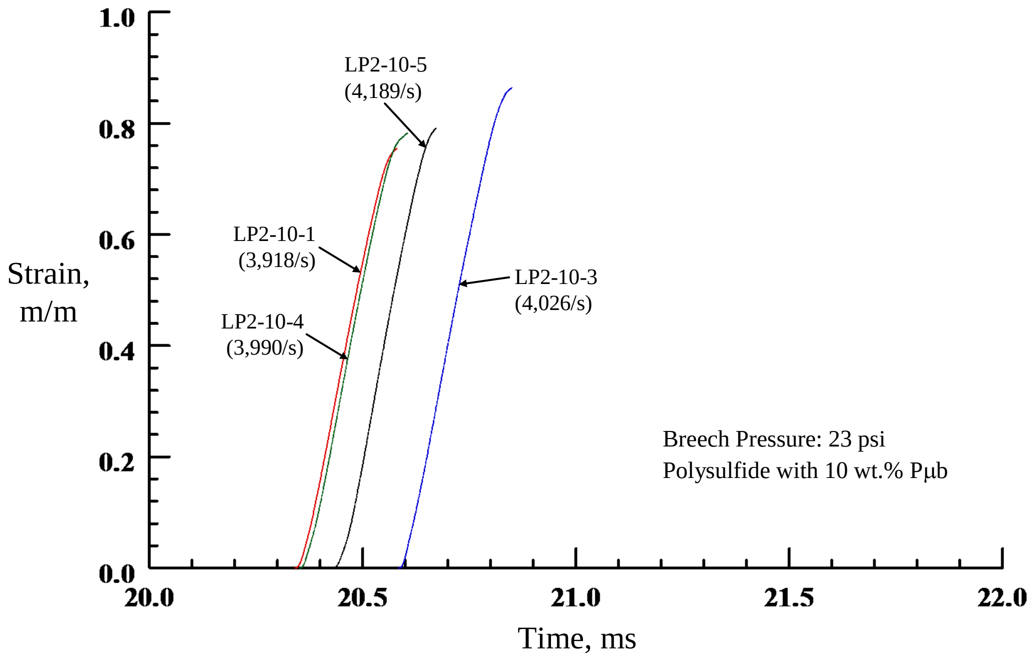

Figure A.18 Strain-Time response of 10 wt.% Pμb-filled LP2 at breech pressure 0.16 MPa

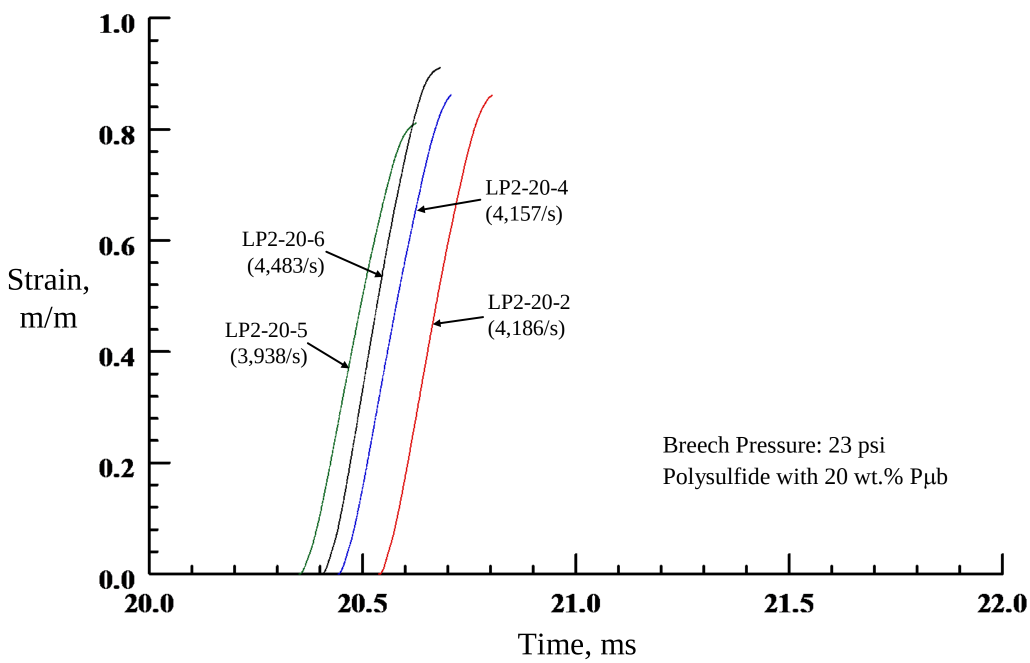

Figure A.19 Strain-Time response of 20 wt.% Pμb-filled LP2 at breech pressure 0.16 MPa

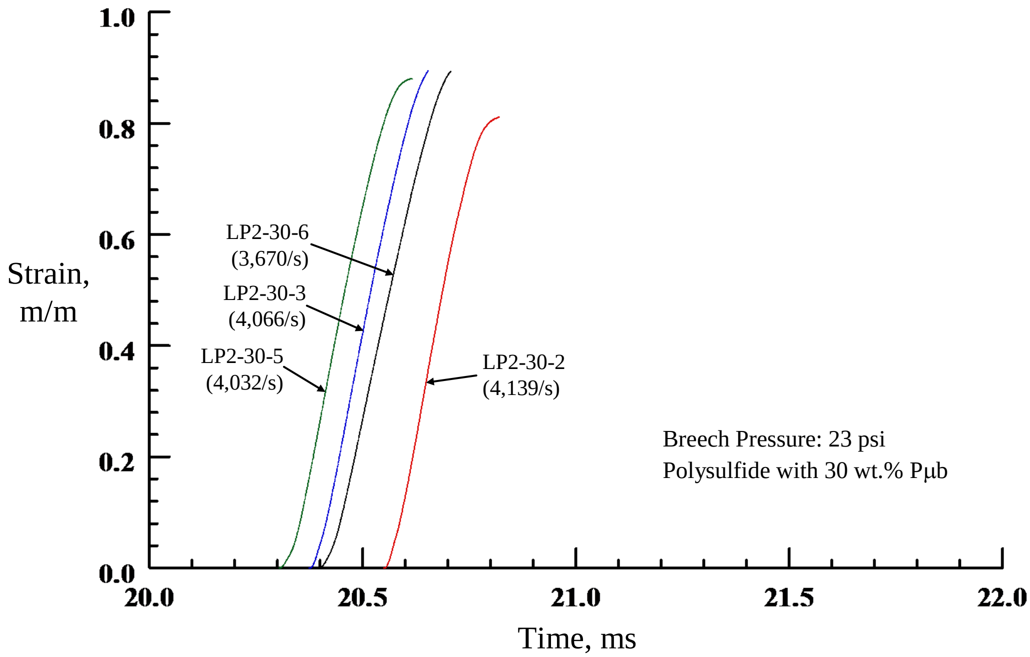

Figure A.20 Strain-Time response of 30 wt.% Pμb-filled LP2 at breech pressure 0.16 MPa

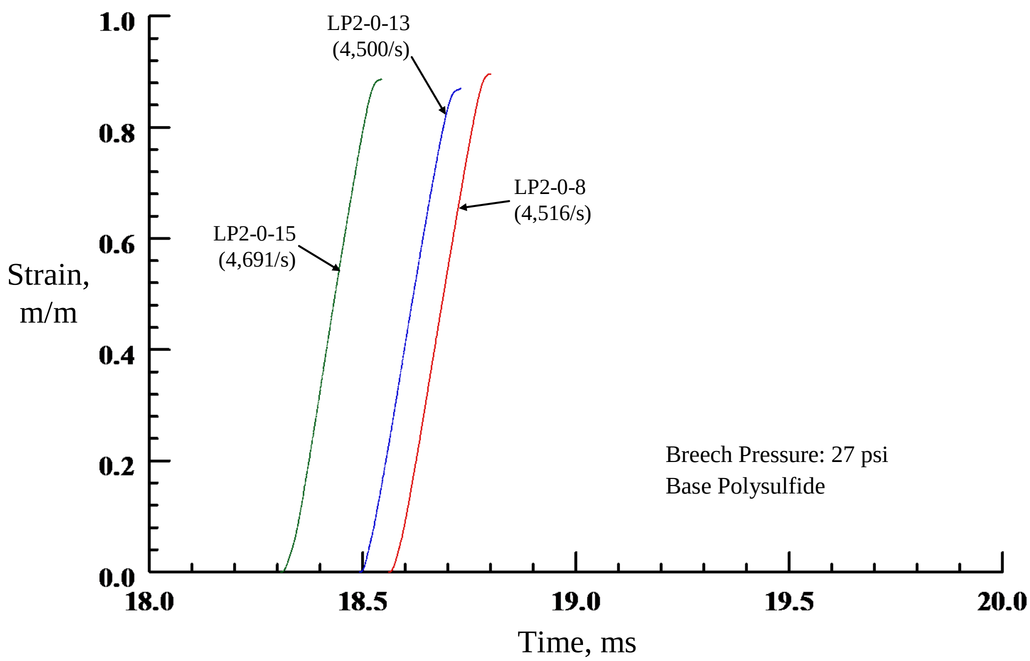

Figure A.21 Strain-Time response of base LP2 at breech pressure 0.19 MPa

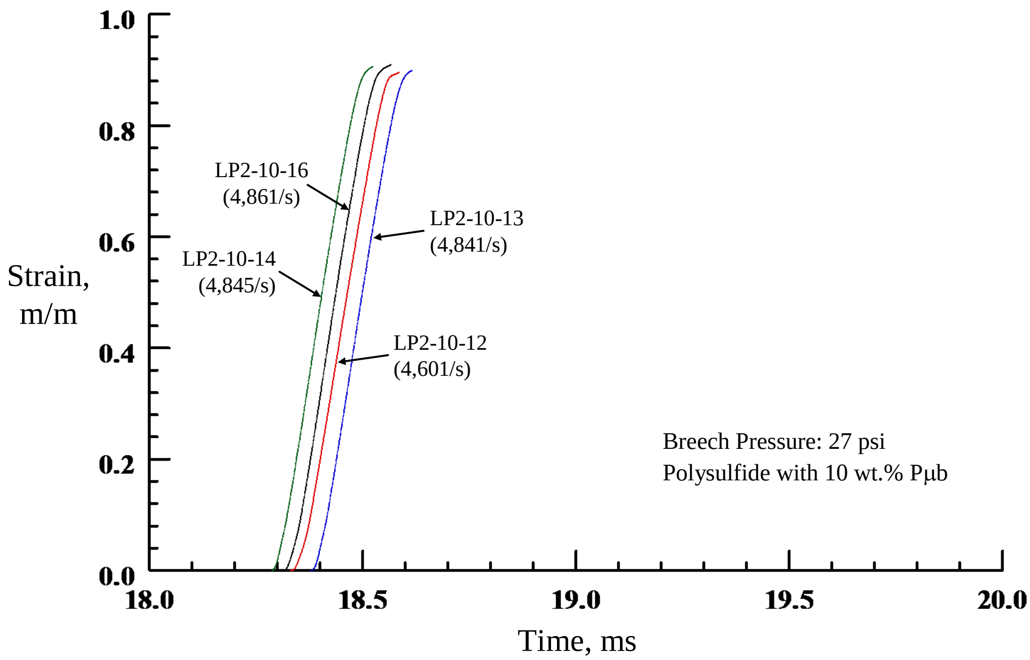

Figure A.22 Strain-Time response of 10 wt.% Pμb-filled LP2 at breech pressure 0.19 MPa

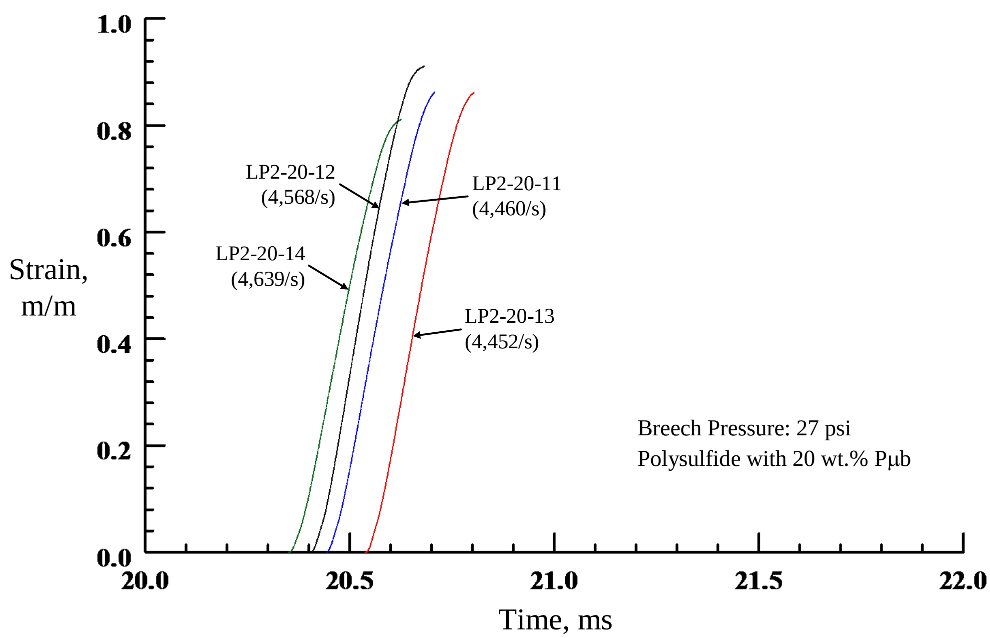

Figure A.23 Strain-Time response of 20 wt.% Pμb-filled LP2 at breech pressure 0.19 MPa

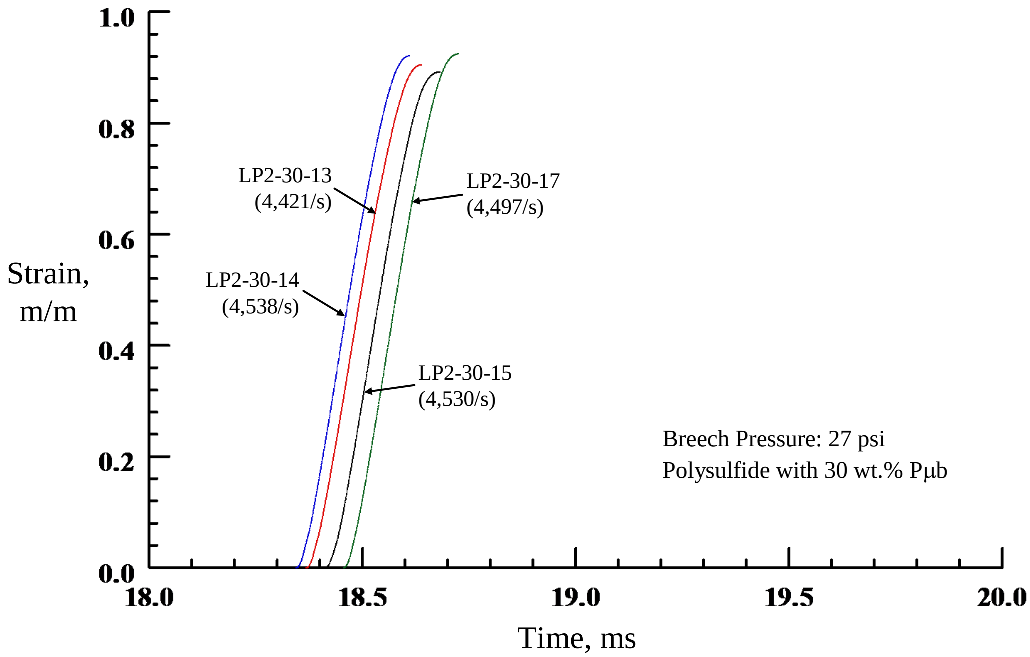

Figure A.24 Strain-Time response of 30 wt.% Pµb-filled LP2 at breech pressure 0.19 MPa